TENSOR POLARIZED DEUTERON CAPTURE BY ^{3}He AT AND ABOVE THE FUSION RESONANCE REGION

by

Mark Joseph Balbes

Department of Physics
Duke University

Date: February 10, 1992

Approved:

Henry R. Weller, Supervisor

Calvin R. Howell

Dissertation submitted in partial fulfillment of the requirements for the degree of Doctor of Philosophy in the Department of Physics in the Graduate School of Duke University

1992

ABSTRACT

(Physics-Nuclear)

TENSOR POLARIZED DEUTERON CAPTURE BY ^{3}He

AT AND ABOVE THE FUSION RESONANCE REGION

by

Mark Joseph Balbes

Department of Physics
Duke University

Date: February 10, 1992

Approved:

Henry R. Weller, Supervisor

Calvin R. Howell

An abstract of a dissertation submitted in partial fulfillment of the requirements for the degree of Doctor of Philosophy in the Department of Physics in the Graduate School of Duke University

1992

Abstract

Tensor-Polarized Deuteron Capture by ^{3}He at and above the Fusion-Resonance Region

The absolute differential cross section and vector and tensor analyzing powers of the $^3\mathrm{He}(\vec{d},\gamma)^5\mathrm{Li}$ reaction have been measured at three energies: $E_d(\mathrm{lab}) = 8.6$ MeV, $E_d(\mathrm{lab}) = 0.8$ MeV where the beam was stopped in the target, and $E_d(\mathrm{lab}) = 0.6$ MeV where the beam lost 0.3 MeV in the target. Additionally, absolute cross sections were measured at $E_d(\mathrm{lab}) = 0.8$ MeV where the beam lost 0.4 MeV in the target, and $E_d(\mathrm{lab}) = 0.4$ MeV where the beam was stopped in the target.

Transition matrix element (TME) analyses of the observables at or below $E_d(\mathrm{lab}) = 0.8$ MeV concluded that the reaction proceeds predominantly through s-wave (E1) capture, with small admixtures of M1 or E2 radiation. While multiple TME solutions exist, multichannel Resonating Group Model calculations performed at the peak of the fusion resonance at $E_d(\mathrm{lab}) = 0.45$ MeV unambiguously select the solution with >89% $^4s_{3/2}$(E1) TME strength as the physically preferred one. In the RGM picture, the strong capture cross section in the fusion resonance region is a consequence of the tensor force, which couples the $[d+^3\mathrm{He}]^{S=3/2}_{J=3/2}$ channel to the $[p+^4\mathrm{He}]^{S=1/2}_{J=3/2}$ channel in the scattering wave function, enabling the capture reaction to proceed via the $\Delta S=0$ (E1) transition to the ground state.

At $E_d = 8.6$ MeV, a transition matrix element fit indicates that the capture cross-section strength is dominated by s-wave E1 capture with an admixture of ~20% d-wave E1 capture. In an RGM calculation at this energy, a non-zero tensor force is necessary to get agreement between data and theory for the relative strengths of the TME's. As with the $E_d(\mathrm{lab}) = 0.45$ MeV calculation, the strong $^4s_{3/2}$(E1) capture strength is due to the coupling of the $[d+^3\mathrm{He}]^{S=3/2}_{J=3/2}$ scattering channel to the $[p+^4\mathrm{He}]^{S=1/2}_{J=3/2}$ scattering channel by the tensor force.

Acknowledgments

This dissertation is the result of many years of hard work by many people. To the Capture Group past-and-future at TUNL, James Langenbrunner, Mark Whitton, John Riley, Bob Chasteler, Greg Schmid, and Mark Godwin, thanks guys for working so hard on my runs. Heartfelt gratitude and appreciation goes to Laird Kramer and Zandy Williams, my cohorts for the last five years, who have dedicated a non-negligible fraction of their lives to this research. I couldn't have done it without you guys. Our post-doc Jerry Feldman graciously left the comforts of Seattle to spend several years here endowing us with the benefits of his experience and physical insights. Evans Hayward and Ron Tilley have provided me with a rich history and sense of continuity for the experiments we have conducted. And of course I couldn't have done any of this without the wisdom and advise of Henry Weller. His enthusiasm and encouragement, coupled with his tremendous knowledge of the field have pushed this research to fruition.

It was only through the love and support of my parents that I embarked on a career in the sciences. They taught me how to be curious about just about everything. Thanks, Mom and Dad, for encouraging me all these years.

I can never repay the dedication and support given to me during my graduate school years by my wife, Lisa. She kept me sane and happy when the world looked bleakest and gave me a reason to get out of school quickly. This dissertation is dedicated to her. Thanks Pooder! I love you.

This dissertation is also dedicated to my son Jack, without whom I would never have known that there were other reasons for doing overnights.

Table of Contents

Figures

Tables

Chapter 1: Introduction

Light nuclei are important for understanding the two-body nuclear force which includes spin-orbit and tensor components. With small, uncomplicated systems the fundamental physical effects become easier to untangle from each other. Capture reactions are particularly well suited for probing these small systems since the photon only weakly perturbs the nuclear medium. Also, the electromagnetic interaction is well understood from Maxwell's equations allowing a strong theoretical foundation with which to interpret empirical results. In this dissertation, the results of experiments to study polarized-deuteron capture by ^{3}He are discussed. These experiments have been conducted in two energy regions: at $E^*_{^5Li}$=21.5 MeV and at $E^*_{^5Li}$=16.7 MeV which corresponds to the $J^\pi=3/2^+$ resonance at E_d(lab) = 0.45 MeV above the d+^{3}He threshold.

From a practical point of view, the d+^{3}He reaction is important because of its potential as a fuel for an energy-producing fusion reactor. Current fusion technology relies on the d+^{3}H reaction because of the lower ignition temperature necessary for a sustained burn. In both reactions, the energy yield is enhanced by the existence of a $J^\pi=3/2^+$ resonance (called the "fusion" resonance) which exists only a few hundred keV above fusion-reactor energies. The advantage that the d+^{3}He reaction offers over the d+^{3}H reaction is a source of cleaner energy. Tritium (^{3}H) itself is radioactive and tends to contaminate the work environment. The process of fusing it with deuterium creates a large source of neutrons from the ^{3}H(d,n)^{4}He reaction which are a health hazard both by themselves and by creating unstable isotopes through neutron-induced nuclear reactions. Using the d+^{3}He reaction eliminates the neutrons, instead producing protons from the ^{3}He(d,p)^{4}He reaction which are easily stopped in matter. Unfortunately, current technology is unable to reach the temperatures necessary to ignite the d+^{3}He plasma, but

the more knowledge which is available increases the probability of someday building just such a device.

Even in the d+^{3}H reactors which are being designed and studied today, the ^{3}He(d,γ)^{5}Li reaction is being considered as a possible diagnostic for the plasma since γ-rays interact relatively weakly with matter and are therefore more easily detected outside of the reactor than other particles. The reaction comes about from the deuterium fusing with ^{3}He which is created in the d(d,n)^{3}He reaction. The γ-rays from this reaction, along with the previously measured ^{3}He(d,γ)^{5}Li-to-^{3}He(d,p)^{4}He branching ratio gives a direct measure of the fusion energy production rate of the reactor [Cec85a].

The properties of the fusion resonance were originally determined primarily by studies of the ^{3}He(d,p)^{4}He reaction [Bon52, Freier54, and Yar53]. The isotropic cross section indicates that the resonance is formed via s-wave capture indicating that the resonance has positive parity. Since the spins of the deuteron and ^{3}He can only couple to S=1/2 or S=3/2, the total spin (L+S) of the fusion resonance can only be $J^\pi=1/2^+$ or $J^\pi=3/2^+$. If a one-level approximation is made, then the total cross section has an upper bound of

$$\sigma \leq \pi(2J+1)/6k^2. \qquad [1.1]$$

where k is the wave number of the deuteron in the center-of-mass. The measurements of the absolute cross section falls between the upper limits for J=1/2 and J=3/2. Since Eqn. 1.1 is an upper bound the resonance must have $J^\pi=3/2^+$. Subsequent ^{4}He(p,p)^{4}He phase shift analyses [Hou78, Pla72, and Sch71] have confirmed this initial spin and parity assignment. A phase shift analysis of the ^{3}He(d,d)^{3}He reaction by [Jen80] found a solution where the $^2s_{1/2}$ phase shift is approximately 5° while the $^4s_{3/2}$ phase shift is

resonant. This indicates that any L=0, S=1/2 background is on the order of two magnitudes less than the L=0, S=3/2 resonance.

Shell-model calculations of ^{5}Li predict both a $3/2^+$ state and a $1/2^+$ state at excitation energies above the $1/2^-$ first excited state [Van83]. Coupled-channel calculations disperse the strength of the $1/2^+$ state because it couples strongly to the α+p channel [Bur83 and HofPri]. The $3/2^+$ state couples to the α+p channel only through the tensor and spin-orbit forces and therefore has a relatively narrow width. Resonating Group Model calculations in the fusion-resonance region also require the presence of a tensor force to predict the strength of the ^{3}He(d,p)^{4}He low-energy cross section [Blu90].

For our investigation of this $J^\pi=3/2^+$ "fusion" resonance region of ^{5}Li, capture reactions with tensor-polarized deuterons are well suited for probing tensor-force effects because of the constraints imposed by the $\Delta S=0$ selection rule for E1 radiation. As stated above, this resonance is populated predominantly by deuterons with L=0 and S=3/2. The $J^\pi=3/2^-$ ground state of ^{5}Li, on the other hand, is predominantly L=1, S=1/2 (as seen in the single-particle model, where the ^{5}Li ground state consists predominantly of a proton in the $p_{3/2}$ orbital above a closed $s_{1/2}$ ^{4}He core). Therefore, in keeping with the $\Delta S=0$ selection rule which says that the dominant term of the E1 operator does not affect channel spin, there are at least two likely mechanisms for an E1 γ-ray transition from the predominantly S=3/2 resonance to the predominantly S=1/2 ground state. First, the S=3/2 resonance can decay directly to the S=3/2 component of the ground state which may be large due to tensor force mixing in the ground state. Second, the tensor force can mix the S=3/2 and S=1/2 scattering states, allowing the transition to the S=1/2 component of the ground state.

The cross section for the ^{3}He(d,γ)^{5}Li reaction was first measured by Blair, Hintz, and Van Patter [Bla54]. An excitation-function measurement showed the fusion

resonance at $E_d(\text{lab}) = 0.45$ MeV with an angle-integrated total cross section of $50 \pm 10\,\mu$b. An angular distribution taken at $E_d = 0.58$ MeV was consistent with isotropy to within 10%. [Bus68] also measured an isotropic angular distribution (at $E_d = 0.48$ MeV) but claim a lower total cross section of $21 \pm 4\,\mu$b. [Kra68] measured an excitation function at 90° with a total cross section of $38\,\mu$b at resonance.

Analyzing powers of the $^3\text{He}(\vec{d},\gamma)^5\text{Li}$ reaction have not been measured previously. However, a study has been made by [Ril89] of the $^3\text{H}(\vec{d},\gamma)^5\text{He}$ reaction in the region of the ^{5}He fusion resonance. An analysis of the data concluded that the isotropic cross section was dominated by S=3/2 (E1) capture, which contributed 95% of the cross section strength. Admixtures of 2.6% S=1/2 (E1) and 2.0% S=3/2 (M1) capture strengths were required to fit the data of that experiment, especially the tensor analyzing power $A_{yy}(\theta)$. From charge-symmetry considerations, similar results are expected for the $^3\text{He}(\vec{d},\gamma)^5\text{Li}$ reaction.

Above the fusion resonance, the $^3\text{He}(d,\gamma)^5\text{Li}$ reaction has been studied from 2-26 MeV by [Tom67], [Del68], [Sch70], [Kin72], and others (see [Ajz88]). [Tom67] suggests the existence of a broad state at 20 MeV with a possible spin assignment of $3/2^+$ or $5/2^+$, whereas [Sch70] also considers a spin assignment of $1/2^+$. [Del68] found no clear evidence for the existence of any state at this energy. [Kin72] measured an excitation function from 17 MeV $\leq E^*_{^5\text{Li}} \leq$ 26 MeV, and several angular distributions within this energy range. The γ_0 and γ_1 transition intensities were extracted, the analysis of which was consistent with a $1/2^+$ state around 18 MeV and a $5/2^+$ state around 20 MeV. If such states do exist, then the current experiment at $E^*_{^5\text{Li}}$=21.5 MeV lies on the high-energy side of the 20 MeV resonance. Angular distributions by [Kin72] indicate a non-isotropic cross section around these energies. Analyzing powers of the $^3\text{He}(\vec{d},\gamma)^5\text{Li}$ reaction have not previously been measured.

The following chapters present the experimental techniques, methods of analysis, and results of our recently concluded study of the $^{3}He(\vec{d},\gamma)^{5}Li$ reaction. Cross sections and analyzing powers have been measured in the fusion resonance region ($E^{*}_{5_{Li}}$=16.7 MeV) and at $E^{*}_{5_{Li}}$=21.5 MeV. The results of Legendre and transition matrix element fits to the data are presented along with interpretations of these results. The results of a Direct Capture calculation at the fusion-resonance energy is reported, along with the more sophisticated Resonating Group Model calculation which was performed in both energy regions. Finally, conclusions about the reaction and the role of the tensor force will be discussed.

Chapter 2: Experimental Techniques

The following is a discussion of the experimental techniques used for beam creation and acceleration, and photon and particle detection. Deuteron beams of 8.85 MeV (which resulted in an 8.6 MeV beam at the center of the target) and approximately 3.3 MeV (subsequently degraded to provide 0.8 MeV, 0.6 MeV, and 0.4 MeV beams on target) were created in three sources and accelerated by the TUNL FN tandem Van de Graaff to one of two gaseous ^{3}He targets. The signals from two NaI spectrometers were processed by fast CAMAC electronics and sorted by the VAX 11/780 computer using the XSYS data acquisition system.

2.1 Sources

The simplest of the three sources that will be discussed is the **Direct Extraction Negative Ion Source (DENIS).** In this source, hydrogen or deuterium is bombarded by electrons supplied by a hot filament. The negative ions are then accelerated by an electric field away from the neutral gas. The entire source is biased to -50 kilovolts with respect to the lab which further accelerates the beam out of the source. The beam travels through a parallel-plate chopper followed by an auxiliary square-wave chopper. It is then deflected by a magnetic field and passes through a double-drift bunching system [Mil79 and Wen80]. This allows the creation of a pulsed beam with 2 to 4 ns long bursts every 200 ns.

The **Lamb Shift Polarized Ion Source (LSPIS)** [Cle74] has been decommissioned since the completion of this experiment. In that source, low-energy positive ions from a duoplasmatron were passed through a cesium vapor in a charge-exchange canal. Approximately 1/3 of these particles exited the canal as neutral particles in the metastable $2S_{1/2}$ state. Negatively charged particles (which resulted from the exchange of two electrons) were deflected out of the beam by an electric field. The beam then traveled through a spin filter [McK68] which consisted of static and radio-frequency

electric fields which selectively quenched all but one hyperfine state of the metastable atoms. In order to select out the polarized $2S_{1/2}$ atoms from the ground-state atoms and also to allow for subsequent acceleration of the beam, the atoms were passed through an argon charge-exchange canal. The probability for the polarized metastable atoms to pick up an extra electron is much greater than for the unpolarized ground state atoms. After exiting the argon region, the beam typically had a 10% to 25% unpolarized background. The beam was then focused and accelerated to 50 keV in preparation for injection into the tandem accelerator. If a pulsed beam was needed, the anode signal of the duoplasmatron could be ramped [How82] to prebunch the beam before passing through the double-drift bunching system .

The LSPIS was replaced by an intense **Atomic Beam Polarized Ion Source (ABPIS)** [CleTBP]. In this new source, deuterium molecules are dissociated by an applied radio-frequency field and drift into the region of a sextupole magnet which splits the six hyperfine levels of the deuterium atoms and defocuses the three lower energy states out of the beam. Weak and strong field rf cavities selectively induce transitions between the three higher-energy populated states and the three lower-energy unpopulated states thus polarizing the atoms. The neutral atoms are then passed through a plasma created by ionized nitrogen to create positively charged ions. They are then accelerated through gaseous Cs in order to pick up two electrons. Finally, the source itself is at -50 kilovolts with respect to the lab, which accelerates the negative ions out of the source. This source is followed by a Wien Filter (described below) and a set of chopper plates which are identical to those following the DENIS source.

The quantization axis of the polarized particles emitted by the above polarized-ion sources points in the direction of the beam momentum axis. In order to be able to measure the full range of analyzing powers, the quantization axis must be rotated into other orientations. This is accomplished with a **Wien Filter**, which previously was

located after the LSPIS and now follows the ABPIS. The Wien Filter consists of crossed electric and magnetic fields which point in the plane normal to the beam momentum. The magnetic field, which is read by a calibrated Hall probe, precesses the particle spins in the plane normal to the direction of the magnetic field. The entire assembly can be rotated about the beam-momentum axis to allow for spin precession to any desired orientation. The electric field is then tuned so that there is no net deflection of the deuterons.

2.2 Acceleration and Transport

The negatively-charged deuterium ions are accelerated by means of an **FN tandem Van de Graaff** accelerator. The negative ions are attracted to the positively charged terminal located at the center of the accelerator tank. A thin (~10μg) ^{12}C foil strips the two electrons from the negative ions at the terminal and the now-positive ions are accelerated back to ground potential at the high-energy end of the tank.

The accelerator is followed by two high-resolution 90° bending magnets. Their fields are set by means of a calibrated NMR probe in the first 90° magnet such that particles of the correct charge-to-mass ratio pass through a pair of control slits located between the magnets. Beam-energy stabilization of the Tandem accelerator is achieved by means of an optically-coupled, fast-feedback circuit which applies a voltage, derived from the slit-current difference, to the accelerator terminal stripper. Thus the calibrated magnet is used to control and regulate the beam energy.

The beam is transported to target by means of several sets of electromagnetic steerers, magnetic-quadrupole focusing devices, and a switching magnet which deflects the beam into the desired beam-line. After passing through the target, the beam is collected in a Faraday cup. The total charge is read by a beam-current integrator, digitized, and counted by a scaler whose output is stored in the computer.

2.3 NaI Spectrometers

Capture γ rays were detected in two anticoincidence-shielded 25.4 cm x 25.4 cm NaI(Tl) spectrometers [Wel81]. Each spectrometer was surrounded by 10 cm of Pb shielding as well as 20 cm of lithium-carbonated paraffin to moderate neutrons. Cadmium or boron sheets in front of the spectrometers also absorbed thermal neutrons. A tapered collimator in the front Pb shield defined a solid angle which completely illuminated the back face of the spectrometer.

The NaI crystals, which were manufactured by the Bicron Corporation, are viewed from the rear by six RCA 8575 photomultiplier tubes. The tubes have been gain matched for increased resolution and the output signals have been passively added. LED pulsers in the crystals provide light pulses for gain stabilization. All but the back face of the NaI crystals are surrounded by five inches of NE 110 plastic scintillator. This plastic shield is viewed by 8 XP 1031 photomultiplier tubes, 2 of which are mounted on the side to view the front volume of the shield. The remaining six tubes are equally spaced on a circle in the rear of the shield to view the remaining volume.

A coincidence condition between the shield and the NaI spectrometer rejects signals which occur within 60 ns of each other. This allows the rejection of ~99% of the cosmic ray events in the NaI crystal. As well as rejecting cosmic ray event, the shield rejects events in which some radiation has leaked out of the crystal. An example of this (although relatively unimportant at the energies of this experiment) would be a γ ray which enters the crystal and is Compton scattered into the shield. The shield gain was run in high-rejection mode which also rejects the 511 keV and 1022 keV escape peaks, due to escaping radiation from e^+-e^- annihilation in the NaI crystal. This decreases the efficiency of the detector system but increases its resolution to a total of ~3% of the γ-ray energy for 15-25 MeV γ rays.

There is a finite probability that a good γ-ray event will be rejected due to an accidental coincidence with a shield event. The probability of this occurring depends on the rate of signals from the shield, and the maximum length of time between shield and NaI signals which is considered coincident. The accidental rate can be measured approximately by setting up a second coincidence circuit where the NaI signals are now delayed by about 300 ns. Most coincidences occuring in this circuit are from uncorrelated events, giving an estimate of the number of accidental coincidences in the undelayed coincidence circuit.

At 8.85 MeV, the beam was pulsed at 5 MHz. A Time to Amplitude Converter (TAC) with the NaI signal as the start and the signal from a pickoff capacitor (located upstream from the target) as the stop, was used to create a time profile of the events in the NaI crystals. Good separation between γ-ray events and neutron events allowed rejection of the neutron events from the energy spectra. Occasionally, a stop signal will not be generated and a crystal event with the proper timing will be rejected. By storing the number of pickoff capacitor signals in a scaler counter and knowing the frequency of the beam bursts, the spectra can be corrected for this effect. Fig. 3.4 shows a typical γ-ray TAC spectrum. The experiments in the fusion resonance region used an unpulsed beam and therefore no time profile of events could be generated.

2.4 Solid-State Detectors

Solid state detectors have been used for three different purposes during this experiment. In the 8.6 MeV configuration, a solid state detector was used to detect elastically scattered deuterons in order to monitor the stability of the beam and target thickness. In the fusion-resonance experiments, a calibrated solid-state detector was used to set the beam energy and gas pressure needed, again by detecting elastically scattered deuterons. Two transmission-mount solid-state detectors are also installed in the

polarimeter in order to detect α particles which are needed to measure the beam polarization out of the ABPIS.

Despite the different purposes of these detectors they have the same electronics configuration. The detector is connected to a preamplifier which has inputs for the voltage bias and pulser test signal and outputs for an energy signal and a fast-timing signal. The energy signal is fed into the control room and the signal is amplified by a Spectroscopy Amplifier. The unipolar output of the Spec. Amp. is used as the linear input of a Linear Gated Stretcher operating in the gated, coincidence mode. The bipolar output of the Spec. Amp. is fed into a Single Channel Analyzer (SCA), which creates the gate for the Linear Gated Stretcher. In this way, the SCA can be used to set energy thresholds.

2.5 Target Configurations

Two distinctly different target geometries were used for the two energy regions studied in this experiment. Fig. 2.1 shows the target geometry for the experiment at E_d = 8.6 MeV. The gaseous ^{3}He target (Research Grade 99.95% pure) was operated at a pressure of 69.0 kPa with a 1.27 μm Nickel beam-entrance foil and a 2.54 μm Havar beam-exit foil. To create the 8.6 MeV beam at the center of the target, an 8.85 MeV beam from the accelerator was used. According to an energy-loss calculation, this beam lost 60 keV in the Ni entrance foil and 150 keV in the four inches of gas between the Ni entrance foil and the center of the target. Another 150 keV was lost in the remaining ^{3}He gas, and 115 keV was lost in the Havar foil. Lead and tungsten shadow bars were used to prevent the NaI spectrometers from viewing these foils and allowed the spectrometers to see a region of gas which was 3.58 cm long when the spectrometer was at 90°, corresponding to a target thickness of 0.301 mg/cm^2 and a solid angle of 23 msr. As an additional monitor of the experiment, an Ortec transmission mount, 500 μm thick, solid-state detector was mounted inside the target chamber at 30° and was doubly collimated to view

the center of the target. A spectrum with no gas in the target was taken in this configuration to determine the γ-ray background from the foils. No background in the energy range of interest was detected. Fig. 2.2 shows a typical d+^{3}He γ-ray spectrum. Fig. 2.3 shows the corresponding solid-state detector spectrum.

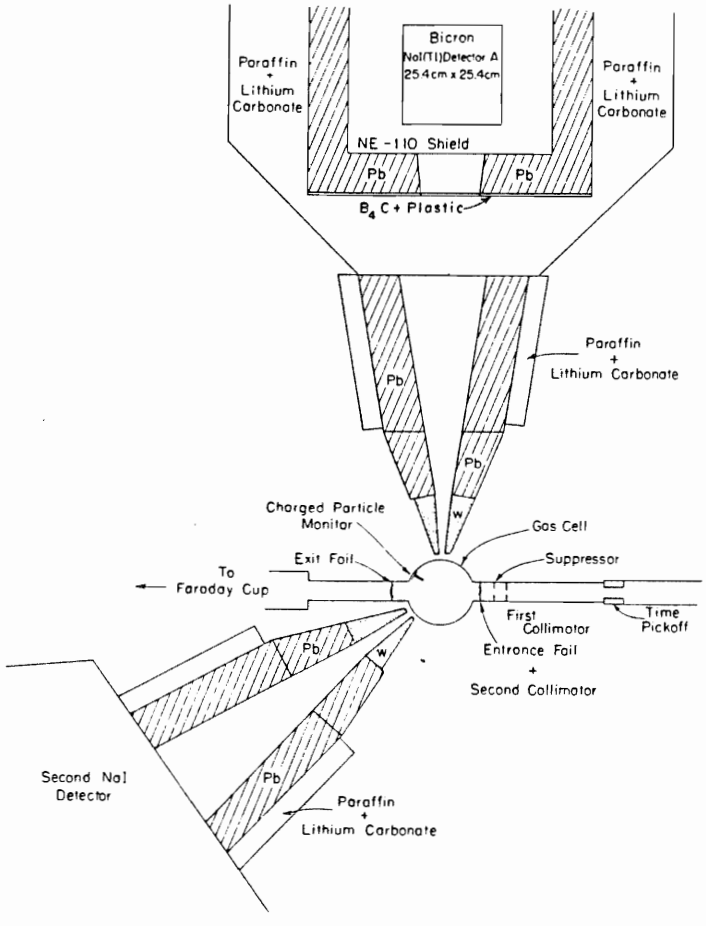

Fig. 2.1 The target geometry for the experiment at $E_d = 8.6$ MeV.

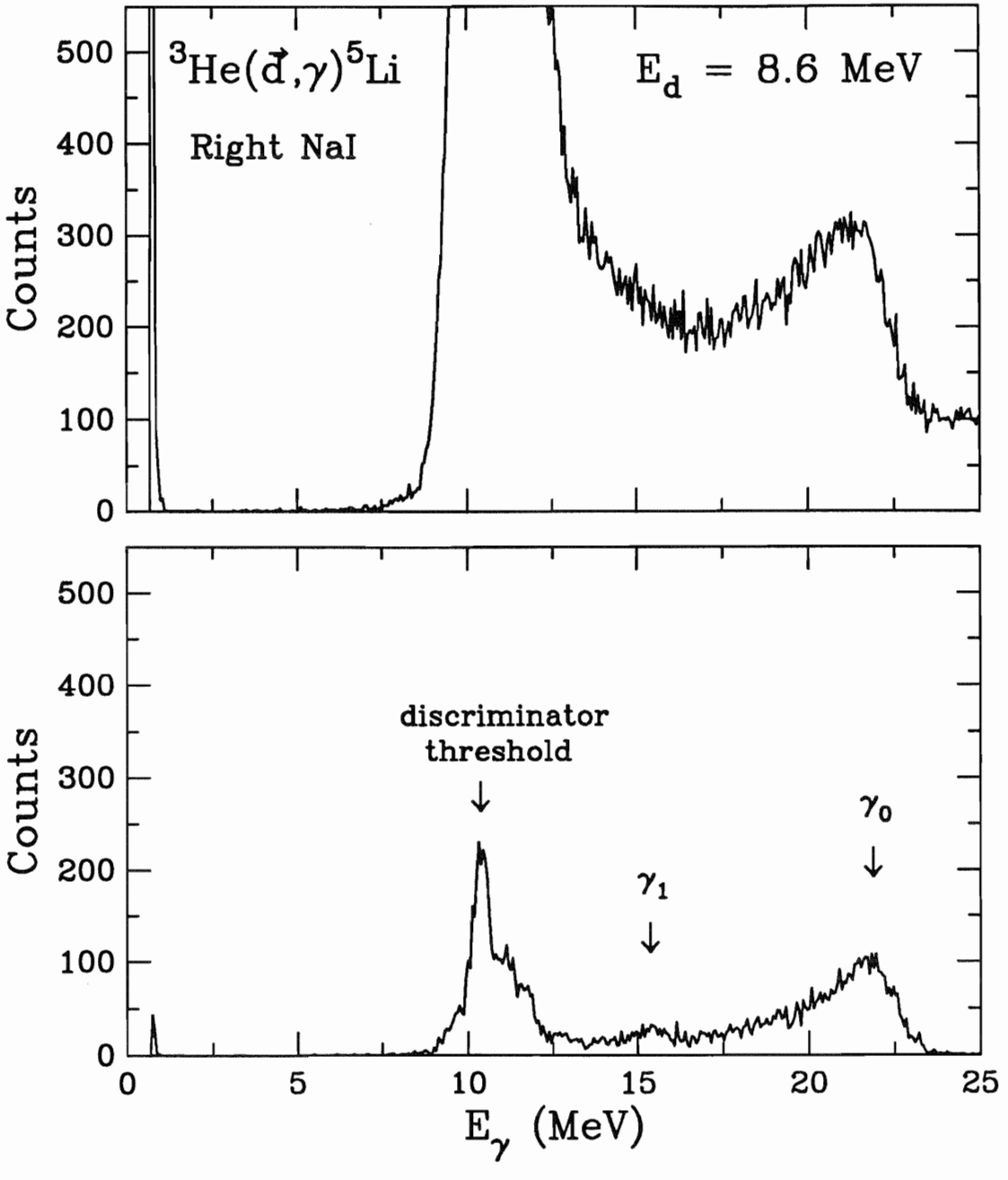

Fig. 2.2 A typical γ-ray energy spectrum from the ^{3}He(d,γ)^{5}Li reaction at E_d=8.6 MeV. Top Panel: The spectrum of all events in the NaI crystal. Bottom Panel: The same spectrum after the shield anticoincidence condition and TAC condition have been applied. The small peak marked γ_1 may be due to capture to the first excited state of ^{5}Li

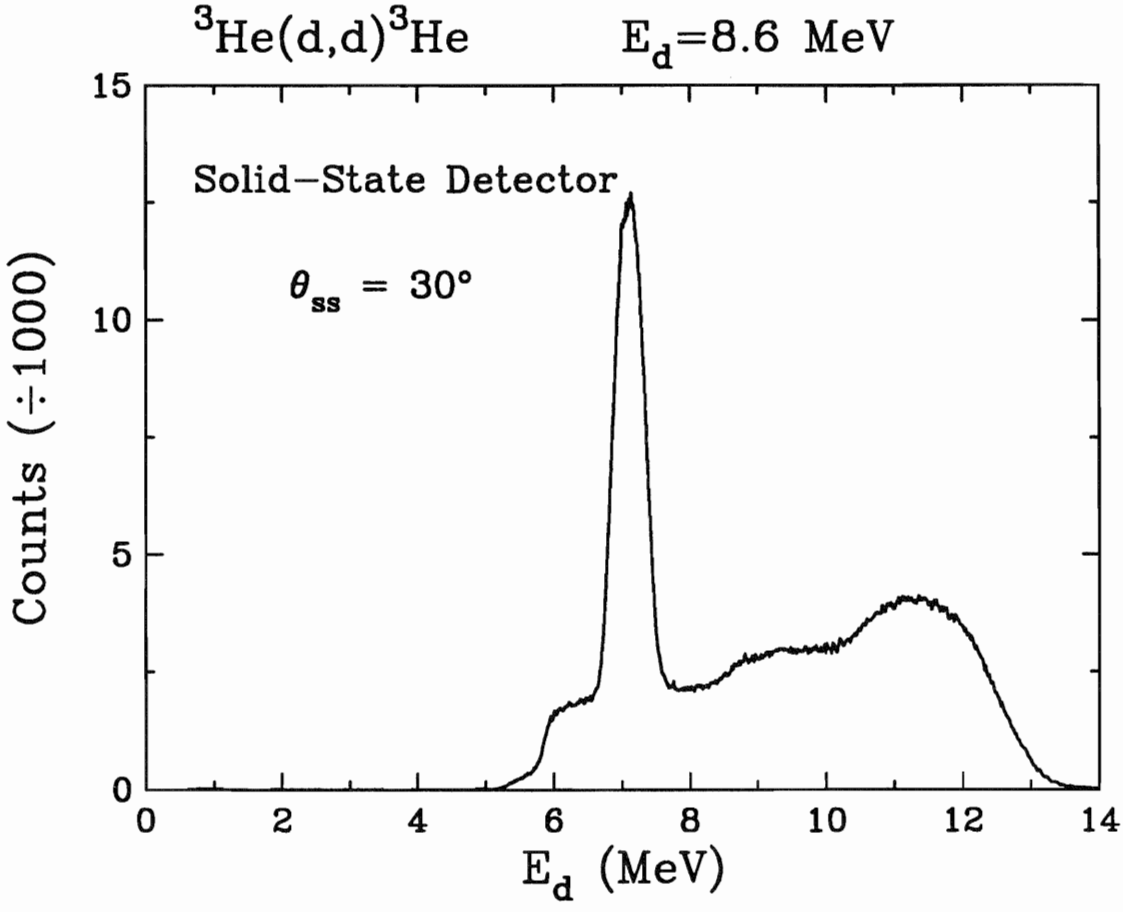

Fig. 2.3 A solid-state detector spectrum from the ^{3}He(d,d)^{3}He reaction at E_d=8.6 MeV. The high peak is from the elastically scattered deuterons. The background is due to high-energy protons from the ^{3}He(d,p)^{4}He reaction which are not stopped in the detector.

In the fusion resonance energy region, deuteron beams of several different energies were passed through 6.35 μm Havar foils which degraded the beam energy to the desired value. A 2.54 cm long cylindrical gas cell (see Fig. 2.4) was filled with ^{3}He gas (Research Grade 99.95% pure). Table 2.1 lists the conditions for each experiment. Accurate beam-current integration was achieved by electrically isolating the gas cell and applying a suppression voltage to prevent the escape of low energy electrons. (The gas cell could not be used for the 8.6 MeV experiment due to the high-energy background in the γ-ray spectra which was generated due to the NaI detectors viewing the beam stop.) The back faces of the NaI spectrometers were placed 106 cm from the target center, defining a solid angle of 45 msr. Spectra from a ^{3}He target and a ^{4}He background target along with the resultant background-subtracted spectrum are shown in Fig. 2.5.

Table 2.1 Target conditions for measurements made in the fusion-resonance region. E_{beam} is the beam energy before entering the Havar degrading foils, E_i is the energy immediately after the foils, and E_f is the beam energy when exiting the target. The uncertainties $\Delta E = \frac{1}{2}\Gamma$, where Γ is the full width at half maximum (FWHM) of the deuteron peaks as seen in the solid-state detector spectrum.

E_{beam} (MeV)	# of Ha foils (6.35 μm)	^{3}He Pressure (kPa)	$E_i \pm \Delta E_i$ (MeV)	$E_f \pm \Delta E_f$ (MeV)	Observables
3.43	4	414	0.80±0.09	0.0	σ, A_y, A_{yy}, T_{20}
3.43	4	124	0.80 ±0.09	0.41±0.12	σ
3.33	4	93.8	0.60±0.08	0.30±0.14	σ, A_y, A_{yy}
3.28	4	89.7	0.4 ± 0.12	0.0	σ

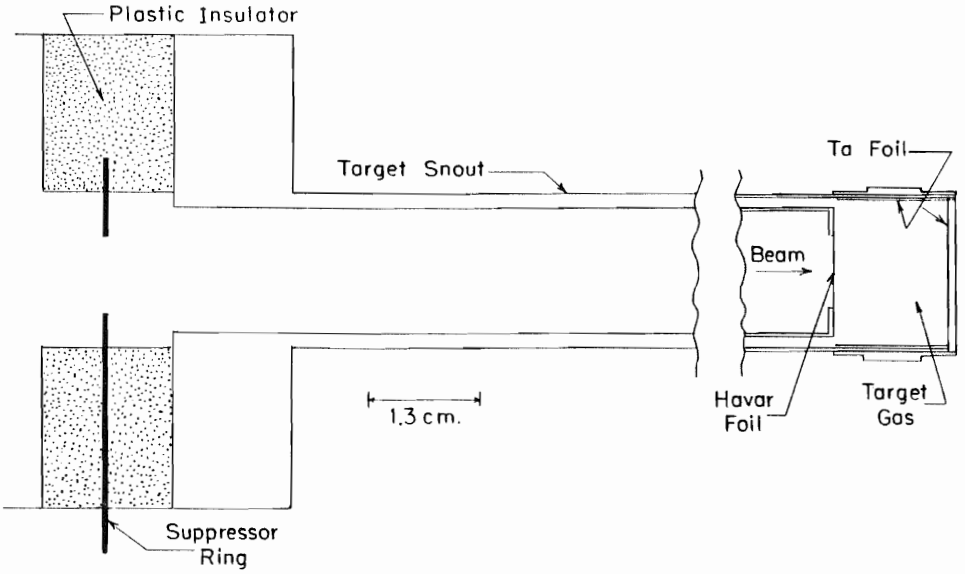

Fig. 2.4 The 2.54 cm long cylindrical gas cell used in the $^{3}He(\vec{d},\gamma)^{5}Li$ reaction experiments in the fusion-resonance energy region.

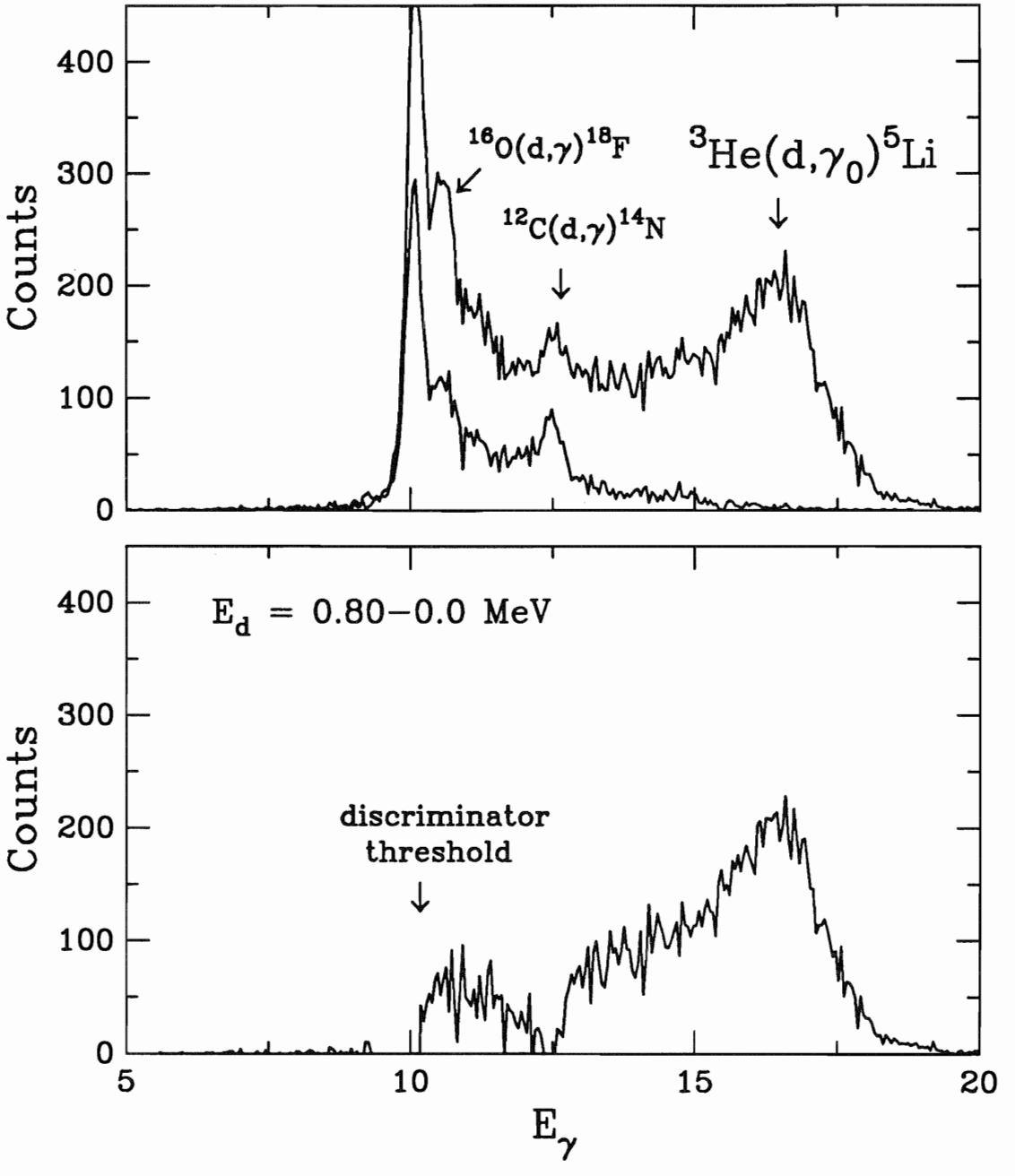

Fig. 2.5 Top Panel: The upper energy spectrum is from the $^{3}He(d,\gamma)^{5}Li$ reaction at E_d=0.8 MeV where the beam is stopped in the target. The lower energy spectrum is from the same target configuration with the ^{3}He replaced by ^{4}He. Contaminant peaks from 3.43 MeV deuteron capture by ^{12}C and ^{16}O are also visible. Bottom Panel: The resultant background-subtracted spectrum.

2.6 Beam-energy calibration

For the experiment at E_d = 8.6 MeV, the beam energy was set using the calibration for the 90°-90° high-resolution magnet system in the high-transmission mode. From experience, it has been found that the beam has less than a 50 keV uncertainty and less than an 8 keV dispersion [Wes84].

In order to set the beam energy and gas pressure for the fusion-resonance experiments, the deuteron beam was tuned into the 60° beam-leg scattering chamber and scattered from a thin (~10 μg) ^{12}C foil into a calibrated solid-state detector located at θ_{ss}=30°. The procedure for creating an 0.8 MeV beam began by rotating four Havar degrading foils into position between the target and the detector. The accelerator voltage was then adjusted to give an 0.8 MeV deuteron peak in the solid-state detector spectrum. The foils were rotated out of position, giving an undegraded scattered-deuteron peak with an energy of 3.43 MeV. Therefore the beam energy before scattering needs to be set to 3.43 MeV since no scattering takes place in the capture experiments. The beam energy was adjusted such that a 3.275 MeV scattered-deuteron peak was seen in the solid-state detector spectrum, corresponding to a 3.43 MeV deuteron beam. Having accounted for the kinematic shift due to the scattering, these same Havar degrading foils were transferred back to the capture set-up to ensure uniformity in foil thickness. The above procedure was also used to produce 0.6 MeV and 0.4 MeV deuteron beams.

In order to determine the gas pressure needed, the solid-state detector was placed inside a small air-tight chamber with a Havar entrance foil and the whole assembly was placed inside the scattering chamber. The scattered-deuteron energy was set by evacuating the chamber and measuring the energy deposited in the calibrated solid-state detector. The chamber was then pressurized with ^3He until the deuterons reaching the detector had the desired energy. (See Table 2.2) As their energy loss became greater, the deuterons had more energy spreading. Therefore, the gas pressure was increased in small

increments in order to determine the peak energy in the spectrum more accurately. The distance from the foils to the detector is 3.81 cm. The pressure used in the 2.54 cm long gas cell was one and a half times the pressure in the solid state detector chamber so that the ^{3}He target thicknesses measured in atoms/cm^2 were equal. Figs. 2.6 and 2.7 show four solid-state detector spectra corresponding to scattered deuterons with no degrading foil, scattered deuterons whose energy has been degraded from E_d=3.43 MeV to 0.80 MeV, scattered and degraded deuterons after losing 0.40 MeV through the ^{3}He gas, and scattered and degraded deuterons after losing all of their energy through the ^{3}He gas.

Table 2.2 Energy loss of deuterons in ^{3}He gas. $E_{initial}$ is the energy of the deuterons entering the gas. E_{final} is the energy of the deuterons after passing through 3.81 cm of gas. Also listed is the gas pressure and the FWHM of the deuterons (as measured in the solid-state detector) after passing through the gas.

$E_{initial}$ (keV)	Pressure (kPa)	E_{final} (keV)	FWHM (keV)
798	0.0	804	174
798	55.2	570	225
798	82.7	414	237
798	110.3	235	350
798	172.4	Almost all particles are stopped.	
798	241.3	All particles are stopped.	
595	0.0	595	155
595	34.5	455	211
595	48.3	380	223
595	57.9	324	265
595	62.1	295	281

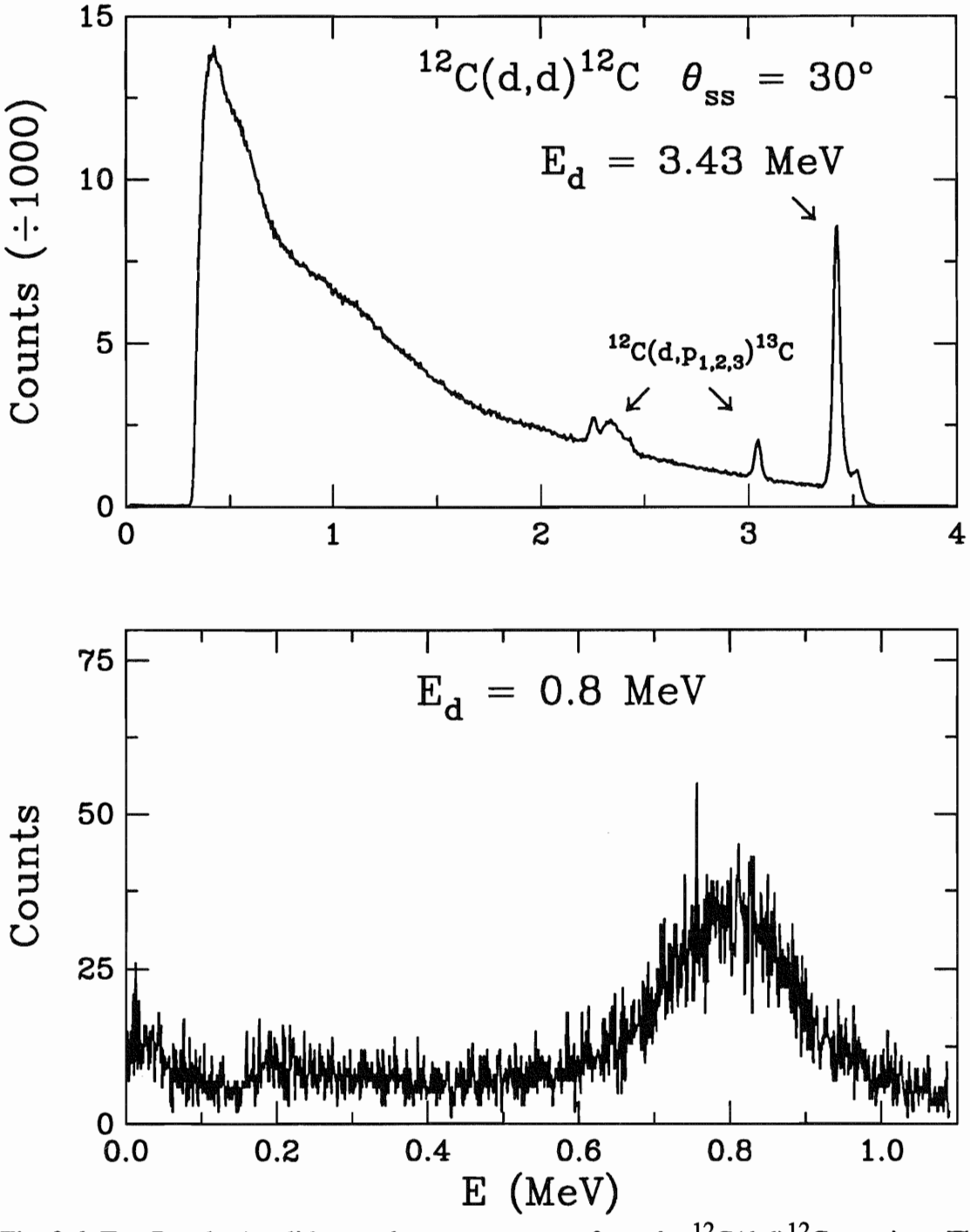

Fig. 2.6 Top Panel: A solid-state detector spectrum from the $^{12}C(d,d)^{12}C$ reaction. The scattered-deuteron peak is at 3.43 MeV. Three peaks from the $^{12}C(d,p_{1,2,3})^{13}C$ reaction are also visible. Bottom Panel: Spectrum after the deuterons have been degraded by 4 Havar foils (placed between the ^{12}C target and the solid-state detector) to 0.8 MeV.

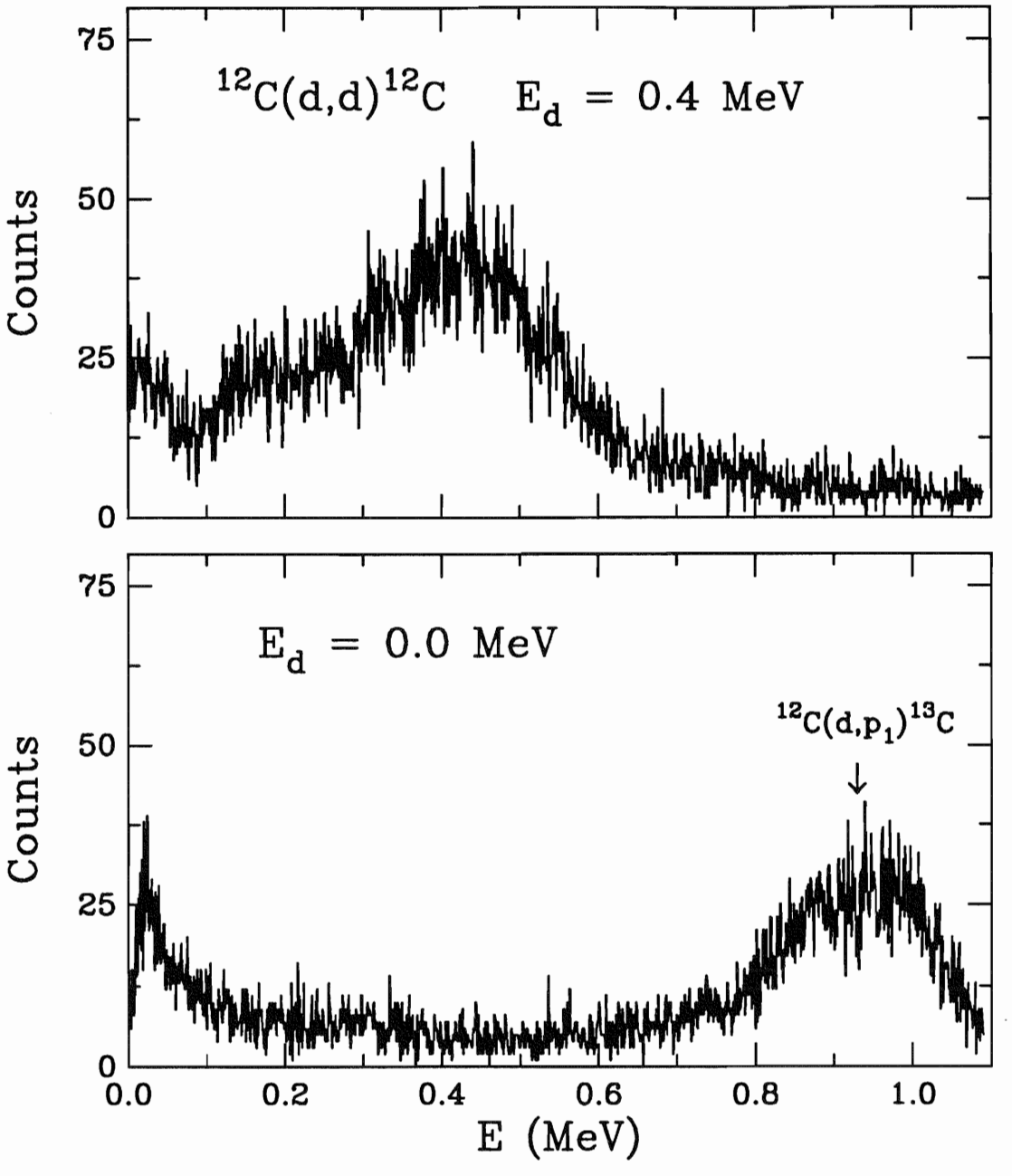

Fig. 2.7 Top Panel: Spectrum from the $^{12}C(d,d)^{12}C$ reaction after the deuterons have been degraded by 4 Havar foils to 0.8 MeV and lost an additional 0.4 MeV in ^{3}He gas. Bottom Panel: Spectrum from the same reaction after the deuterons have been degraded by 4 Havar foils to 0.8 MeV and stopped in the ^{3}He gas. The peak in the spectrum at 0.9 MeV is caused by protons from the $^{12}C(d,p_1)^{13}C$ reaction.

2.7 Polarimetry

The polarization of the beam from the LSPIS was measured inside the source itself using the quench ratio method [Ohl71]. By quenching out the polarized particles, the beam which remained was completely unpolarized. The ratio of beam current from the quenched and unquenched beams gave a direct measure of the unpolarized background. The major disadvantage to this method is that, although the fraction of the beam which is polarized is determined, the specific state of the polarization at the target is unknown.

In order to allow greater knowledge of the beam polarization, a polarimeter was constructed which measures vector and tensor polarized deuterons from E_d = 5-12 MeV using the ^{3}He(d,p)^{4}He and ^{3}He(d,α)^{1}H reactions. Based on the Stephenson polarimeter at Wisconsin, the polarimeter consists of a ^{3}He gas-target cell, two CsI detectors at 27.5° and one CsI detector at 0°, all for proton detection, and two transmission-mount solid-state detectors in front of the 27.5° CsI's for detecting recoil α particles. For an extensive discussion of the polarimeter see [Ste80].

For the detectors on the left side of the polarimeter, the yield in each detector, $N_L(\theta)$, can be expressed as:

$$N_L(\theta) = K_L\sigma_0(\theta)[1+2iT_{11}(\theta)\mathrm{Re}(it_{11}) + T_{20}(\theta)t_{20} + 2T_{21}(\theta)\mathrm{Re}(t_{21}) + 2T_{22}(\theta)\mathrm{Re}(t_{22})], \quad [2.1]$$

where K_L contains the target thickness and detector efficiency, the T_{ij}'s are the reaction's tensor observables, and the t_{ij}'s are the tensor moments of the beam. Similarly, for a detector on the right side:

$$N_R(\theta) = K_R\sigma_0(\theta)[1-2iT_{11}(\theta)\mathrm{Re}(it_{11}) + T_{20}(\theta)t_{20} - 2T_{21}(\theta)\mathrm{Re}(t_{21}) + 2T_{22}(\theta)\mathrm{Re}(t_{22})]. \quad [2.2]$$

The analyzing powers for the ^{3}He(d,p)^{4}He and ^{3}He(d,α)^{1}H reactions have been measured in [Ste80]. Therefore, it is only necessary to solve five equations, one for each detector, for four unknowns to get the beam polarization. Using all five detectors gives a

redundancy check on the accuracy of the measurement. A Fortran code (see Appendix B) reads the yields in each detector directly from gates set in the spectra on the computer. It then performs the MINUIT χ^2 minimization procedure to determine the polarization moments of the beam and their associated errors. The accuracy of the analyzing-power measurements used to compute the beam polarization limits the polarimeter to no better than 2% accuracy.

Chapter 3: Absolute Cross Sections

3.1 Introduction

An angular distribution measurement of a differential cross section is conceptually simple to perform. For a given number of particles passing through a target of known thickness, the events in a detector with a known efficiency and set at a given angle are counted. More specifically, the differential cross section is:

$$\frac{d\sigma(\theta)}{d\Omega} = \frac{Y(\theta)}{N t \varepsilon d\Omega} \qquad [3.1]$$

where

$Y(\theta)$ = the number of events coming from the reaction of interest in the detector at the angle θ.

θ = the angle between the beam-momentum vector and the vector pointing from the target to the detector .

N = the total number of particles which passed through the target .

t = the target thickness in units of particles/ cm^2.

ε = the efficiency of the detector.

$d\Omega$ = the solid angle subtended by the detector.

In practice, this becomes a very difficult measurement because complete knowledge of the beam, target, and detector geometry is needed. In addition, estimates must be made of how many counts were lost due to instrumental and/or computer effects.

In a perfect spectrum containing only one peak which comes from the reaction of interest, it would be a straightforward procedure to sum the total number of counts in the spectrum to get $Y(\theta)$. However, background radiation from beam-induced reactions and natural radiation from the Earth complicate matters by obscuring the low-energy portion of the γ-ray peak. It is therefore only possible to sum a portion of the γ-ray peak and estimate the fraction of the total counts which were summed. To do this, the peak of

interest must be fitted with a physically reasonable response function which extends to zero energy. The area of the entire response function is then compared to the area of the region which was summed. For a monoenergetic γ ray this functional form is simply the line-shape response of the NaI detector system. For a transition to an unbound state such as the ground state of ^{5}Li, however, the functional form must be a convolution of the NaI line-shape with the energy distribution of γ-rays coming from the reaction.

The measurements of all the various contributions needed for a determination of the absolute cross section are discussed below. Errors for each contribution are estimated and then tabulated in Table 3.3.

3.2 Beam Current Integration

Deuteron beam currents on target ranged from 50 to 250 nA. For the experiment at $E_d = 8.6$ MeV, the beam was deposited in a tantalum-lined Faraday cup located about $4\frac{3}{4}$ meters beyond the target. For the fusion resonance experiments, the beam was stopped either in the target or at the back end of the gas cell. The cell was electrically isolated from the beam-line and a suppressor ring biased to -300 Volts prevented recoiling electrons from escaping the gas cell. The total charge was integrated by a Model 1000 Brookhaven Instruments Corporation Current Integrator (BCI). The procedure to manually zero the current scale and input balance introduces less than a 1% uncertainty in the total charge accumulated.

3.3 Target Thickness

The target geometries used in the experiments are described in **Experimental Techniques**. The density of ^{3}He gas at 310.93 K is given in [Mat80] as 25,537.6 cm^3/mole. By applying the Ideal Gas Laws to correct for room temperature and pressure conditions and by multiplying by the length of gas viewed by the detectors, the target thickness in atoms/cm^2 can be calculated. The gas pressure of the target was measured by a Penwalt gauge which could be read to better than 0.2 PSIA. The pressure tended to

increase over time by 0.2 to 0.4 PSIA over the original fill pressure due to heating of the gas by the beam. For consistency, and since there was no evidence of a gas leak, the original fill pressure was used for the absolute cross section calculations. The absolute temperature of the ^{3}He gas is not known just after filling the chamber since the rapid expansion of the gas may tend to cool it. However, even temperature variations of 5° C introduce less than 2% uncertainty in the target density.

For the 8.6 MeV geometry, the target thickness was 6.03×10^{19} atoms/cm^2 at θ_{lab}=90°. A Monte Carlo calculation was performed by S. E. King [Kin83] to find the variation in target thickness as a function of detector angle. The correction factor was within 2% of the first-order correction of $\frac{1}{\sin(\theta)}$. Therefore, only the first-order correction has been used for this data.

For the cross section measurements in the fusion-resonance region, the target thickness remained constant with angle since the entire 2.54 cm long gas cell was viewed by the NaI spectrometers. However, for the two cross section measurements where the beam was stopped in the target (E_d=0.8 MeV and E_d=0.4 MeV), the actual target length is known only to about 5%. This comes about due to the discrepancy in the range calculation for deuterons traversing ^{3}He as computed by the energy-loss code BABEL and the extrapolated target thickness from the measured energy losses of Table 2.2. In all fusion-resonance measurements, the ^{3}He was replaced by an equal pressure of ^{4}He in order to obtain a background spectrum while maintaining the energy loss of the deuterons through the target. Table 3.1 lists the target thicknesses used.

Table 3.1 Target thickness for measurements made in the fusion resonance energy region. E_i is the beam energy entering the target and E_f is the beam energy exiting the target. The uncertainties are given by $\Delta E = \frac{1}{2}\Gamma$, where Γ is the full width at half maximum (FWHM) of the deuteron peaks as seen in the solid-state detector spectrum. The errors for the target thickness are computed from the uncertainties in target length, ^{3}He temperature, and ^{3}He pressure

$E_i \pm \Delta E_i$ (MeV)	$E_f \pm \Delta E_f$ (MeV)	target thickness (atoms/cm^2)
0.80±0.09	0.0	$(1.54\pm0.14)\times10^{20}$
0.80±0.09	0.41±0.12	$(7.69\pm0.18)\times10^{19}$
0.43±0.22	0.0	$(5.56\pm0.31)\times10^{19}$
0.60±0.08	0.30±0.14	$(5.82\pm0.15)\times10^{19}$

3.4 Efficiency

The measurement of the two NaI-spectrometer efficiencies is crucial for the calculation of the absolute cross section. The absolute γ-ray efficiency was measured at $E_\gamma = 15.1$ MeV and $\theta_\gamma = 125^\circ$ by populating a resonance in ^{13}N via the ^{12}C $(p,\gamma)^{13}$N reaction using the thick-target technique of [Mar77]. The product of the detector efficiency (ε) and solid angle (dΩ) is extracted by comparing to the absolute yield given by [Mar77]. For a typical region of the spectrum which was summed, $\varepsilon d\Omega = 6.6$ msr and 5.7 msr for the left and right NaI spectrometers, respectively.

The efficiencies of the NaI spectrometers were confirmed by a second, independent method which utilized the ^{3}H$(p,\gamma)^4$He reaction at $E_\gamma = 26$ MeV. A spectrum was measured with no paraffin in front of the NaI. The full line-shape was summed and corrected for lost counts due to the attenuation through the plastic shield [HayPri]. A

spectrum was then measured and summed for a fully shielded detector. The ratio of the shielded to unshielded yields is the detector efficiency at 26 MeV, assuming that the efficiency of the unshielded detector is nearly 100% for the full response function [Pau74]. Using the known energy dependence [McB82 and Wel81], the efficiency was calculated for 15.1 MeV γ-rays and found to agree with the first measurement to within 5% of the value.

3.5 Line-shape measurement

The NaI detector line-shape response function was measured using the $^3H(p,\gamma)^4He$ reaction at $E_p = 2.5$ MeV, yielding γ rays with $E_\gamma = 21.6$ MeV. The response of the detector to these incident γ rays yields a spectrum with finite resolution (~3%) and a long low-energy tail (see Fig. 3.1). In order to use the line-shape to fit other NaI γ-ray peaks, it must be parameterized in a convenient functional form. It has been found that a composite function of two exponentials with quartic arguments can describe the line-shape quite well. In fact, until the recent addition of a new NaI with improved resolution, only cubic arguments had been needed. The functional form for the line-shape parameterization is:

$$F(E) = \begin{cases} 0 & E \geq E_{high} \\ e^{C_5 + C_6E + C_7E^2 + C_8E^3 + C_9E^4} & E_J \leq E < E_{high} \\ e^{C_0 + C_1E + C_2E^2 + C_3E^3 + C_4E^4} & E_{low} \leq E \leq E_J \\ \frac{F(E_{low})}{E_{low}} E & E < E_{low} \end{cases} \qquad [3.2]$$

where the two exponentials are required to match smoothly at the joint E_J, which usually is positioned high on the low-energy side of the peak (see Fig. 3.1). E_{low} is the low-energy cut-off point below which the line-shape is extrapolated linearly to zero energy.

E_{high} is the high-energy cut-off point above which the line-shape is zero. A χ^2 minimization code (see Appendix C) using the routine MINUIT has been written in order to fit F(E) to ^{3}H+p γ-ray spectra accumulated with the left and right NaI spectrometers. The results of these fits are listed in Table 3.2. Fig. 3.1 shows a typical fit to the γ-ray spectrum.

Table 3.2 The results from a search of χ^2 space for solutions of Eqn. 3.2 for the left and right NaI spectrometers. Parameters are given to extreme precision due to the large cancellation effects in F(E).

	Left NaI	Right NaI
C_0	505.941760	1446.01464
C_1	-120.991939	-325.455574
C_2	10.8054336	27.4027008
C_3	-0.426110365	-1.02228202
C_4	0.00627399981	0.0142771522
C_5	177032.628	438922.787
C_6	29665.4010	-80895.7846
C_7	-1856.87722	5586.461089
C_8	51.4420715	-171.313332
C_9	-0.532014012	1.96830020
E_J	21.701	21.060
E_{low}	14.000	15.000
E_{high}	23.500	23.000
Centroid	21.820	21.512

The energy of the γ ray entering the crystal in a given experiment is not always the same as a γ-ray energy for which a line-shape has been measured. It has been assumed in the present experiments that the percent resolution, $\Delta E/E_\gamma$, is constant in the region of interest for the current experiment [Wel81]. It is then a simple procedure to transform the line-shape response function at 21.6 MeV into a response function for any γ-ray energy. This is accomplished by linearly transforming the line-shape energy such that the centroid corresponds to the desired γ-ray energy. For example, to create a line-shape response function at E_γ=10.8 MeV, F(E) is mapped to E/2, which maps the centroid at F(E=21.6 MeV) to E=10.8 MeV. It is therefore necessary to specify the γ-ray energy E_γ when discussing the the response function, which from now on shall be denoted as $F(E,E_\gamma)$.

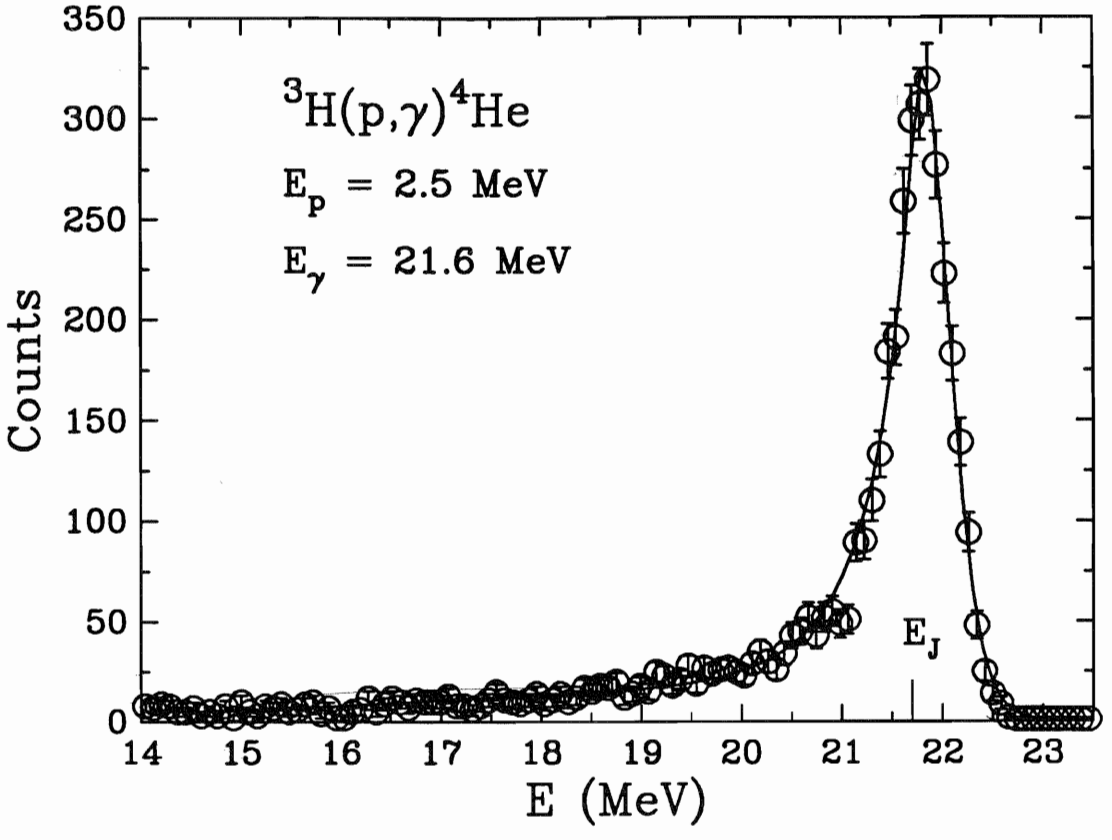

Fig. 3.1 Spectrum of the NaI detector response function as measured in the ^{3}He(p,γ)^{4}He reaction at E_p = 2.5 MeV. The error bars represent the statistical uncertainties in the measurement. The solid curve represents the best fit to the data. E_J (see Eqn. 3.2) is the energy at which the composite function F(E) is joined.

3.6 NaI Spectrum fitting with a convolution function

In order to get consistent summing regions with different spectra, it is necessary to fit the spectra with a physically reasonable functional form. For γ-ray spectra coming from reactions with transitions to bound states, this form is simply the line-shape response of the NaI crystal as described in Section 3.5. Complications arise when the final state is unbound as in the case of ^{5}Li.

According to the theory of resonance reactions [Lan58], the energy distribution of γ rays which are produced in an electric-dipole transition to an isolated resonance with a p+α breakup channel can be described in terms of a Breit-Wigner form:

$$BW(E_\gamma) \propto \frac{1}{k^2} \frac{E_\gamma^3 \Gamma_p(E_p)}{\left[\left(E_\gamma - E_{res} + \Delta(E_p)\right)^2 + \left(\frac{\Gamma_p}{2}\right)^2\right]} \qquad [3.3]$$

where Γ_p is the width of the p+α channel, E_p is the nucleon emission energy, and E_γ^3 is the energy-dependent term of the γ-ray width Γ_γ. It is assumed that Γ_γ is much less than Γ_p so that the total width $\Gamma = \Gamma_p + \Gamma_\gamma \approx \Gamma_p$. This formalism is discussed further in Appendix A.1.

In the E_d= 8.6 MeV experiment, the γ-ray spectra from the NaI spectrometers were fit using the minimization code MINUIT with a convolution of the measured energy-dependent response function of the NaI spectrometer and the Breit-Wigner resonance shape described above. The functional form used is

$$F'(E) \propto \int F(E,E_\gamma)\, BW(E_\gamma)\, dE_\gamma \qquad [3.4]$$

where the overall height of F'(E) was varied, and the entire convoluted form was shifted up or down in energy to allow for spectrum calibration errors. The value for the width of the ^{5}Li ground state, extracted in a previous study [Bal91], was fixed at

$\Gamma_p(E_{res}) = 2.44$ MeV. Fig. 3.2 shows the best fit to the ^{5}Li spectrum at 8.6 MeV, as well as the NaI response function and the $BW(E_\gamma)$ function used in the convolution.

A further complication arose when fitting the spectra from experiments in the fusion energy region. In these experiments, the energy loss of the beam in the target was comparable to the width of the ground-state resonance. This additional spreading was taken into account by a second convolution with a Gaussian function. Although the Gaussian width was treated as a free parameter, the full width at half maximum was always consistent with the energy loss of the beam in the target. A typical fit is shown in Fig. 3.3. Appendix A.2 contains the Fortran code for the fitting routine.

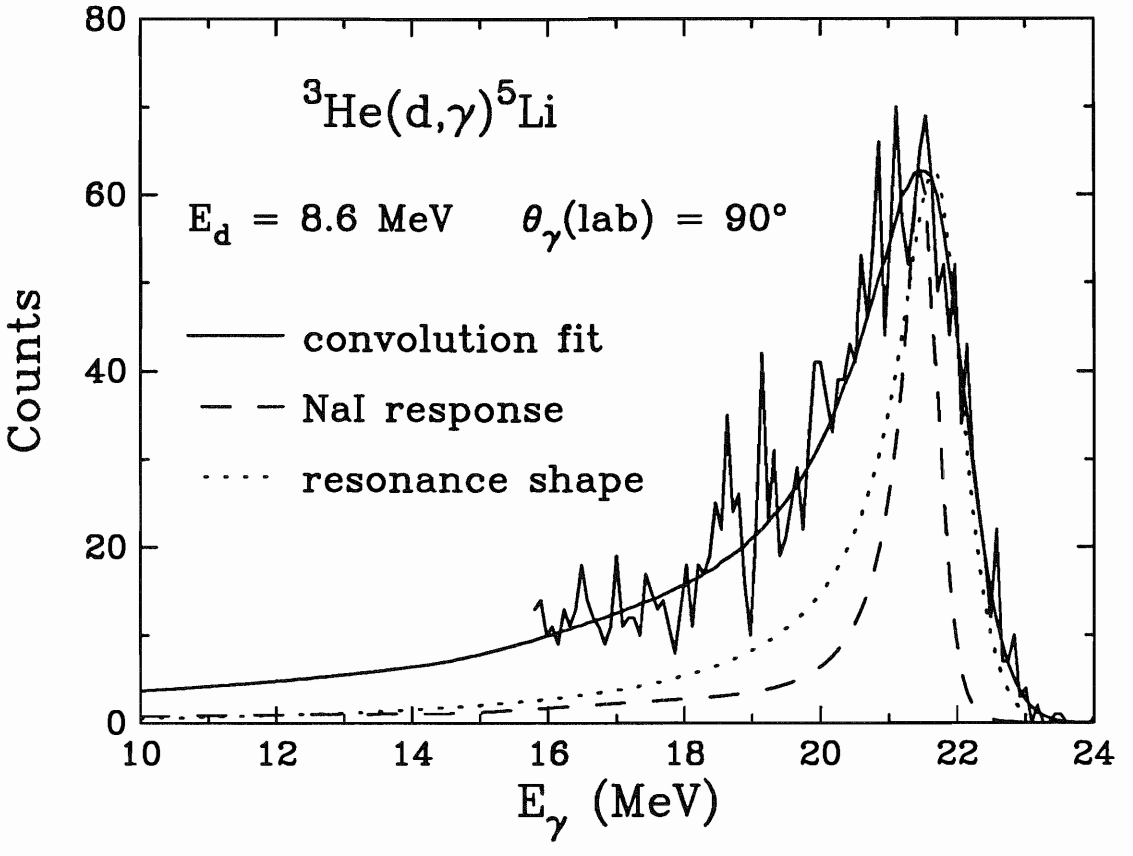

Fig. 3.2 A typical γ-ray spectrum for the ^{3}He(d,γ)^{5}Li reaction at E_d=8.6 MeV and θ_{lab}=90°. The convolution of the NaI response function and the resonance shape was fitted in the range 19.0 MeV ≤ E_γ ≤ 24.0 MeV. The spectrum is not plotted below 16 MeV.

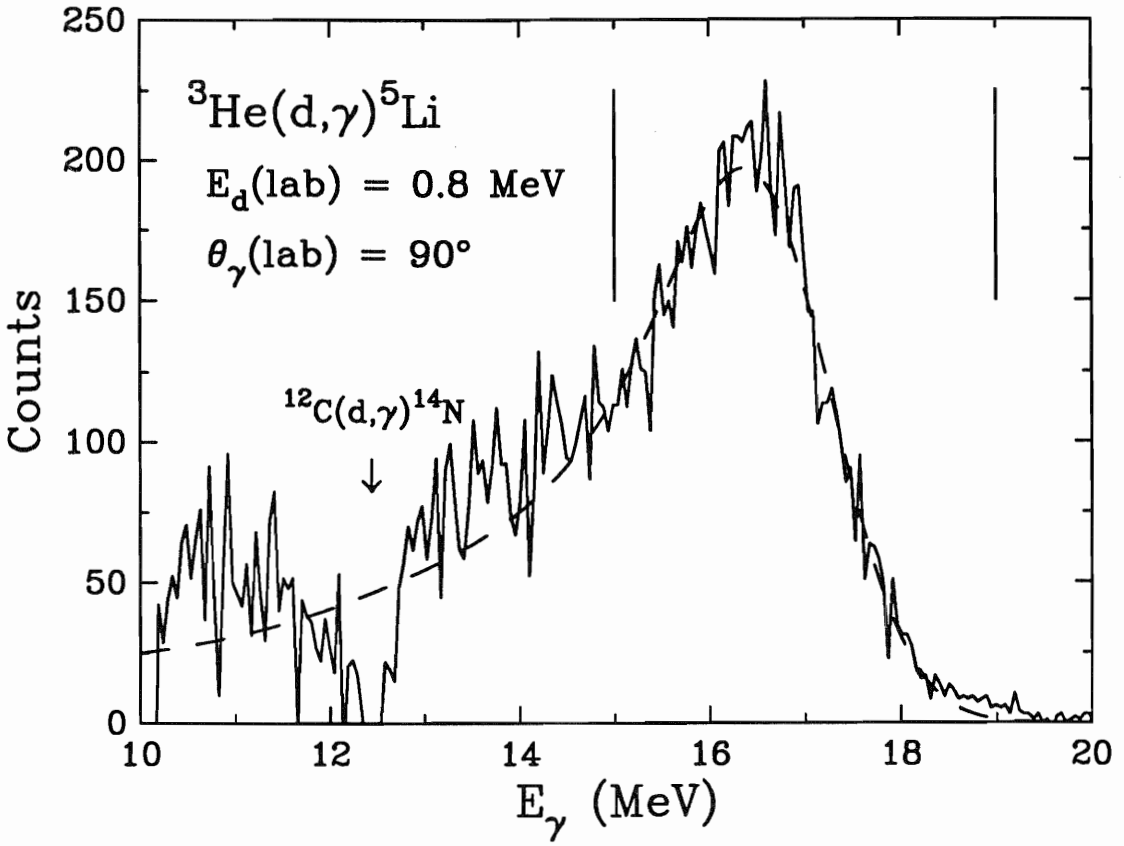

Fig. 3.3 A typical background-subtracted γ-ray spectrum from the ^{3}He(d,γ)^{5}Li reaction for an 0.8 MeV beam which was stopped in the target. The dashed curve represents a convolution fit to the data, where the vertical lines denote the fitted region. This is also the region of the peak that was summed to calculate the observables. The dip in the spectrum at 12.5 MeV is caused by background subtraction of a peak from the ^{12}C(d,γ)^{14}N reaction.

3.7 Dead-Time Correction

Dead time may arise from the fact that the computer cannot process an event because it is still busy processing a previous event or other information. Higher count rates and multiple active processes increase this effect. Fortunately, it is easy to measure this dead time and correct the spectra for the lost counts. A high frequency ("deadtime-less") scaler counter keeps track of the total number of gate signals going into the computer. Each gate corresponds to one event. Summing the full energy spectrum gives the total number of events processed by the computer. To correct for dead time, yields are multiplied by the factor:

$$\text{Dead Time Correction (DTC)} = \frac{\text{\# of gates for energy signals}}{\text{\# of counts in full energy spectrum}} \qquad [3.5]$$

This correction is used for the NaI spectrometers where the complete NaI spectrum is summed before any coincidence or timing conditions are applied. The same method is used to correct for dead time effects in the solid state detector spectra. Typically, dead times are kept below 10% and were usually less than 4% for the current experiments.

Other sources of dead time are the electronic modules used to process the signals before storing them in the computer. However, these effects are negligible compared to the computer dead time. For example, for 10 μs after an event in the NaI crystal no other signals are accepted by the electronics. This is to prevent the pile up of multiple signals. This 10 μs is dead time. A typical run lasts about one hour with less than 100,000 NaI signals reaching the computer. Then the amount of time that the electronics are idle is $\sim 10^5$ counts x 10×10^{-6} s = 1 s. The dead time correction is then:

$$\text{Electronics DTC} \sim \frac{3600\ \text{s}}{3600\text{s} - 1\text{s}} = 1.0003$$

which is a small correction compared to the computer dead time.

3.8 Accidental-Coincidence Correction

A small fraction of good events in the NaI crystal are rejected due to accidental coincidences with shield events. The number of good events which have been accidentally rejected are estimated electronically in a delayed-coincidence circuit which is described in Section 2.3. Knowing the total number of coincidences (COIN) and accidental coincidences (ACC), the multiplicative correction for this effect is:

$$\text{Accidental Correction (AC)} = \frac{1}{1 - \frac{\text{ACC}}{\text{COIN}}} \qquad [3.6]$$

where the true yield is equal to the accidental correction times the measured yield. The accidental corrections for this experiment were typically 1 to 4% in the current experiments.

This correction factor is only an estimate of the true accidental correction due to correlated events which can take place. For example, a cosmic-ray shower may produce a secondary event 300 ns after the initial event is detected. This coincides with the delay in the accidental-coincidence circuit and therefore gives rise to an accidental-coincidence count. Assuming that 10% of the accidentals are not true accidentals, then the yields should actually be corrected by:

$$\text{Actual Accidental Correction (AAC)} = \frac{1}{1 - \frac{0.9\text{ACC}}{\text{COIN}}} \cdot \qquad [3.7]$$

In a typical run, the number of coincidences is about 30,000 and the number of accidentals is perhaps 500. Then AC = 1.017 and AAC=1.015. In other words, there is less than a 0.2% discrepancy.

3.9 Pickoff Correction

For the experiment at 8.6 MeV, the beam was pulsed at 5 MHz with the beam compressed into 2 to 3 ns long bursts. A timing profile (TAC spectrum) for the events in the NaI was generated (see Fig. 3.4) by measuring the time between the beam burst

passing through a capacitive pickoff, located before the target, and an event in the crystal. Since neutrons travel slower than γ rays, counts from the two events are separated in the time spectrum. The neutrons can then be gated out of the energy spectrum by allowing only events which arrive at the detector at the right time to be sorted into the energy spectrum. This sorting process is done by software in the computer. The TAC window size was set visually during on-line sorting. Therefore, it is possible for some good events to be outside this window. By summing the TAC spectrum using a wider window it has been determined that at most 5% of the good counts are outside the original TAC window.

Occasionally, a pickoff signal from a beam burst is not strong enough to get through the discriminator. Any events from this burst are then rejected by the timing condition. To correct for this, the number of signals (S) from the pickoff capacitor are counted. The frequency (f) of the beam pulsing and the length of time (t) of each run are known. Then the multiplicative pickoff correction is given by:

$$\text{Pickoff Correction} = \frac{ft}{S} \qquad [3.7]$$

where the true yield of γ rays is equal to the pickoff correction times the measured yield. Pickoff corrections varied from 0.1% to 7% and were typically under 2%. With no beam on target, background noise produced in the pickoff circuit is typically less than 0.1%.

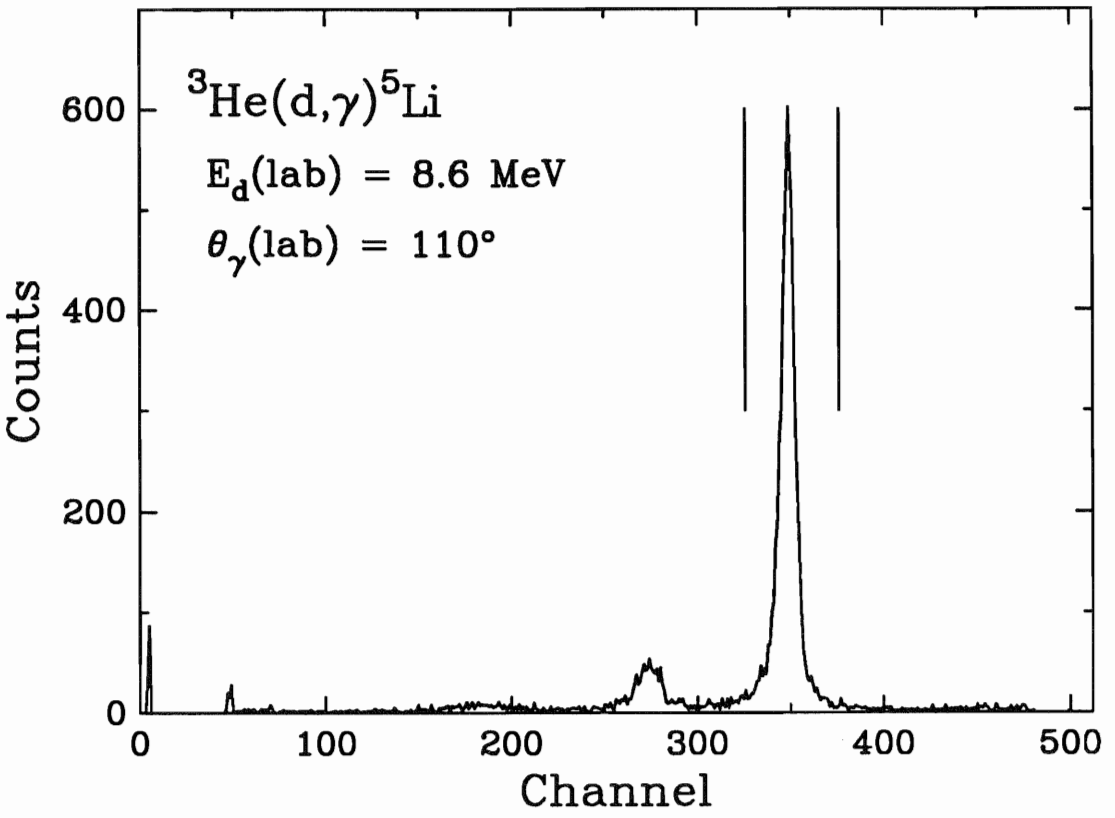

Fig. 3.4 A TAC spectrum from the ^{3}He($\vec{d}$,γ)^{5}Li reaction at E_d = 8.6 MeV. The vertical lines denote the gate from which a TAC-gated energy spectrum was constructed (as in Fig. 3.2).

3.10 Results

Independent measurements of the angular distributions of the absolute differential cross sections were made in the left and right NaI spectrometers. These two angular distributions were then nomalized to each other by an overall averaging factor and then the data at each angle were combined in an weighted averaging procedure. The overall averaging factor was typically about 0.95 for the right NaI data and 1.05 for the left NaI data. This falls well within the systematic errors of the experiment.

The absolute differential cross section (obtained from the weighted averaging procedure described above) for $E_d = 8.6$ MeV, $E_d = 0.8\text{-}0.0$ MeV, $E_d = 0.8\text{-}0.4$ MeV, $E_d = 0.4\text{-}0$ .0 MeV, and $E_d = 0.6\text{-}0.3$ MeV are listed in Table 3.3. Figs. 3.5-3.9 plot these cross sections, respectively, along with the cross sections obtained individually from the left and right NaI spectrometers. Table 3.4 lists the various sources of errors of these measurements as discussed in Sections 3.2-3.9.

Previous studies of the $^3He(\vec{d},\gamma)^5Li$ reaction at the peak of the fusion resonance measured absolute cross sections which range from 1.7 μb/sr [Bus68] to 4 μb/sr [Bla54]. The current measurements energy-integrate over four regions of the resonance and are therefore underestimates of the on-resonance cross section. However, they do fall within the range of the previously measured values, indicating that the measurement of [Bus68] may be too low. Present measurements of angular distributions in the fusion resonance region are nearly isotropic, which is also consistent with these previous experiments.

Measurements of the differential cross section at $\theta=90^\circ$ near $E_d=8.6$ MeV indicate that the cross section is between 3 and 4 mb/sr [Del68 and Kin72]. This is significantly higher than the current measurement of 2.4 μb/sr, however the angular distributions are similar in shape (see Section 5.3.4)

Table 3.3 The absolute differential cross section of the $^{3}He(d,\gamma)^{5}Li$ reaction in the center-of-mass system as measured in the present experiment. The errors represent the statistical uncertainty of the data.

$\theta_{c.m.}$ (deg)	8.6 MeV (μb/sr)
36.280	1.694 ± 0.018
51.703	1.945 ± 0.025
72.077	2.225 ± 0.022
92.196	2.396 ± 0.055
112.050	2.361 ± 0.019
131.662	2.121 ± 0.169
151.080	2.150 ± 0.052

$\theta_{c.m.}$ (deg)	0.8-0.0 MeV (μb/sr)
30.252	1.747 ± 0.072
50.386	1.802 ± 0.027
70.473	1.868 ± 0.015
90.502	1.917 ± 0.015
110.471	1.907 ± 0.033
130.384	1.890 ± 0.067
150.250	1.838 ± 0.038

$\theta_{c.m.}$ (deg)	0.8-0.4 MeV (μb/sr)
30.252	1.984 ± 0.057
50.386	2.037 ± 0.027
70.473	2.111 ± 0.037
90.502	2.105 ± 0.059
110.471	2.099 ± 0.072
130.384	2.151 ± 0.025
150.250	2.122 ± 0.062

$\theta_{c.m.}$ (deg)	0.4-0.0 MeV (μb/sr)
30.238	1.549 ± 0.075
50.364	1.507 ± 0.070
70.446	1.530 ± 0.024
90.474	1.558 ± 0.022
110.445	1.652 ± 0.058
130.362	1.574 ± 0.029
150.236	1.739 ± 0.108

$\theta_{c.m.}$ (deg)	0.6-0.3 MeV (μb/sr)
35.289	1.957 ± 0.074
50.386	1.854 ± 0.069
70.473	1.877 ± 0.028
90.502	1.822 ± 0.134
110.471	1.935 ± 0.011
130.384	1.938 ± 0.029
145.287	1.836 ± 0.091

Table 3.4 Sources of error for the absolute cross section measurements listed in Table 3.1. These errors are discussed in Sections 3.2 through 3.9.

Sources of Error	Error (%)				
	8.6 MeV	0.8-0.0 MeV	0.8-0.4 MeV	0.4-0.0 MeV	0.6-0.3 MeV
Beam-current integration	1	1	1	1	1
Gas Pressure	2.0	0.3	1.1	1.5	1.5
Gas Temperature	2	2	2	2	2
Target Length	2	5	0	5	0
Efficiency Measurement	10	10	10	10	10
Dead Time Correction	0.03	0.03	0.03	0.03	0.03
Accidental Correction	0.2	0.2	0.2	0.2	0.2
TAC Gate Error	5	-	-	-	-
Pickoff Correction	0.1	-	-	-	-
Statistical Uncertainty	2.3	2.0	2.3	3.6	2.4
TOTAL	12	12	11	12	11

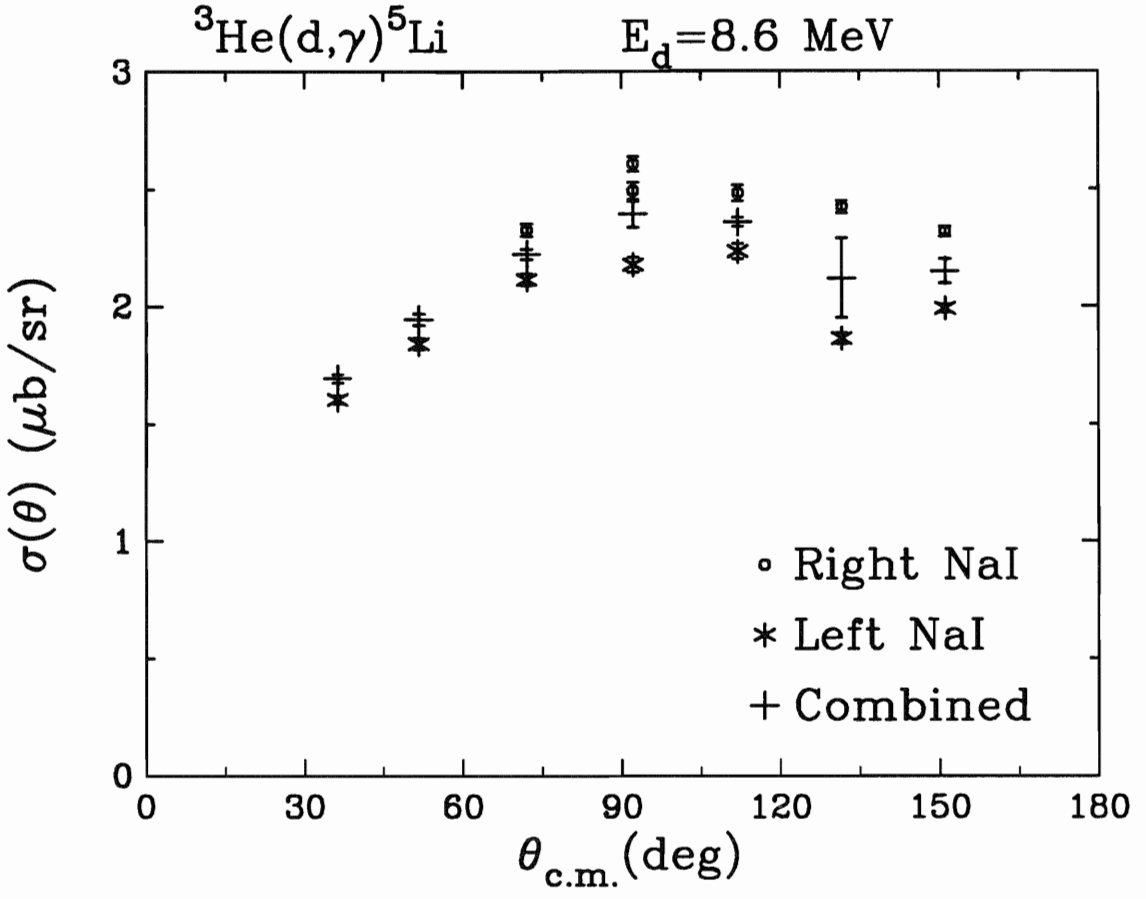

Fig. 3.5 The absolute differential cross section for the ^{3}He($\vec{d}$,γ)^{5}Li reaction at E_d(lab) = 8.6 MeV as measured in the left and right NaI spectrometers. The combined result is derived from a normalization and weighted-averaging procedure as described in the text. The error bars represent the statistical uncertainty of the measurements.

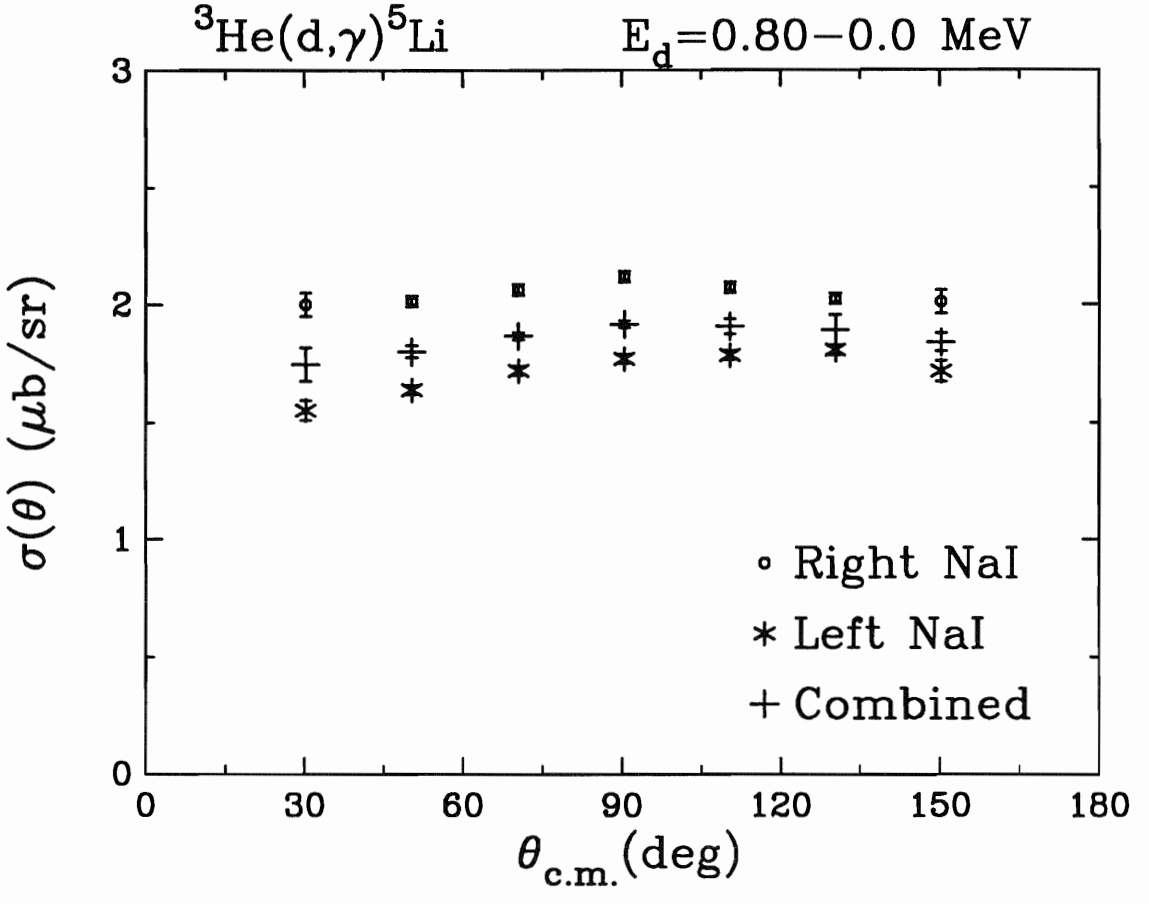

Fig. 3.6 The absolute differential cross section for the $^3He(\vec{d},\gamma)^5Li$ reaction at E_d(lab) = 0.8 MeV, where the deuteron beam was stopped in the target, as measured in the left and right NaI spectrometers. The combined result is derived from a normalization and weighted-averaging procedure as described in the text. The error bars represent the statistical uncertainty of the measurements.

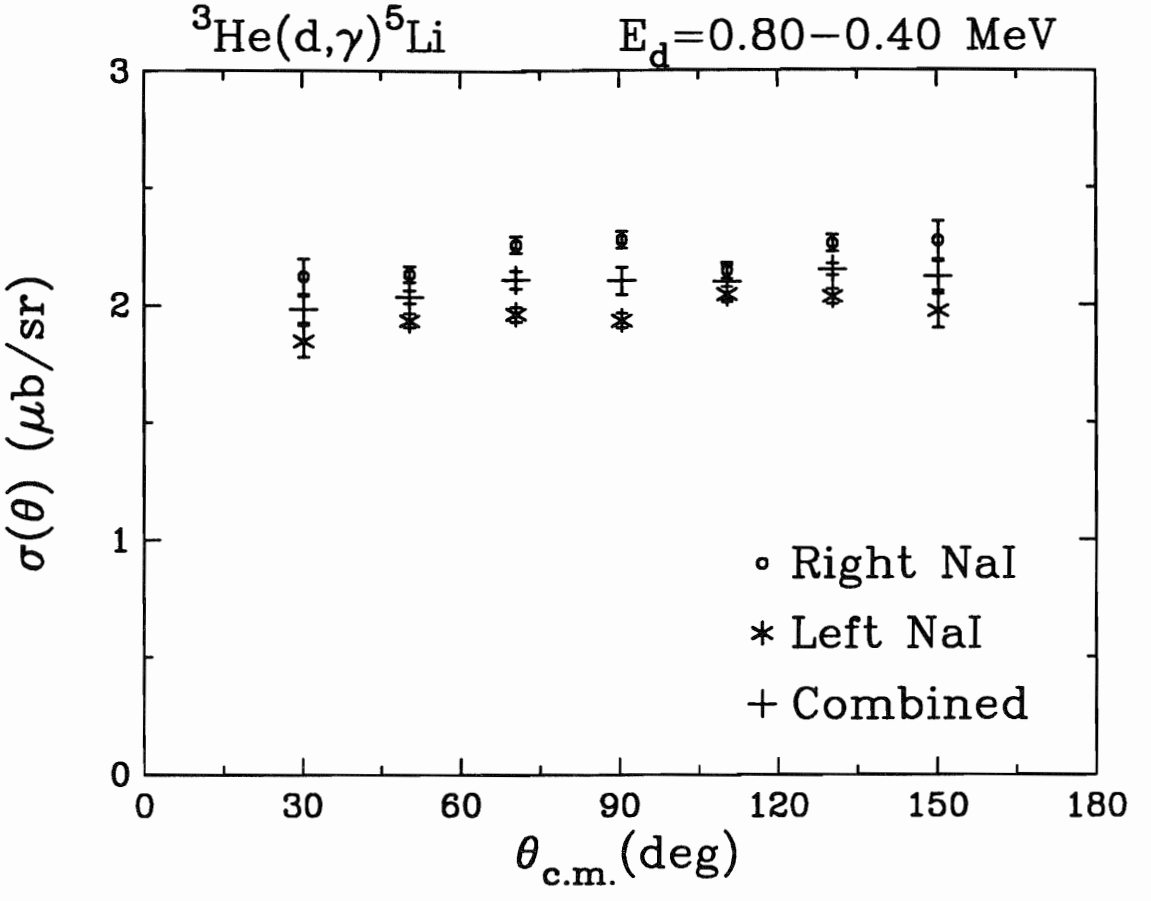

Fig. 3.7 The absolute differential cross section for the $^3He(\vec{d},\gamma)^5Li$ reaction at $E_d(lab) = 0.8$ MeV, where the deuteron beam exited the target with $E_d = 0.4$ MeV, as measured in the left and right NaI spectrometers. The combined result is derived from a normalization and weighted-averaging procedure as described in the text. The error bars represent the statistical uncertainty of the measurements.

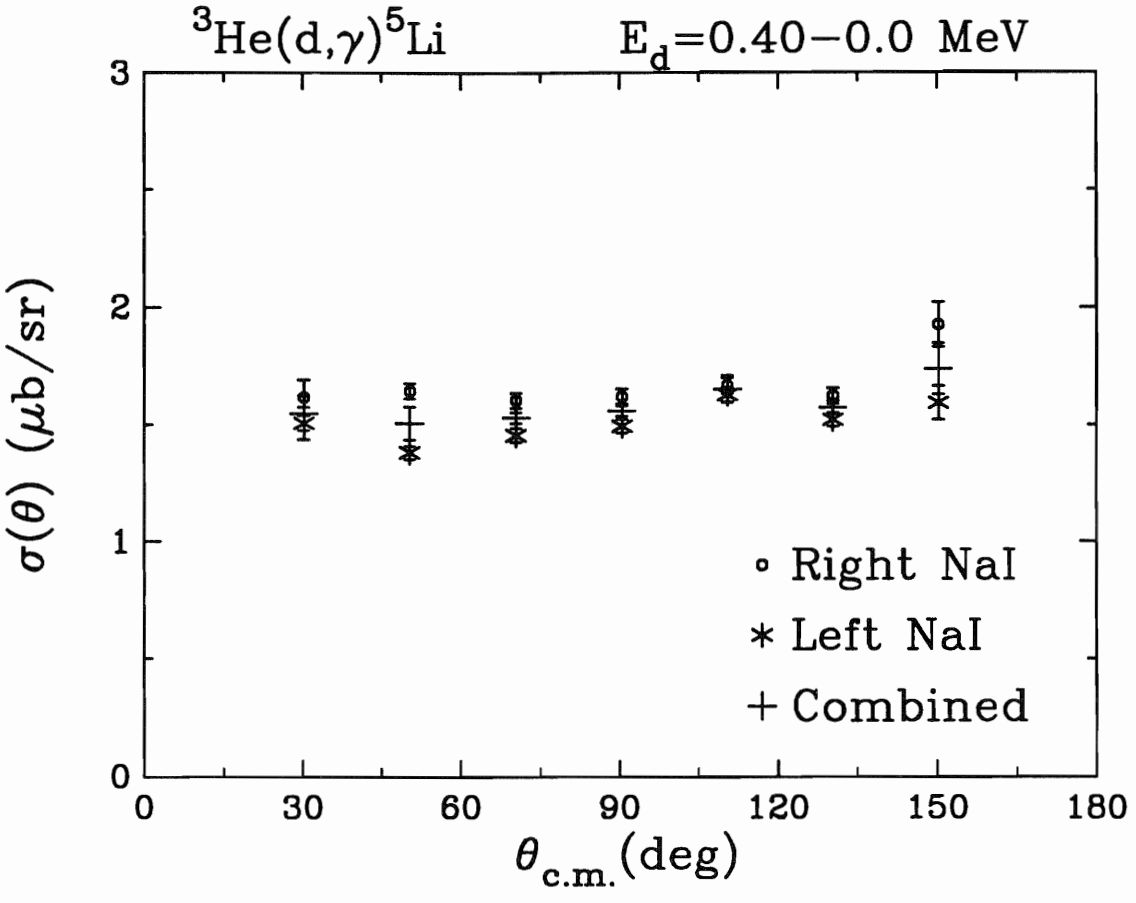

Fig. 3.8 The absolute differential cross section for the $^3He(\vec{d},\gamma)^5Li$ reaction at E_d(lab) = 0.4 MeV, where the deuteron beam was stopped in the target, as measured in the left and right NaI spectrometers. The combined result is derived from a normalization and weighted-averaging procedure as described in the text. The error bars represent the statistical uncertainty of the measurements.

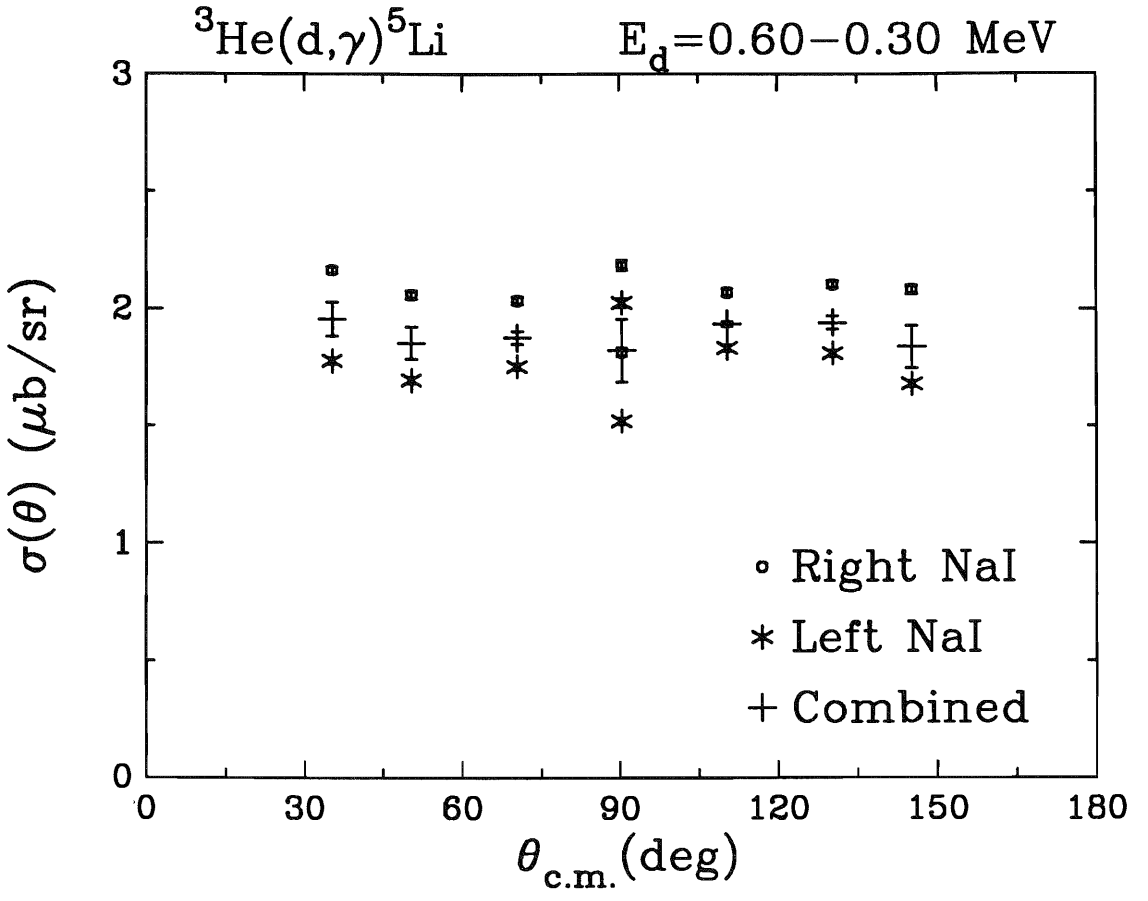

Fig. 3.9 The absolute differential cross section for the $^3He(\vec{d},\gamma)^5Li$ reaction at $E_d(lab) = 0.6$ MeV, where the deuteron beam exited the target with $E_d = 0.3$ MeV, as measured in the left and right NaI spectrometers. The combined result is derived from a normalization and weighted-averaging procedure as described in the text. The error bars represent the statistical uncertainty of the measurements.

Chapter 4: Polarization Observables

4.1 Introduction

One of the advantages of conducting experiments at TUNL is being able to utilize the polarized proton and deuteron beams to measure the analyzing powers of reactions. This chapter will discuss the mathematical and physical properties which describe polarization phenomena for the case of the spin-1 deuteron as well as presenting the results of experimental measurements of the vector and tensor analyzing powers of the $^3He(\vec{d},\gamma)^5Li$ reaction. All formalism is discussed under the guidelines of the Madison Convention [Bar71]

When an external magnetic field (**B**-field) is applied to a deuterium atom, the degenerate energy levels of the electron split due to the hyperfine interaction. Fig. 4.1 shows a plot of the level splitting as a function of applied B-field strength. $\mathbf{B_c}$ is the **B**-field applied to the electron due to it's motion through the electric field of the nucleus. At field strengths less than $\mathbf{B_c}$ (weak fields), the proton and electron spins are strongly coupled so that the total spin of the atom **F** and its associated magnetic quantum number m_f are good quantum numbers. Here $\mathbf{F} = \mathbf{s} + \mathbf{I}$, where **s** is the spin of the electron, **I** is the spin of the nucleus, and **F** is the vector sum of **s** and **I**. Bold-face type indicates these are vector quantities. At field strengths much greater than $\mathbf{B_c}$ (strong fields), the electron and nuclear spin become decoupled such that m_s and m_I are good magnetic quantum numbers. Since all experiments described in this dissertation were conducted with $\mathbf{B} > \mathbf{B_c}$, only the strong field case shall be discussed further.

In a strong field, the non-degenerate energy levels can be labeled by their nuclear magnetic substate m_I (+1, 0, or -1) and the electron magnetic substate m_s ($\pm$ 1/2). Alternatively, these states are often referred to as states 1, 2, and 3 for the three higher energy states with m_I = +1, 0, and -1 respectively, and states 4, 5, and 6 for the three

lower energy states with m_I = -1, 0, and +1 respectively. The relative populations of these states determine the polarization of the deuteron beam.

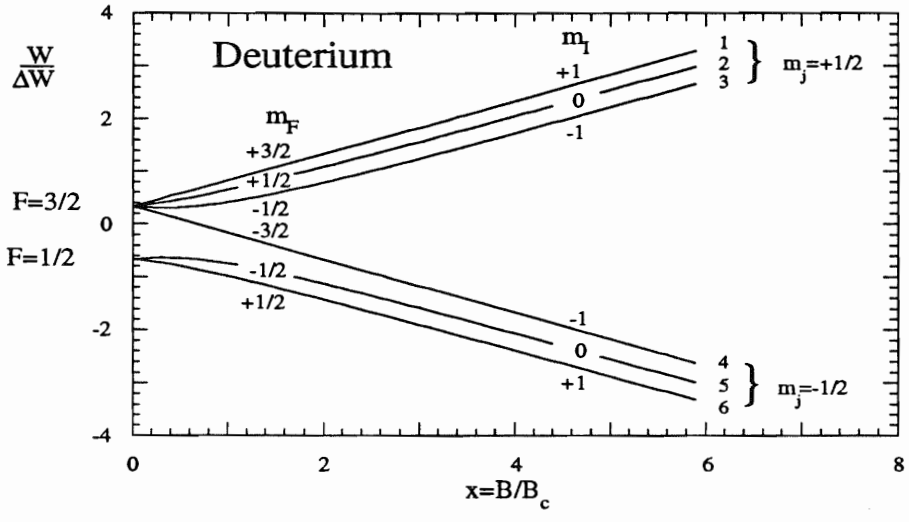

Fig. 4.1 Plot of the hyperfine splitting of deuterium as a function of applied B-field strength. $\mathbf{B_c}$ is the **B**-field applied to the electron due to it's motion through the electric field of the nucleus.

4.2 The Madison Convention

Fig. 4.2 illustrates the Madison-convention coordinate system. The z-axis points in the direction of the beam momentum $\mathbf{k_{in}}$. The y-axis is perpendicular to the reaction plane in the direction of $\mathbf{k_{in}} \times \mathbf{k_{out}}$, where $\mathbf{k_{out}}$ points from the target to the detector. β is defined as the angle between the z-axis and the quantization axis ζ. ϕ is defined as the angle due to a rotation of ζ about the z-axis out of the y-z plane.

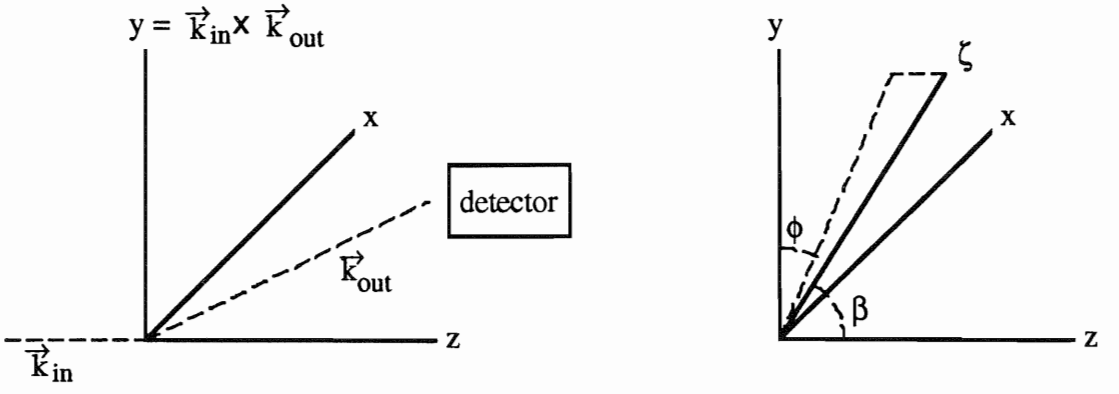

Fig. 4.2 The Madison convention coordinate system. Left figure: The z axis is along the direction of the incident beam momentum vector $\vec{k}_{in}$. The vector $\vec{k}_{out}$ points from the target to the detector. The y axis is defined along $\vec{k}_{in} \times \vec{k}_{out}$. The x axis is defined such that a right-handed coordinate system is formed. Right figure: The angle β is defined by the z axis and the quantization axis ζ. The angle ϕ is defined by the y axis and the projection of ζ on the x-y plane.

The preparation of polarized beams is discussed in Section 2.1. For the purposes of the current discussion, which follows that of W. Haeberli [Hae75], it is assumed that a polarized deuteron beam with a known population of states has been prepared. For a beam which has been polarized along a quantization axis ζ given by the angles β and ϕ, the polarization can be represented by a tensor of rank 2. This tensor can either be expressed in cartesian coordinates with elements p_i and p_{ij}, or in spherical coordinates with elements t_{ij}.

The cartesian spin moments are defined as the expectation values of combinations of the spin operators:

$$p_i = \langle S_i \rangle \qquad i = x,y,z \qquad \text{vector polarization,} \qquad [4.1]$$

and $$p_{ij} = 3/2\langle S_iS_j+S_jS_i\rangle - 2\delta_{ij} \qquad i,j = x,y,z \qquad \text{tensor polarization.} \qquad [4.2]$$

Similarly, the spin tensor moments in spherical coordinates are defined below.

$$t_{00} = 1 \qquad [4.3]$$

$$t_{10} = \sqrt{3/2}\langle Sz\rangle \qquad [4.4]$$

$$t_{11} = -\sqrt{3/2}\langle S_x + iS_y\rangle \qquad [4.5]$$

$$t_{20} = \sqrt{1/2}\langle 3S_z^2 - 2\rangle \qquad [4.6]$$

$$t_{21} = -\sqrt{3/2}\langle (S_x + iS_y)S_z + S_z(S_x + iS_y)\rangle \qquad [4.7]$$

$$t_{22} = \sqrt{3/2}\langle (S_x + iS_y)^2\rangle. \qquad [4.8]$$

Beams prepared in a polarized-ion source have azimuthal symmetry such that ζ points along the z-axis. It is then possible to express the polarization in terms of only two quantities, p_ζ and $p_{\zeta\zeta}$ in cartesian coordinates or τ_{10} and τ_{20} in spherical coordinates. If N_+ is the fraction of particles with spin $m_I = +1$, N_- is the fraction of particles with spin $m_I = -1$, and N_0 is the fraction of particles with spin $m_I = 0$, then p_ζ and $p_{\zeta\zeta}$ can be written as:

$$p_\zeta = (N_+ - N_-) \quad \text{and} \quad p_{\zeta\zeta} = (1 - 3N_0), \qquad [4.9]$$

and τ_{10} and τ_{20} as:

$$\tau_{10} = \sqrt{3/2}\,(N_+ - N_-) \quad \text{and} \quad \tau_{20} = \sqrt{1/2}\,(1 - 3N_0). \qquad [4.10]$$

A Wien Filter with crossed E and B fields located downstream from the polarized-ion source allows ζ to be precessed to any desired orientation. For any rotations β and ϕ of the quantization axis the spin tensor moments are given in spherical coordinates by:

$$t_{10} = \tau_{10}\cos(\beta) \qquad [4.11]$$

$$it_{11} = \tau_{10}\sin(\beta)\,e^{i\phi}/\sqrt{2} \qquad [4.12]$$

$$t_{20} = (1/2)\,\tau_{20}\,(3\cos^2\beta - 1) \qquad [4.13]$$

$$t_{21} = -i\sqrt{3/2}\,\tau_{20}\sin(\beta)\cos(\beta)e^{i\phi} \qquad [4.14]$$

$$t_{22} = -\sqrt{3/8}\,\tau_{22}\sin^2(\beta)e^{2i\phi}. \qquad [4.15]$$

The spin tensor moments in cartesian coordinates may be obtained from linear combinations of the above expressions as denoted in [Bar71, p. *xxix*].

4.3 Analyzing Powers

The cross section $\sigma_P(\theta)$ for a reaction $A(\vec{a},b)B$ with an incident polarized spin-1 particle can be expressed in terms of the unpolarized cross section $\sigma_0(\theta)$ and the spin tensor moments [Hae75 and Dar71].

$$\sigma_P(\theta) = \sigma_0(\theta)[1+2iT_{11}(\theta)\mathrm{Re}(it_{11}) + T_{20}(\theta)t_{20} + 2T_{21}(\theta)\mathrm{Re}(t_{21}) + 2T_{22}(\theta)\mathrm{Re}(t_{22})] \quad [4.16]$$

or

$$\sigma_P(\theta) = \sigma_0(\theta)[1+\tfrac{3}{2}p_\zeta A_y(\theta)\sin(\beta)\cos(\phi) + \tfrac{1}{4}p_{\zeta\zeta}A_{zz}(\theta)(3\cos^2\beta - 1) - p_{\zeta\zeta}A_{xz}(\theta)\sin(\beta)\cos(\beta)\sin(\phi) - \tfrac{1}{4}p_{\zeta\zeta}(A_{xx}(\theta) - A_{yy}(\theta))\sin^2(\beta)\cos(2\phi)]. \quad [4.17]$$

These expressions provide the foundation for measuring the analyzing powers of reactions. By judicious choices of beam polarizations each analyzing power becomes accessible to experimental measurements. For example, a polarized beam where the spin points in the direction of motion has only a t_{20} tensor spin moment. Then equation [4.16] reduces to:

$$\sigma_P(\theta) = \sigma_0(\theta)[1+T_{20}(\theta)t_{20}]. \quad [4.18]$$

A cross-section measurement with a polarized beam followed by a measurement with an unpolarized beam leads to the expression:

$$T_{20}(\theta) = \frac{1}{t_{20}}\left[\frac{\sigma_P(\theta)}{\sigma_0(\theta)} - 1\right]. \quad [4.19]$$

To measure $A_y(\theta)$ and $A_{yy}(\theta)$ simultaneously, the spin-quantization axis is aligned along the y axis ($\beta=90°$, $\phi=0°$). Equation [4.17] then reduces to:

$$\sigma_P(\theta) = \sigma_0(\theta)[1+\tfrac{3}{2}p_\zeta A_y(\theta) + \tfrac{1}{2}p_{\zeta\zeta}A_{yy}(\theta)]. \quad [4.20]$$

With the TUNL Lamb Shift Polarized Ion Source (LSPIS), the beam was polarized into State 1, 2, or 3. For Q defined as the fraction of the beam which is polarized, i.e. there is a (1-Q) unpolarized background, then the polarization in State 1 is p_ζ=Q and $p_{\zeta\zeta}$=Q; for State 2, p_ζ=0 and $p_{\zeta\zeta}$=-2Q; for State 3, p_ζ=-Q and $p_{\zeta\zeta}$=Q. Writing Equation [4.20] for each state and solving for $\sigma_0(\theta)$, $A_y(\theta)$, and $A_{yy}(\theta)$ gives:

$$\sigma_0(\theta) = \frac{1}{3}[\sigma_1(\theta) + \sigma_2(\theta) + \sigma_3(\theta)] \qquad [4.21]$$

$$A_y(\theta) = \frac{1}{Q}\left[\frac{\sigma_1(\theta) - \sigma_3(\theta)}{\sigma_1(\theta) + \sigma_2(\theta) + \sigma_3(\theta)}\right] \qquad [4.22]$$

$$A_{yy}(\theta) = \frac{1}{Q}\left[\frac{\sigma_1(\theta) + \sigma_3(\theta) - 2\sigma_2(\theta)}{\sigma_1(\theta) + \sigma_2(\theta) + \sigma_3(\theta)}\right] \qquad [4.23]$$

where $\sigma_i(\theta)$ denotes the polarized cross section in state i (i=1,2,3).

To measure $A_y(\theta)$ and $A_{yy}(\theta)$ simultaneously using the Atomic Beam Polarized Ion Source (ABPIS), the beam was polarized using the Strong Field 2, 3↔5 transition. The theoretical maxima for p_ζ and $p_{\zeta\zeta}$ are $\frac{1}{3}$ and -1, respectively. Typically, the actual polarizations are about 80% of these values. By measuring $\sigma_P(\theta)$ and $\sigma_0(\theta)$ for a left and right detector, the analyzing powers are given by:

$$A_y(\theta) = \frac{1}{3p_\zeta}\left[\frac{\sigma_{LP}(\theta)}{\sigma_{L0}(\theta)} - \frac{\sigma_{RP}(\theta)}{\sigma_{R0}(\theta)}\right] \qquad [4.24]$$

$$A_{yy}(\theta) = \frac{1}{p_{\zeta\zeta}}\left[\frac{\sigma_{LP}(\theta)}{\sigma_{L0}(\theta)} + \frac{\sigma_{RP}(\theta)}{\sigma_{R0}(\theta)} - 2\right]. \qquad [4.25]$$

4.4 Statistical Errors of Analyzing Powers

To derive the statistical errors for the analyzing powers, it is necessary to start with the expression for the error of a function which contains contributions from several uncorrelated, independent measurements [Bev69].

$$\Delta F(x_i) = \sqrt{\sum \left(\frac{\partial F}{\partial x_i}\right)^2 (\Delta x_i)^2} \qquad [4.26]$$

Using equations [4.19] and [4.26] the error in $T_{20}(\theta)$ is given as :

$$\Delta T_{20}(\theta) = \frac{1}{t_{20}} \sqrt{\left(\frac{1}{\sigma_0}\right)^2 (\Delta\sigma_P)^2 + \left(\frac{\sigma_P}{\sigma_0^2}\right)^2 (\Delta\sigma_0)^2}. \qquad [4.27]$$

$\Delta\sigma_P$ and $\Delta\sigma_0$ are the errors in the cross section measurement defined as:

$$\Delta\sigma_i = n_i \sqrt{Y_i} \qquad [4.28a]$$

$$n_i = \frac{\sigma_i}{Y_i}. \qquad [4.28b]$$

The proportionality constant n_i depends on experimental parameters such as the target thickness and detector efficiency. (See Sections 3.3 and 3.4)

For $A_y(\theta)$ and $A_{yy}(\theta)$ in the LSPIS configuration, equations [4.22], [4.23], and [4.26] give:

$$\Delta A_y(\theta) = \frac{1}{Q}\frac{1}{\Sigma^2} \sqrt{(\sigma_2+2\sigma_3)^2(\Delta\sigma_1)^2+(\sigma_1-\sigma_3)^2(\Delta\sigma_2)^2+(2\sigma_1+\sigma_2)^2(\Delta\sigma_3)^2}, \qquad [4.29]$$

and $$\Delta A_{yy}(\theta) = \frac{3}{Q}\frac{1}{\Sigma^2} \sqrt{(\sigma_2)^2(\Delta\sigma_1)^2+(\sigma_1+\sigma_3)^2(\Delta\sigma_2)^2+(\sigma_2)^2(\Delta\sigma_3)^2}, \qquad [4.30]$$

where $\Sigma = \sigma_1(\theta) + \sigma_2(\theta) + \sigma_3(\theta)$.

For $A_y(\theta)$ and $A_{yy}(\theta)$ in the ABPIS configuration, equations [4.24], [4.25], and [4.26] give:

$$\Delta A_y(\theta) = \frac{1}{3p_\zeta}\sqrt{D} \qquad [4.31]$$

$$\Delta A_{yy}(\theta) = \frac{1}{p_{\zeta\zeta}}\sqrt{D} \qquad [4.32]$$

$$D = \left(\frac{\Delta\sigma_{LP}}{\sigma_{L0}}\right)^2 + \left(\frac{\sigma_{LP}\Delta\sigma_{L0}}{(\sigma_{L0})^2}\right)^2 + \left(\frac{\Delta\sigma_{RP}}{\sigma_{R0}}\right)^2 + \left(\frac{\sigma_{RP}\Delta\sigma_{R0}}{(\sigma_{R0})^2}\right)^2. \qquad [4.33]$$

There are two basic effects in the error equations. First, the error goes inversely as the square root of the total number of counts. Second, the error goes inversely as the polarization. Therefore it is very important to have the maximum polarization possible. If the polarization drops by a factor of two, the error doubles. It then takes four times as many counts (and four times as long) to make up for the lost precision.

4.5 Results

The analyzing powers of the the $^3He(\vec{d},\gamma)^5Li$ reaction have been measured in three energy regions, using the methods discussed above. The analyzing powers $A_y(\theta)$ and $A_{yy}(\theta)$ were measured at $E_d = 8.6$ MeV and $E_d = 0.8$ MeV (where the beam was stopped in the target) using the LSPIS configuration. Independent measurements were made in this configuration for the left and right NaI spectrometers and the results were combined by a weighted averaging procedure. $T_{20}(\theta)$ was measured at $E_d = 0.8$ MeV using the ABPIS configuration. Finally, the ABPIS was used to measure the analyzing powers $A_y(\theta)$ and $A_{yy}(\theta)$ at $E_d = 0.6$ MeV where the deuteron beam lost 0.3 MeV in the target.

In Chapter 3, many sources of errors were discussed for the cross section measurement. One of the nice properties of analyzing powers is that they are expressed

as ratios of cross sections. This means that many systematic errors in the cross section do not affect the analyzing powers. Target thickness, detector efficiency, and the solid angle of the detector all cancel out in Eqn. 4.19 and Eqns. 4.21-4.25. The dominant systematic errors in analyzing power measurements are from the uncertainty in the beam polarization. This is usually less than 10% but no better than 2% (see Section 2.7). The results of the analyzing power measurements are given in Tables 4.1-4.3 and Figs 4.3-4.6. The quoted errors represent the statistical uncertainty of the data. The analysis and interpretation of the measured cross sections and analyzing powers are discussed in the next chapter.

Table 4.1 The results of an angular distribution measurement of the analyzing powers for the $^3He(\vec{d},\gamma)^5Li$ reaction at $E_d = 8.6$ MeV. The errors represent the statistical uncertainty of the measurement.

$\theta_{c.m.}$	$A_y(\theta)$	$A_{yy}(\theta)$
36.280	-0.026±0.013	-0.002±0.019
51.703	-0.040±0.017	0.056±0.023
72.077	-0.009±0.011	0.049±0.035
92.196	-0.023±0.013	0.044±0.019
112.050	-0.002±0.011	0.016±0.031
131.662	0.026±0.016	0.019±0.018
151.080	0.027±0.012	-0.009±0.017

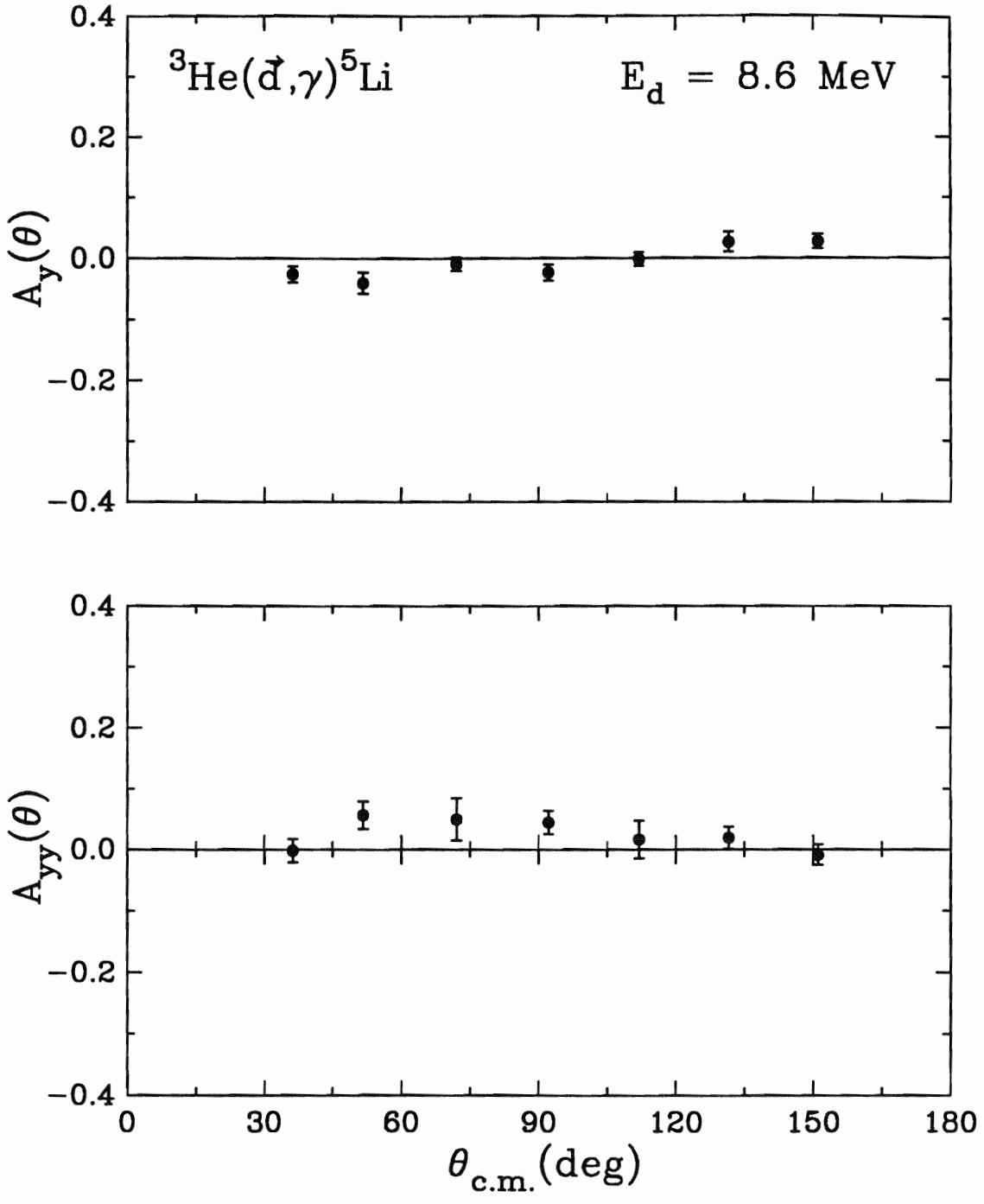

Fig. 4.3 Plot of the angular distribution of the analyzing powers for the ^{3}He($\vec{d}$,γ)^{5}Li reaction at $E_d = 8.6$ MeV. The errors represent the statistical uncertainty of the measurement.

Table 4.2 The results of an angular distribution measurement of the analyzing powers for the $^3He(\vec{d},\gamma)^5Li$ reaction at $E_d = 0.8$ MeV where the deuteron beam was stopped in the target. The errors represent the statistical uncertainty of the measurement.

$\theta_{c.m.}$	$A_y(\theta)$	$A_{yy}(\theta)$	$T_{20}(\theta)$
30.252	0.052±0.052	0.188±0.069	-0.19±0.02
50.386	-0.018±0.019	0.174±0.026	-0.05±0.02
70.473	0.064±0.026	0.201±0.035	0.04±0.03
90.502	0.011±0.037	0.082±0.049	0.10±0.02
110.471	0.004±0.029	0.172±0.039	
120.434			0.00±0.04
130.384	0.012±0.026	0.158±0.034	
150.250	0.114±0.054	0.043±0.073	-0.20±0.03

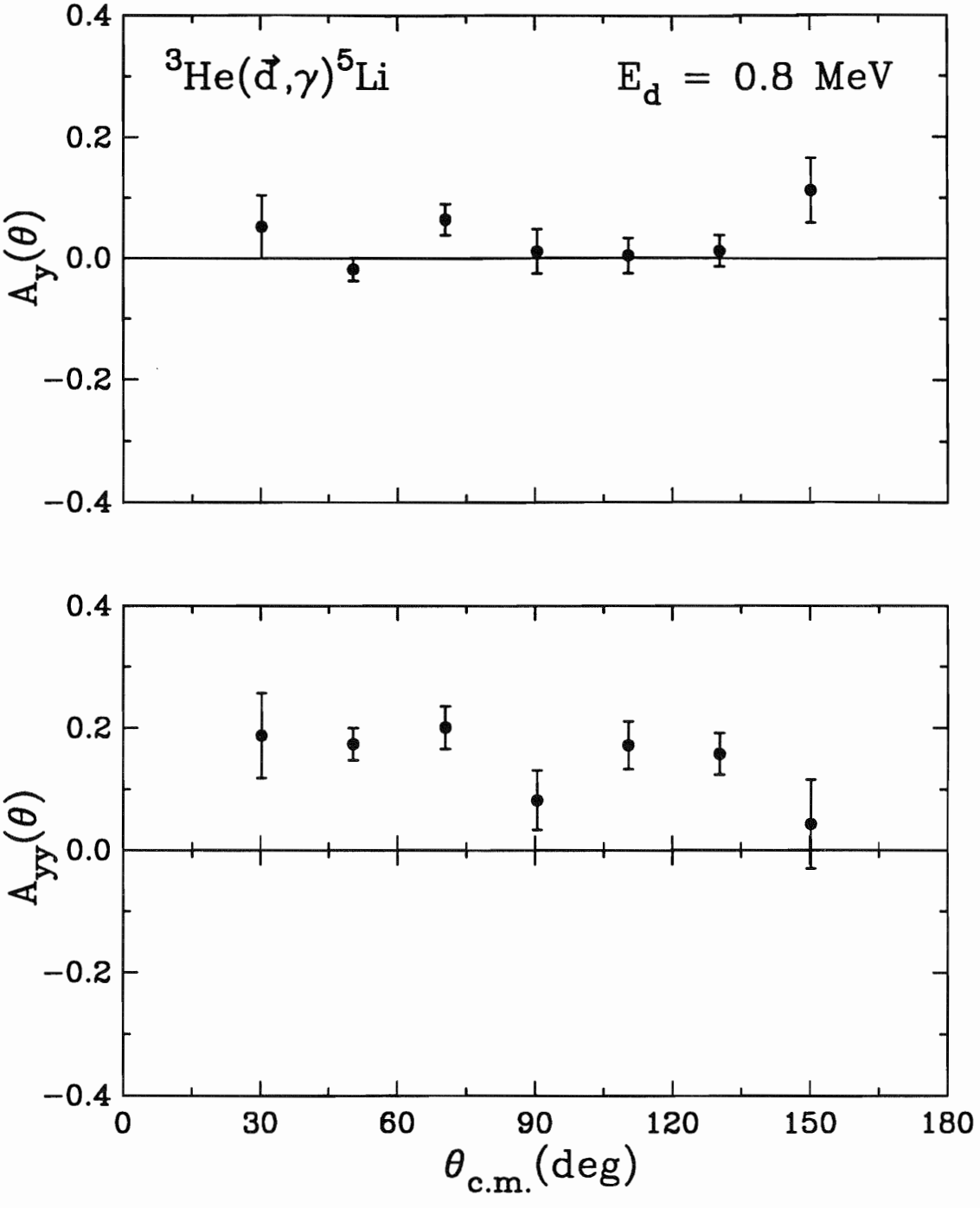

Fig. 4.4 Plot of the angular distribution of the analyzing powers $A_y(\theta)$ and $A_{yy}(\theta)$ for the ^{3}He($\vec{d}$,γ)^{5}Li reaction at E_d = 0.8 MeV where the deuteron beam was stopped in the target. The errors represent the statistical uncertainty of the measurement.

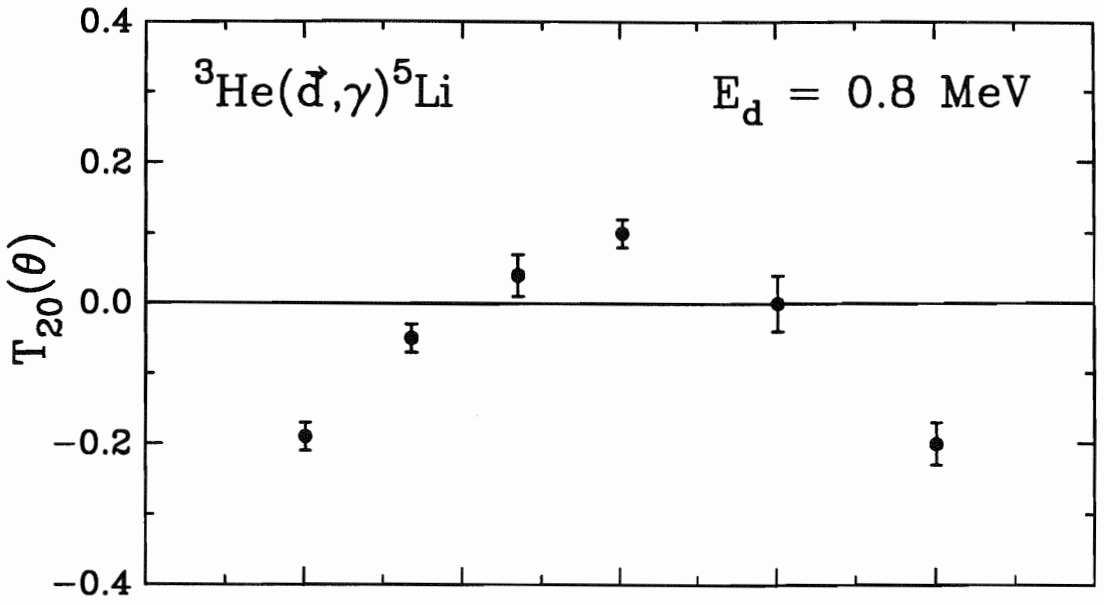

Fig. 4.5 Plot of the angular distribution of the analyzing power $T_{20}(\theta)$ for the $^3He(\vec{d},\gamma)^5Li$ reaction at E_d = 0.8 MeV where the deuteron beam was stopped in the target. The errors represent the statistical uncertainty of the measurement.

Table 4.3 The results of an angular distribution measurement of the analyzing powers for the $^3He(\vec{d},\gamma)^5Li$ reaction at $E_d = 0.6$ MeV where the deuteron beam lost 0.3 MeV in the target. The errors represent the statistical uncertainty of the measurement.

$\theta_{c.m.}$	$A_y(\theta)$	$A_{yy}(\theta)$
35.289	-0.028±0.016	0.194±0.015
50.386	-0.017±0.022	0.218±0.020
70.473	-0.018±0.019	0.241±0.017
90.502	-0.047±0.023	0.223±0.021
110.471	0.000±0.019	0.222±0.017
130.384	0.020±0.019	0.169±0.018
145.287	0.033±0.020	0.212±0.019

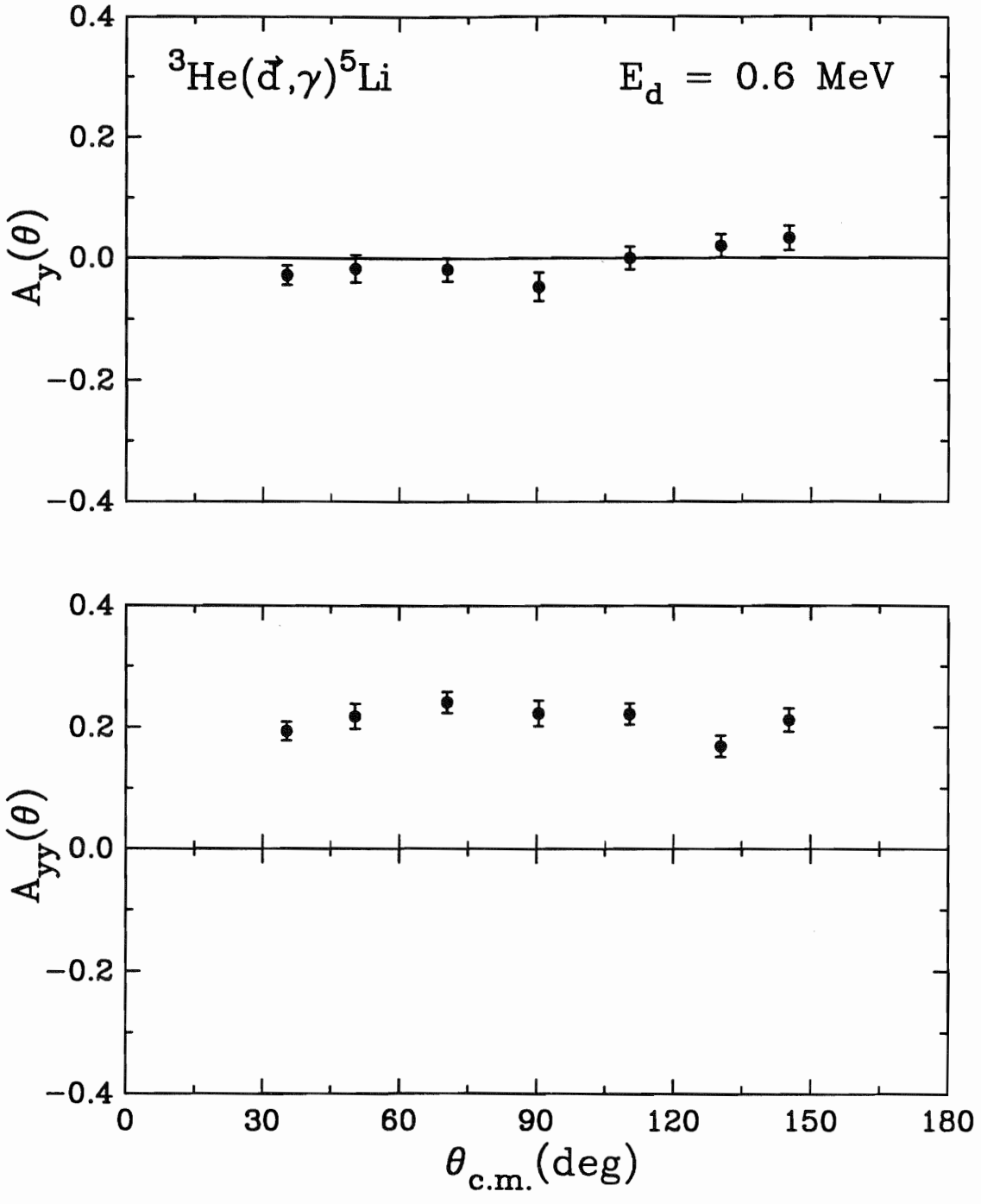

Fig. 4.6 Plot of the angular distribution of the analyzing powers $A_y(\theta)$ and $A_{yy}(\theta)$ for the ^{3}He($\vec{d}$,γ)^{5}Li reaction at E_d = 0.6 MeV where the deuteron beam lost 0.3 MeV in the target. The errors represent the statistical uncertainty of the measurement.

Chapter 5: Legendre and Transition Matrix Element Analyses

5.1 Introduction

The analysis of the angular distributions of the cross section and analyzing powers proceeds in two steps. Initially, the observables are fitted with Legendre or associated Legendre polynomials. As well as yielding the Legendre coefficients, these fits provide two more very useful pieces of information. First, the sum of polynomials terminates at twice the highest multipole of radiation involved in the reaction. Second, interference between different multipoles of radiation creates asymmetries in the observables about 90° which are reflected in the odd coefficients of the fits.

The second method of analysis, which offers more insight than the Legendre fitting, is the transition matrix element (TME) analysis which uses the formalism of [Sey79]. In this method, the cross section and analyzing powers are expressed in terms of irreducible transition matrix elements which contain the dynamical physics involved in the reaction. The values of the TME's are extracted by fitting them directly to all of the data at one energy. The advantage of this method is that all observables can be fit simultaneously, thereby increasing the sensitivity of the analysis. However, since the number of possible TME's involved in a reaction generally exceeds the number of data points being fit, one must be careful to include in the fits all TME's which have a significant effect while keeping the total number of free parameters of the fit reasonably small.

5.2 Allowed Transitions

The decomposition of the incident d+^{3}He scattering wave function is expressed in the LS coupling scheme [Sey79]. For the reaction a(x,λ)c (in this case ^{3}He($\vec{d}$,γ)^{5}Li), the angular momenta of the system are defined as follows:

a = the spin of the target,

x = the spin of the projectile,

L = the orbital angular momentum of the projectile,

b = the spin of the gamma emitting state,

λ = the multipolarity of the γ-ray,

c = the spin of the residual nucleus

and p = the mode of the γ-ray (1=electric, 0=magnetic).

Then in the LS coupling scheme:

$$x + a = S, \qquad [5.1a]$$

$$L + s = b, \qquad [5.1b]$$

$$\lambda + c = b. \qquad [5.1c]$$

For the $^3He(\vec{d},\gamma)^5Li$ reaction, a = 1/2 and x = 1.

Continuum states of $J^\pi=1/2^+,3/2^+$, and $5/2^+$ can radiate to the $J^\pi= 3/2^-$ ground state of ^5Li via E1 radiation which changes parity and transfers 1 unit of angular momentum. In the continuum, the intrinsic spin of the deuteron (1^+) couples with the intrinsic spin of ^3He ($1/2^+$) to a total channel spin of $S=1/2^+$ or $3/2^+$. Table 5.1 lists the channel spin S, orbital angular momentum L, and total angular momentum J = L+S for the continuum waves which can decay to the ground state of ^5Li via the E1, M1, and E2 operators.

Table 5.1 Some coupling schemes for L, S, and J quantum numbers which can couple to the $J^{\pi} = 3/2^{-}$ ground state of ^{5}Li via E1, M1, and E2 radiation.

l	S	J	$^{2S+1}L_J$	Eλ,Mλ
0	1/2	1/2	$^{2}s_{1/2}$	E1
0	3/2	3/2	$^{4}s_{3/2}$	E1
1	1/2	1/2	$^{2}p_{1/2}$	M1, E2
1	1/2	3/2	$^{2}p_{3/2}$	M1, E2
1	3/2	1/2	$^{4}p_{1/2}$	M1, E2
1	3/2	3/2	$^{4}p_{3/2}$	M1, E2
1	3/2	5/2	$^{4}p_{5/2}$	M1, E2
2	1/2	3/2	$^{2}d_{3/2}$	E1
2	1/2	5/2	$^{2}d_{5/2}$	E1
2	3/2	1/2	$^{4}d_{1/2}$	E1
2	3/2	3/2	$^{4}d_{3/2}$	E1
2	3/2	5/2	$^{4}d_{5/2}$	E1

5.3 The Legendre Polynomial Expansions

5.3.1 Definitions of the Legendre Polynomial Expansions

According to [Sey79], for a tensor-polarized beam the associated Legendre polynomial coefficients b_k, c_k, d_k, and e_k are defined by the equation,

$$\sigma(\theta,\phi) = \sum_k A_k P_k + B_k P_k^1 p_y + C_k P_k t_{20} + D_k P_k^1 \mathrm{Re}(t_{21}) + E_k P_k^2 \mathrm{Re}(t_{22}). \quad [5.2]$$

The unitless, lower-case coefficients are given by dividing the above coefficients by A_0, e.g. $\tilde{a}_k = A_k/A_0$. By comparison with

$$\sigma(\theta,\phi) = \sigma_u(\theta)[1+\tfrac{3}{2}p_y A_y(\theta)+t_{20}T_{20}(\theta)+2\mathrm{Re}(t_{21})T_{21}(\theta)+2\mathrm{Re}(t_{22})T_{22}(\theta)], \quad [5.3]$$

it is found that:

$$\sigma_u(\theta) = \sum_k A_k Q_k P_k(\cos\theta), \quad [5.4]$$

$$\sigma_u(\theta)A_y(\theta) = \tfrac{2}{3}\sum_k B_k Q_k P_k^1(\cos\theta), \quad [5.5]$$

$$\sigma_u(\theta)T_{20}(\theta) = \sum_k C_k Q_k P_k(\cos\theta), \quad [5.6]$$

$$\sigma_u(\theta)T_{21}(\theta) = \tfrac{1}{2}\sum_k D_k Q_k P_k(\cos\theta), \quad [5.7]$$

and $$\sigma_u(\theta)T_{22}(\theta) = \tfrac{1}{2}\sum_k E_k Q_k P_k^2(\cos\theta), \quad [5.8]$$

where the Q_k terms account for the finite geometry of the detector. The tensor analyzing power $A_{yy}(\theta)$ can be expressed in terms of $T_{20}(\theta)$ and $T_{22}(\theta)$ as:

$$A_{yy}(\theta) = \frac{-1}{\sqrt{2}}T_{20}(\theta) + \sqrt{3}\,T_{22}(\theta). \quad [5.9]$$

In the experiments with E_d=8.6 MeV and E_d=0.6-0.3 MeV, $A_{yy}(\theta)$ has been measured but $T_{20}(\theta)$ and $T_{22}(\theta)$ have not. Unfortunately, the Legendre and second associated Legendre polynomials do not form a linearly-independent system, making it impossible to get a unique solution from a fit to Eqn. 5.8, with Eqns. 5.6 and 5.7 substituted for $T_{20}(\theta)$

and $T_{22}(\theta)$ respectively. Therefore, $\sigma_u(\theta)A_{yy}(\theta)$ was simply fitted to an expansion in Legendre polynomials of the form:

$$\sigma_u(\theta)A_{yy}(\theta) = \sum_k C_k' Q_k P_k(\cos\theta). \qquad [5.10]$$

5.3.2 Legendre fits at E_d = 0.8-0.0 MeV

Fits to four observables ($\sigma_u(\theta)$, $\sigma_u(\theta)A_y(\theta)$,$\sigma_u(\theta)T_{20}(\theta)$, and $\sigma_u(\theta)T_{22}(\theta)$) have been performed. The results are stated in Table 5.2. The finite odd-k coefficients indicate E1-M1 and/or E1-E2 interference. The small k=3 and 4 coefficients suggest that the contributions from E2 radiation are small. Previous angular distributions of the cross section in the fusion resonance region (see Chapter 1) have indicated that the cross section is isotropic to within 10%. The present cross section has been determined to be consistent with isotropy to within 5% in a Legendre fit to A_0 only.

5.3.3 Legendre fits at E_d = 0.6-0.3 MeV

Fits to three observables ($\sigma_u(\theta)$, $\sigma_u(\theta)A_y(\theta)$, and $\sigma_u(\theta)A_{yy}(\theta)$) have been performed. The results are stated in Table 5.2. Again, the finite odd-k coefficients indicate E1-M1 and/or E1-E2 interference. As with the E_d = 0.8-MeV cross section, the present cross section has been determined to be consistent with isotropy to within 5% in a Legendre fit to A_0 only.

5.3.4 Legendre fits at E_d = 8.6 MeV

Fits to three observables ($\sigma_u(\theta)$, $\sigma_u(\theta)A_y(\theta)$, and $\sigma_u(\theta)A_{yy}(\theta)$) have been performed. The results are stated in Table 5.2. The finite odd-k coefficients indicate E1-M1 and/or E1-E2 interference with the non-negiblie k=3 and 4 coefficients suggesting important contributions from E1-E2 interference.

Table 5.2 The results of the Legendre polynomial fits at $E_d = 0.8\text{-}0.0$ MeV, $E_d = 0.6\text{-}0.3$ MeV, and $E_d = 8.6$ MeV.

	0.8-0.0 MeV	0.6-0.3 MeV	8.6 MeV
A_0 (μb/sr)	1.855 ± 0.012	1.897 ± 0.031	2.147 ± 0.013
$\bar{a}_1$	-0.033 ± 0.018	0.013 ± 0.027	-0.138 ± 0.013
$\bar{a}_2$	-0.056 ± 0.024	-0.007 ± 0.048	-0.203 ± 0.017
$\bar{a}_3$	0.004 ± 0.022	0.053 ± 0.030	-0.023 ± 0.016
$\bar{a}_4$	0.010 ± 0.030	-0.029 ± 0.070	0.010 ± 0.034
$\bar{b}_1$	0.029 ± 0.022	-0.022 ± 0.014	-0.015 ± 0.009
$\bar{b}_2$	-0.015 ± 0.013	-0.022 ± 0.009	-0.020 ± 0.007
$\bar{b}_3$	-0.002 ± 0.015	0.011 ± 0.008	0.007 ± 0.005
$\bar{b}_4$	-0.025 ± 0.014	-0.007 ± 0.007	-0.006 ± 0.005
$\bar{c}_0$	-0.029 ± 0.012		
$\bar{c}_1$	0.008 ± 0.020		
$\bar{c}_2$	-0.262 ± 0.026		
$\bar{c}_3$	0.015 ± 0.041		
$\bar{c}_4$	-0.008 ± 0.046		
$\bar{c}_0'$		0.216 ± 0.009	0.025 ± 0.009
$\bar{c}_1'$		0.006 ± 0.013	0.002 ± 0.012
$\bar{c}_2'$		-0.022 ± 0.025	-0.068 ± 0.023
$\bar{c}_3'$		-0.023 ± 0.026	-0.039 ± 0.032
$\bar{c}_4'$		0.033 ± 0.041	-0.034 ± 0.034
$\bar{e}_2$	-0.045 ± 0.020		
$\bar{e}_3$	-0.027 ± 0.011		
$\bar{e}_4$	0.009 ± 0.005		

5.4 The Transition Matrix Element Analysis

5.4.1 Introduction

The formalism of [Sey79] can be used to express the Legendre polynomial coefficients in terms of the reduced transition matrix elements (TME's), where the TME's are labelled by their continuum state quantum numbers ($^{2S+1}L_J$) and the multipolarity (Eλ or Mλ) of the outgoing γ ray. The relevant TME's can then be fit to all of the data simultaneously, giving a fairly model-independent interpretation of the reaction. In order to maintain a reasonable number of free parameters in the fits, the J dependence of the transition matrix elements has been suppressed in these relationships. Of course, for s-wave capture this assumption is always true because there is only one possible J value for a given S. Appendix D contains the expansion of the Legendre polynomials in terms of the transition matrix elements under this no-J-dependence assumption.

5.4.2 Transition Matrix Element fits at E_d = 0.8-0 MeV

With the low-energy deuterons of this experiment, s-wave capture is expected to dominate the reaction. Considering s-wave capture only, the expressions for the observables in terms of the TME's are quite simple:

$$\sigma(\theta) = 2\,|^2s_{1/2}(E1)|^2 + 4\,|^4s_{3/2}(E1)|^2\,, \qquad [5.11]$$

$$A_y(\theta) = 0, \qquad [5.12]$$

and

$$A_{yy}(\theta) = \frac{0.632\,|^2s_{1/2}(E1)|\,|^4s_{3/2}(E1)|\cos(\delta) + 0.800\,|^4s_{3/2}(E1)|^2}{2\,|^2s_{1/2}(E1)|^2 + 4\,|^4s_{3/2}(E1)|^2}, \qquad [5.13]$$

where δ is the relative phase between the two transition matrix elements. In the $3/2^+$ fusion resonance region, it is expected that the $^4s_{3/2}(E1)$ transition matrix element will dominate the reaction. For pure $^4s_{3/2}(E1)$ capture, $A_{yy} = 0.2$.

The results of a simultaneous fit to all the data are given in Table 5.3 and shown in Figs. 5.1 and 5.2. It was necessary to introduce a small amount of M1 radiation in order to fit the asymmetry of the data. Two statistically significant solutions with nearly-identical total χ^2=25 have been found, one with dominant S=3/2 s-wave capture strength, the second with nearly equal strengths for the S=1/2 and S=3/2 s-wave transition matrix elements. (Note: upon re-analysis, a second solution has also been found for the $^3H(\vec{d},\gamma)^5He$ data of [Ril89] which also has nearly equal S=1/2 and S=3/2 s-wave capture strengths.) Unfortunately, from the analysis alone, it is impossible to choose one solution over the other.

Table 5.3 Transition matrix element relative contributions to the cross section from a TME fit to the cross section and analyzing powers of the $^3He(\vec{d},\gamma)^5Li$ reaction for an 0.8 MeV beam which was stopped in the target. Two solutions with nearly identical χ^2=25 have been found. The phase of the $^4s_{3/2}$ (E1) matrix element has been arbitrarily set to 0.0.

	Solution 1		Solution 2	
TME	Intensity	Phase	Intensity	Phase
$^2s_{1/2}$ (E1)	0.03±0.03	260°±3°	0.48±0.06	145°±3°
$^4s_{3/2}$ (E1)	0.89±0.03	0°	0.44±0.05	0°
^{2}p(M1)	0.01±0.01	69°±2°	0.01±0.01	66°±4°
^{4}p(M1)	0.07±0.02	173°±2°	0.07±0.02	-10°±2°

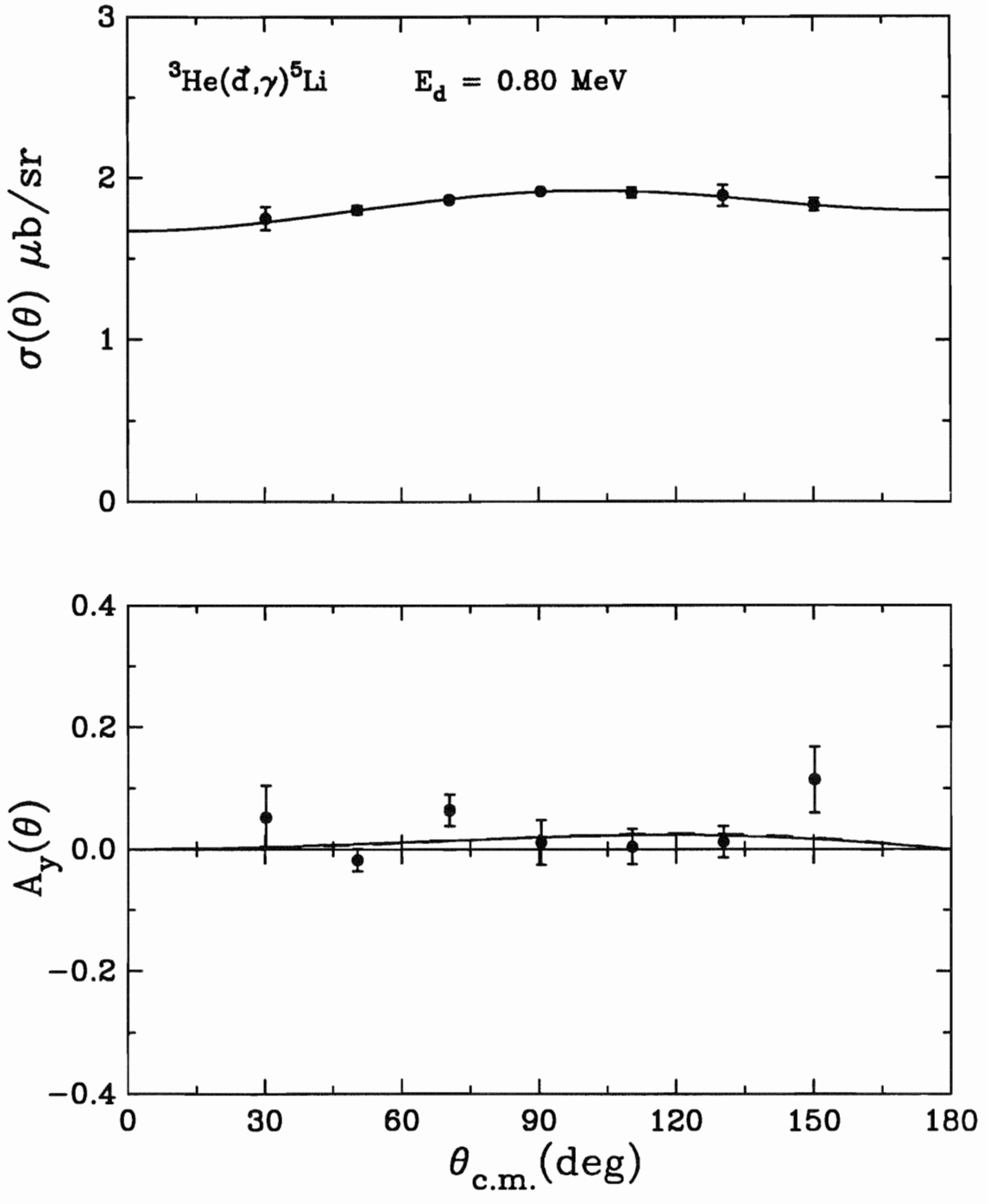

Fig. 5.1 $\sigma(\theta)$ and $A_y(\theta)$ from the ^{3}He(d,γ)^{5}Li reaction at E_d = 0.8-0 MeV are shown along with the results of the two TME solutions. The solid line represents Solution 1 of Table 5.3. The dashed line (which is almost entirely underneath the solid line) represents Solution 2.

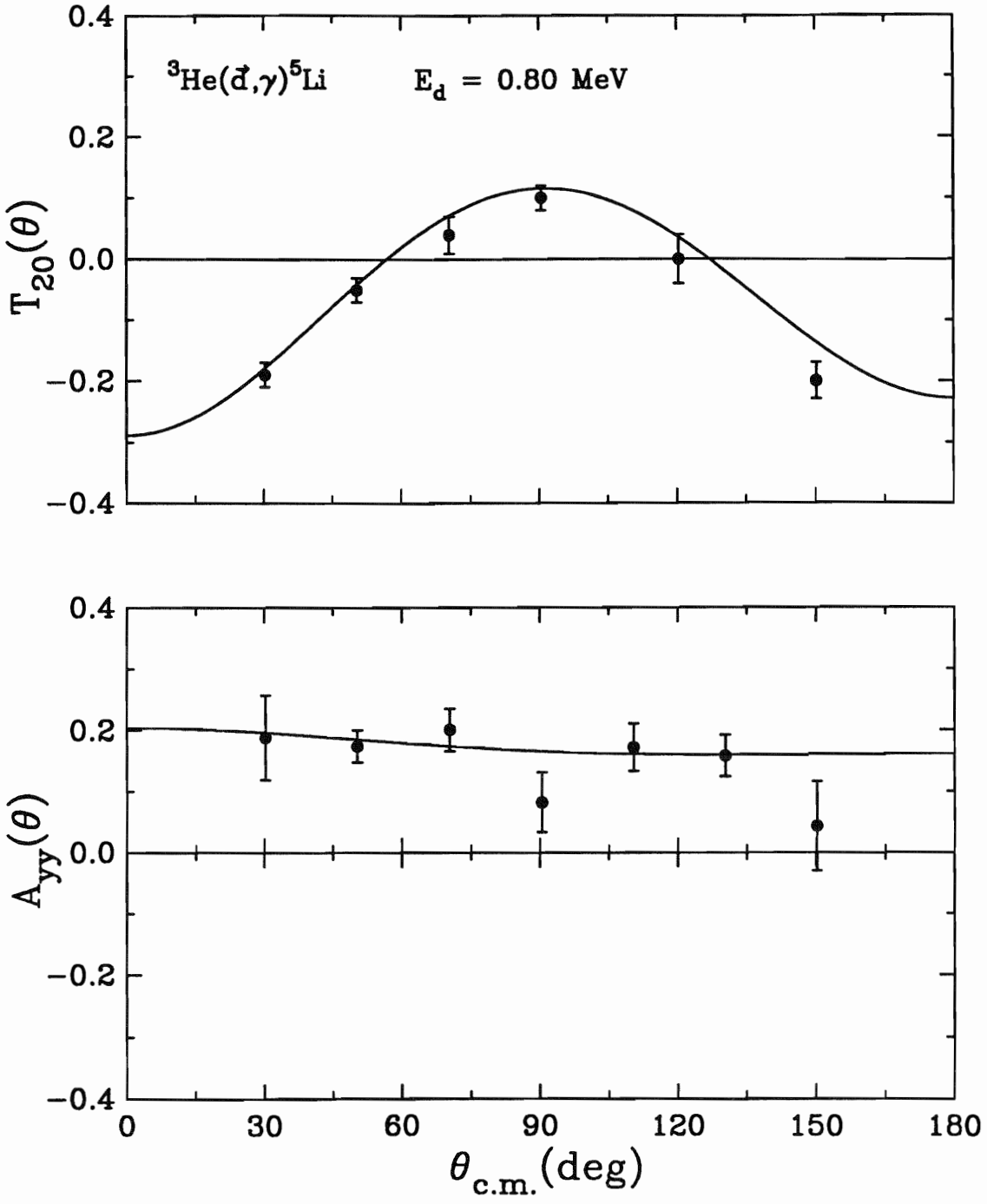

Fig. 5.2 $A_{yy}(\theta)$ and $T_{20}(\theta)$ from the ^{3}He(d,γ)^{5}Li reaction at E_d = 0.8-0 MeV are shown along with the results of the two TME solutions. The solid line represents Solutions 1 and 2 of Table 5.3.

5.4.3 Transition Matrix Element fits at E_d = 0.6-0.3 MeV

In order to understand more fully the physics of the $^3He(\vec{d},\gamma)^5Li$ reaction in the fusion resonance region, angular distributions of $\sigma(\theta)$, $A_y(\theta)$, and $A_{yy}(\theta)$ integrated over the FWHM of this resonance were measured. A transition matrix element analysis which uses the same choices of TME's as the E_d=0.8 MeV work finds, rather than the two previous solutions, one unique solution with a χ^2=19 whose errors nearly span both previous solutions. If, instead of using M1 radiation to account for the asymmetry in the data, E2 radiation is introduced into the fits then the set of two solutions is recovered. These fits do not have quite as good a χ^2 (=25) although they are acceptable from a statistical point of view. The results of these fits are given in Table 5.4 and plotted in Fig. 5.3 and 5.4.

Table 5.4 Transition matrix element relative contributions to the cross section from a TME fit to the cross section and analyzing powers of the $^3He(\vec{d},\gamma)^5Li$ reaction for an 0.6 MeV deuteron beam which lost 0.3 MeV in the target. Three statistically acceptable solutions have been found. Note that for Solution 1, M1 radiation is included, whereas for Solutions 2 and 3, E2 radiation is included. In all cases, the phase of the $^4s_{3/2}$ (E1) matrix element has been arbitrarily set to 0.0.

TME	Solution 1 χ^2=19.5	
	Intensity	Phase
$^2s_{1/2}$ (E1)	0.19±0.17	175°± 6°
$^4s_{3/2}$ (E1)	0.67±0.15	0°
^2p(M1)	0.10±0.03	89°± 5°
^4p(M1)	0.04±0.02	-24°± 9°

TME	Solution 2 χ^2=25.5		Solution 3 χ^2=25.2	
	Intensity	Phase	Intensity	Phase
$^2s_{1/2}$ (E1)	0.01±0.07	174°± 180°	0.45±0.07	8°± 20°
$^4s_{3/2}$ (E1)	0.99±0.08	0°	0.52±0.05	0°
^2p(E2)	0.00±0.01	68°± 62°	0.02±0.04	-84°± 95°
^4p(E2)	0.00±0.01	67°± 117°	0.01±0.01	-85°± 132°

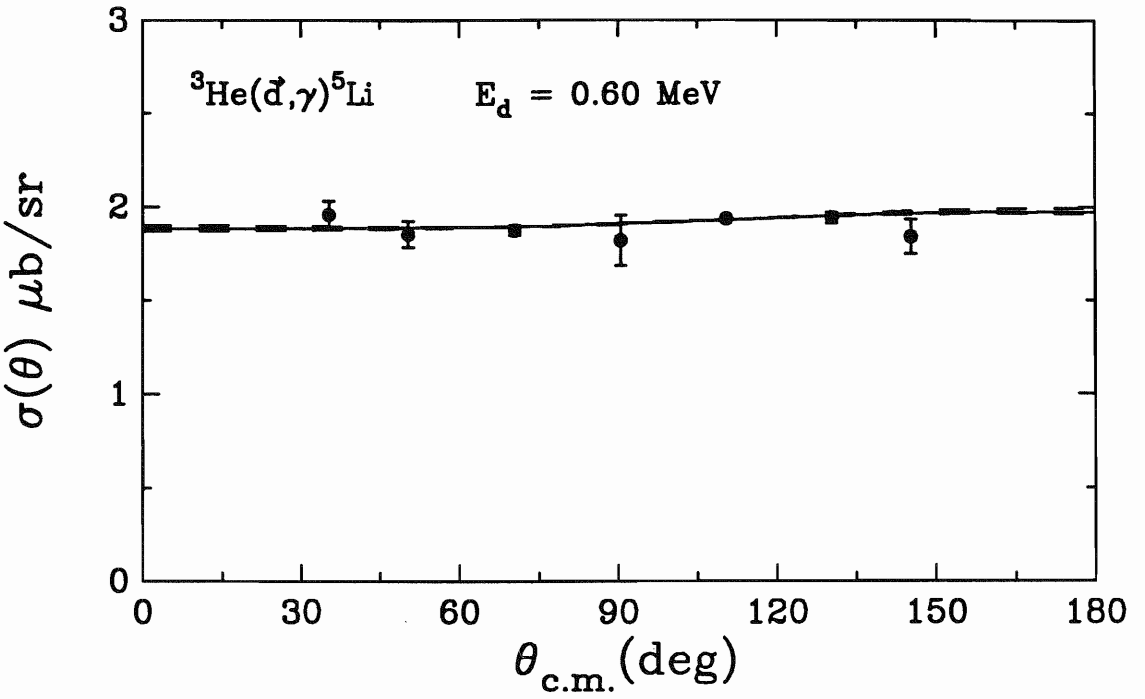

Fig. 5.3 $\sigma(\theta)$ from the ^{3}He(d,γ)^{5}Li reaction at E_d = 0.6-0.3 MeV is shown along with the results of the three TME solutions. The solid line represents Solution 1 of Table 5.4. The dashed-dotted line represents Solution 2, and the dashed line represents Solution 3.

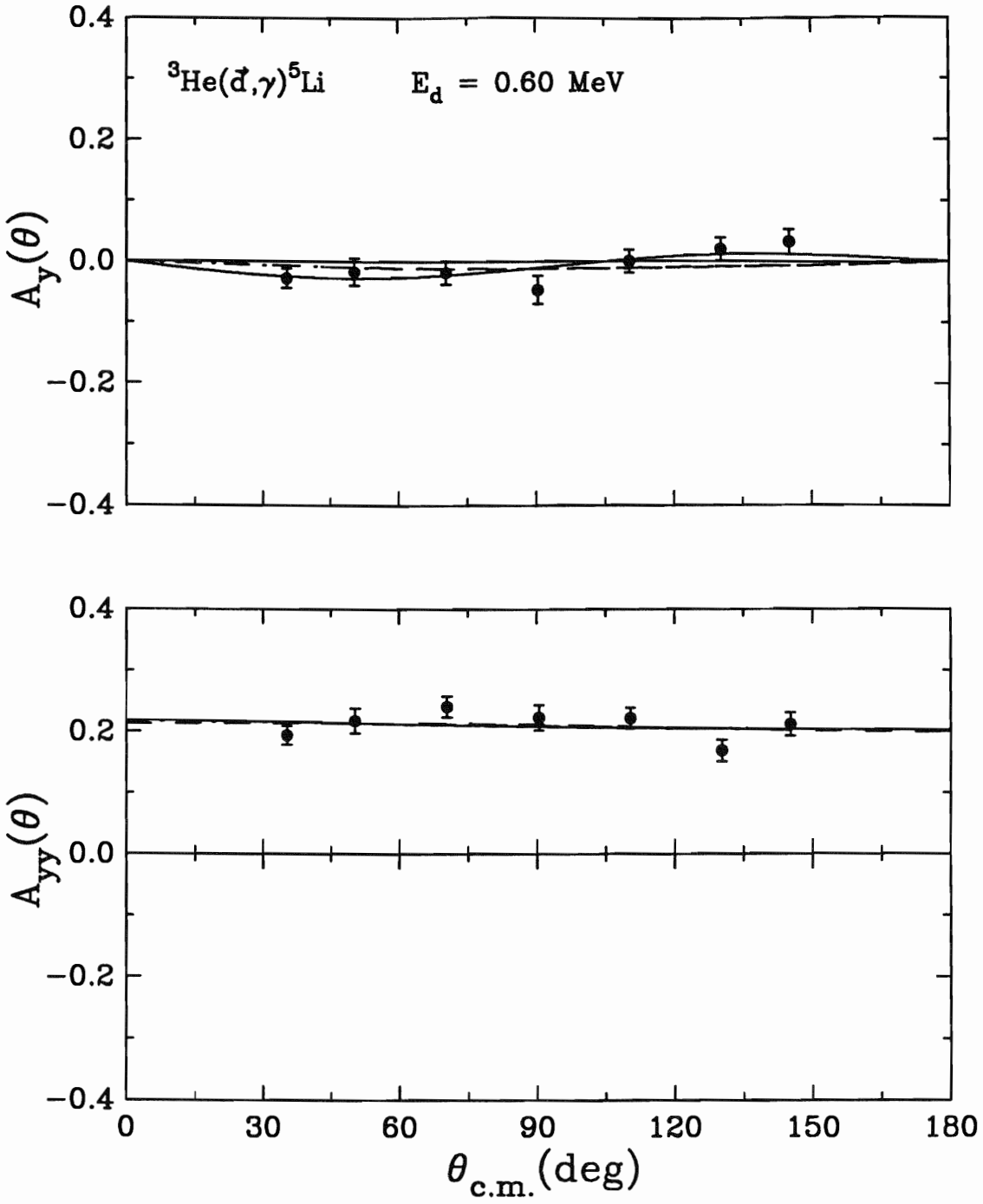

Fig. 5.4 $A_y(\theta)$ and $A_{yy}(\theta)$ from the ^{3}He(d,γ)^{5}Li reaction at E_d=0.6-0.3 MeV is shown along with the results of the three TME solutions. The solid line represents Solution 1 of Table 5.4. The dashed-dotted line represents Solution 2, and the dashed line represents Solution 3.

5.4.4 Transition Matrix Element fits at E_d = 8.6 MeV

At E_d=8.6 MeV, only one solution (with χ^2=7) was found from a fit to the cross section and analyzing powers $A_y(\theta)$ and $A_{yy}(\theta)$. The fit indicates that the capture cross-section strength is dominated by s-wave E1 capture with an admixture of ~20% d-wave E1 capture. The results of a simultaneous fit to all the data are given in Table 5.5 and shown in Figs. 5.5 and 5.6.

Table 5.5 Transition matrix element relative intensities from a TME fit to the cross section and analyzing powers of the $^3He(\vec{d},\gamma)^5Li$ reaction at E_d=8.6 MeV. Only one statistically significant solution (with χ^2=7) has been found. The phase of the $^4s_{3/2}$(E1) matrix element has been arbitrarily set to 0.0.

TME	Intensity	Phase
$^2s_{1/2}$(E1)	0.15±0.02	53°± 5°
$^4s_{3/2}$(E1)	0.65±0.03	0°
^2p(E2)	0.00±0.00	133°± 6°
^4p(E2)	0.00±0.00	179°± 13°
^2d(E1)	0.18±0.02	199°± 3°
^4d(E1)	0.02±0.01	72°± 4°

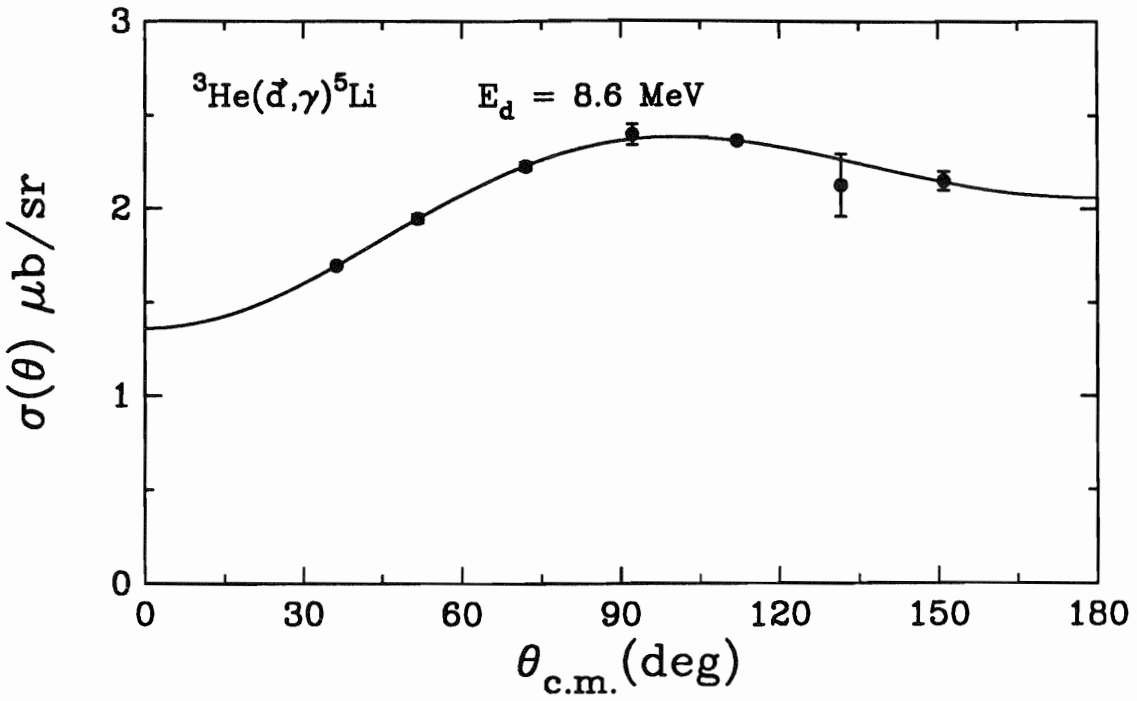

Fig. 5.5 $\sigma(\theta)$ from the ^{3}He(d,γ)^{5}Li reaction at E_d = 8.6 MeV is shown along with the results of the TME solution of Table 5.5.

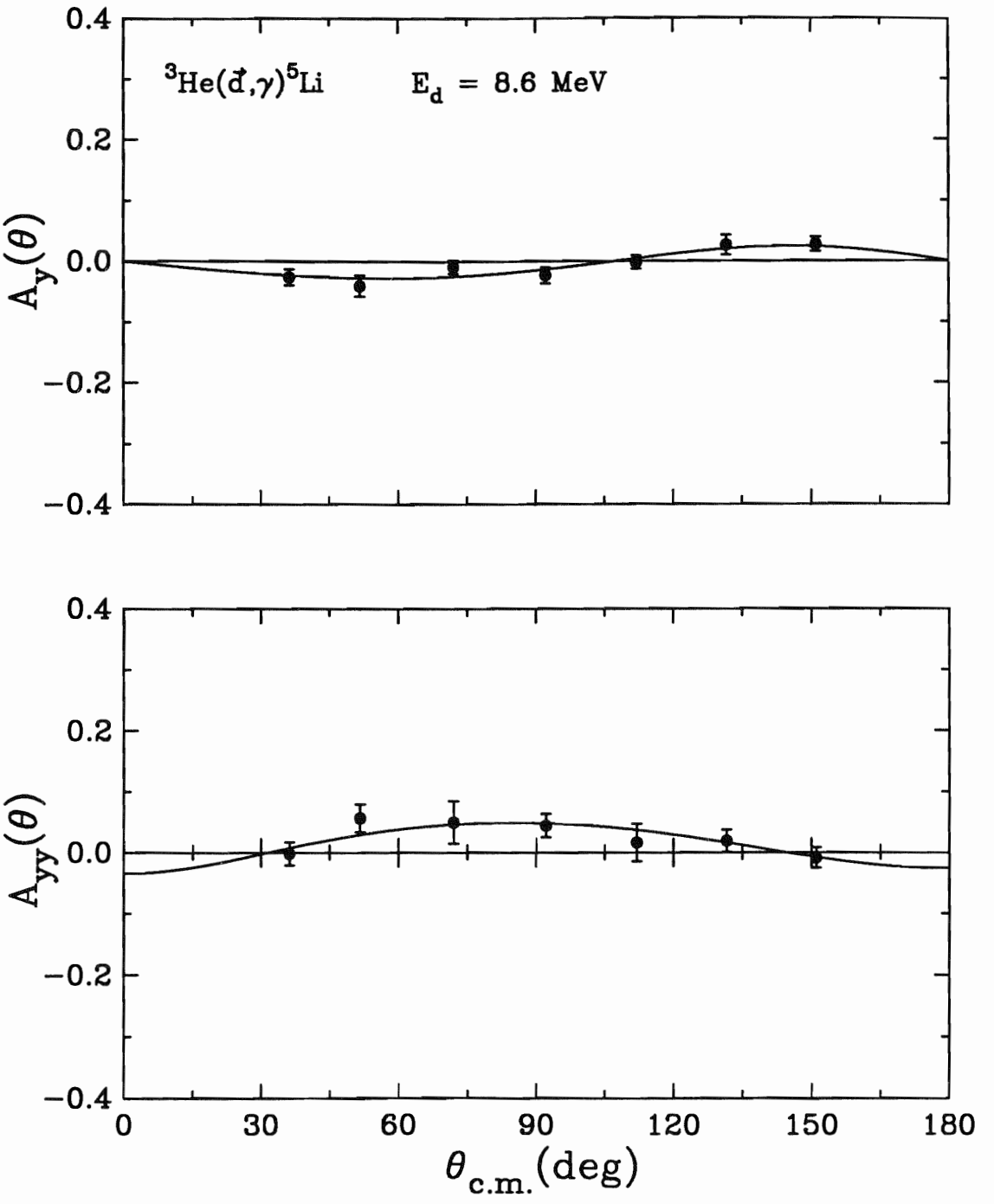

Fig. 5.6 $A_y(\theta)$ and $A_{yy}(\theta)$ from the ^{3}He(d,γ)^{5}Li reaction at E_d = 8.6 MeV are shown along with the results of the TME analysis. The solid lines represent the solution of Table 5.5.

5.4.5 Discussion

It should be noted that the results of all of the TME analyses, both in the fusion-resonance region and at $E_d = 8.6$ MeV, indicate that there are TME's with large intensities which arise from S=3/2 capture to the ground state via E1 radiation. As discussed previously, the dominant term of the E1 operator has a $\Delta S=0$ selection rule, meaning that it does not change the channel spin in the transition from the scattering state to the ground state. The most obvious mechanisms for an E1 γ-ray transition to the $3/2^-$ ground state of ^{5}Li is that the S=3/2 continuum state decays to the S=3/2 component of the ground state. However, in the single-particle model, the ^{5}Li ground state has S=1/2 since it consists predominantly of a proton in the $p_{3/2}$ orbital above a closed $s_{1/2}$ ^{4}He core (in LS coupling L=1, S=1/2). This suggests that capture to the S=3/2 component of the ground state is a small effect unless the tensor force acts to produce a larger-than-expected S=3/2 component. Another mechanism which can cause large S=3/2 capture strengths is the mixing of the S=3/2 and S=1/2 scattering states by the tensor force, allowing the transition to the S=1/2 component of the ground state. In order to investigate this further, it is necessary to employ some nuclear model calculations. The theory and results from a Direct-Capture Model and a Multi-Channel Resonating Group Model will be discussed in the next two chapters.

Chapter 6: The Direct Capture Calculation at E_d = 0.45 MeV

Introduction

Our first effort to investigate the $^3He(\vec{d},\gamma)^5Li$ reaction within a theoretical framework utilized the Direct Capture (DC) model. In the DC model, this reaction is a one-step process in which the scattering states and the ground state are described by a point-deuteron cluster coupled to a point-^3He cluster. Transition matrix elements (TME's) for E1 transitions from the $^2s_{1/2}$ and $^4s_{3/2}$ continuum states to the $P_{3/2}$ ground state of ^5Li were calculated in the fusion resonance region. Since only the non-spin-flip E1 operator is considered, the S (=1/2 or 3/2) of the ground state must be the same as that of the scattering state in the E1-only calculation. In other words, the $^2s_{1/2}$ scattering state captures into the $^2P_{3/2}$ piece of the ground-state wave function. Likewise, the $^4s_{3/2}$ scattering state captures into the $^4P_{3/2}$ piece of the ground-state wave function. Therefore, in this model, the relative strengths of the experimentally determined transition matrix elements are a direct measure of the admixture of S=1/2 and S=3/2 in the ground state.

Wave Functions

The ground-state wave function is generated from an optical model potential of the form:

$$V(r) = V_c(r) + V_n(r) \qquad [6.1]$$

where $V_c(r)$ is the coulomb potential. $V_n(r)$ is a real central potential with the Woods-Saxon form:

$$V_n(r) = \frac{V_n}{1 + e^{(r-r_0)/a_0}} \qquad [6.2]$$

V_n is adjusted such that the calculated binding energy of ^5Li agrees with experimental measurements. Although the ^5Li nucleus is unbound in the p+α channel, it is bound by

16.388 MeV in the d+^{3}He channel which is the only channel included in this DC model. Since no optical model parameters at the fusion resonance energy were available, the optical model parameters r_0 and a_0 were taken to have average values as given in [Per76]. The values of the V_n, r_0, and a_0 which were used are:

$$V_n = -93.04 \text{ MeV}, \quad r_0 = 1.25 \text{ fm}, \quad a_0 = 0.65 \text{ fm} \qquad [6.3]$$

The scattering-state wave function is described by a distorted wave which is derived from the same real optical model as the ground-state wave function.

As discussed in Chapter 1 and Section 5.4.5, the fact that the fusion resonance is seen in the γ-ray channel can be accounted for if a large admixture of the ground state of ^{5}Li is in an S=3/2 state. This is necessary since the $\Delta S=0$ selection rule for the dominant term of the E1 operator will only allow transitions from the $J^\pi=3/2^+$ fusion resonance (which has L=0, S=3/2) to the S=3/2 admixture of the ground state. The ground-state wave function can be written as:

$$\Psi_{g.s.} = \rho \, |S=1/2\rangle + \sqrt{1-\rho^2} \, |S=3/2\rangle, \qquad [6.4]$$

and calculated as a function of ρ.

Results

Transition matrix elements were calculated for several values of ρ using the above wave functions and the Siegert E1 operator. The Legendre coefficients $\bar{a}_2$, $\bar{b}_2$, $\bar{c}_0$, $\bar{c}_2$, and $\bar{e}_2$ (see Section 5.3.1) were then computed as a function of ρ. It was found that only $\bar{b}_2$, $\bar{c}_2$, and $\bar{e}_2$ are sensitive to the spin admixture in the ground state. Fig. 6.1 plots these coefficients as a function of ρ. Also plotted are the values of these coefficients which were extracted in a Legendre fit to the data taken at E_d=0.8-0.0 MeV. Together the DC model and the Legendre fits indicate that the fraction of S=3/2 in the ground state (denoted by $1-\rho^2$) of ^{5}Li is between 0.84 and 0.98.

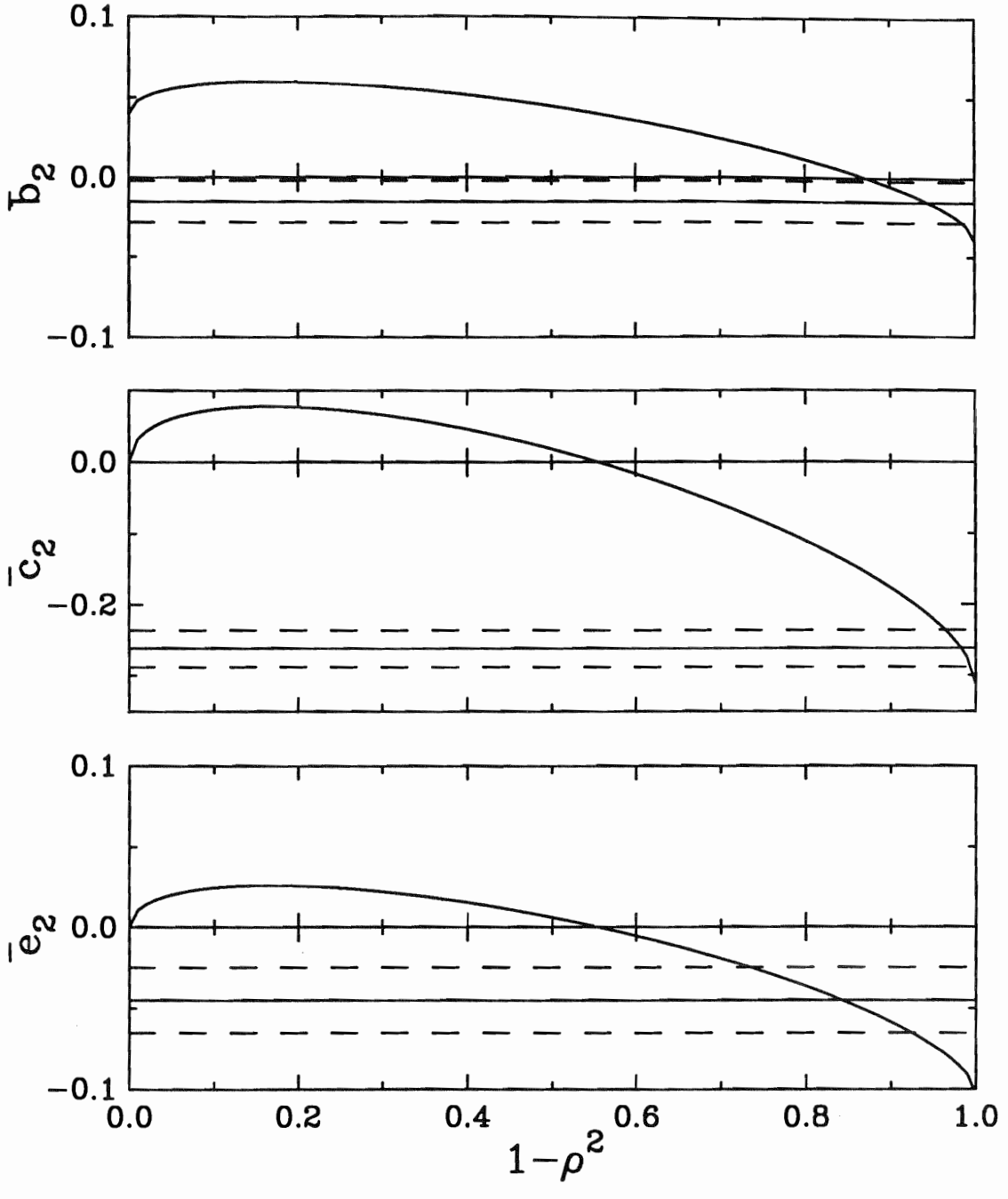

Fig. 6.1 The Legendre coefficients $\bar{b}_2$, $\bar{c}_2$, and $\bar{e}_2$. $1-\rho^2$ represents the fraction of S=3/2 in the ground state of ^{5}Li. The curves are from a Direct Capture calculation. The solid horizontal lines are the values of the coefficients obtained from the Legendre fits to the data taken at E_d=0.8-0.0 MeV. The dashed lines represent the errors on these fits.

Limitations of the model

The DC model prediction of > 80% S=3/2 in the ground-state wave function appears to be unphysical. Certainly from a simple shell-model picture, the ground state of ^{5}Li should be predominantly S=1/2 since it consists of a proton in the $p_{3/2}$ shell above a closed α core. So what has gone wrong in this model?

The first shortfall is in the application of the model. In a resonance region, direct capture is not necessarily the dominant capture process. This poses a large problem if one is trying to calculate the absolute cross section [Bro64], however the analyzing powers and the dimensionless Legendre coefficients are not necessarily affected.

The second, more fundamental problem is that the model is confined to considering only the d+^{3}He cluster configuration. Certainly the ground state, which decays to a proton and an α particle within 10^{-21} seconds, must include the p+α configuration in its wave function. The continuum wave functions must also include p+α channels as evidenced by the large cross section for the ^{3}He(d,p)^{4}He reaction [Ajz88]. In order to include this channel in the theoretical framework, the more sophisticated Resonating Group Model is needed. Chapter 7 presents the results of this calculation. It will be shown that the admixture of S=3/2 in the ground state is small and that the large capture cross section is due to the coupling of the $[d+^3He]^{S=3/2}_{J=3/2}$ scattering channel to the $[p+^4He]^{S=1/2}_{J=3/2}$ scattering channel by the tensor force.

Chapter 7: The Multichannel Resonating Group Model

7.1 Introduction

One of the myriad of problems encountered when modeling nuclear reactions is that of effectively manipulating the large number of degrees of freedom. The Resonating Group Model (RGM), which was first proposed by Wheeler [Whe37] accomplishes this by clustering nucleons into bound substructures which have no internal degrees of freedom. For example, ^{5}Li can be described as an α-particle coupled with a proton, or as a deuteron coupled with a ^{3}He nucleus. The total wave function of the ^{5}Li nucleus is then described as a linear combination of cluster wave functions multiplied by their respective relative-motion wave functions [Hof86]. These wave functions are totally antisymmetrized in order to adhere to the Pauli Principle and optimized according to the prescription of the variational principle. Thus, the calculations can be improved by expanding the model-space to include more clusters or more sophisticated internal cluster wave functions.

7.2 Description of the cluster wave functions

In the current RGM calculation, ^{5}Li is described using three cluster wave functions and the proton. The three clusters are the deuteron, the nucleus of ^{3}He, and the α-particle. The proton is described simply as a point particle. The three clusters have a more complicated radial expression of the form:

$$\Psi(r) = C_1 e^{-b_1 r^2} + C_2 e^{-b_2 r^2}. \qquad [7.1]$$

The C_1, C_2, b_1, and b_2 coefficients for the present case were obtained by H.M. Hofmann using the Ritz variational principle [Mer86] and therefore yield upper bounds on the binding energy of each cluster. The coefficients for the three cluster wave functions as well as the calculated and experimental binding energies of each cluster are listed in Table 7.1.

Table 7.1 The parameters for the three clusters used to describe ^{5}Li are given along with the binding energy of each cluster obtained with these parameters. The experimentally determined binding energy of each cluster is also given for comparison.

cluster	C_1	C_2	b_1 (fm^{-2})	b_2 (fm^{-2})	B.E. (RGM) (MeV)	B.E. (Exp.) (MeV)
deuteron	0.5320	0.1492	0.3204	0.0403	-1.35	-2.23
^{3}He	0.1428	0.0184	0.293	0.084	-3.98	-7.72
α-particle	5.2018	0.0658	0.324	0.084	-21.43	-28.30

7.3 The ground-state wave function of ^{5}Li

Now that the cluster wave functions have been described, they can be combined along with relative-motion wave functions to generate the total ground-state wave function of ^{5}Li. In general, this wave function, as described by [Mer86], is:

$$\mathcal{A}(\psi^{Jj}) = \mathcal{A} \sum_{\alpha m \sigma} c_\alpha^{LSJ} \, (LmS\sigma|Jj) \, |\alpha Lm\rangle |\alpha S\sigma\rangle \qquad [7.2]$$

where L is the relative orbital angular momentum of the cluster pairs, S is their total spin, and J is their total angular momentum L+S. Their projections are denoted by m, σ, and j respectively. All other quantum numbers and all of the different cluster decompositions are denoted by the symbol α. The c_α^{LSJ} coefficients are the free parameters that are minimized in the variational calculation.

For the description of the ^{5}Li ground state, three cluster configurations have been used: $[p+^4He]^{S=1/2}$, $[d+^3He]^{S=1/2}$, and $[d+^3He]^{S=3/2}$, where the cluster pairs are in a relative P-state and their total angular momentum is J = 3/2. The radial wave function for each cluster pair is then described by

$$|\alpha Lm\rangle = (\Psi_1\Psi_2)Y_{Lm}e^{-\gamma r^2}, \qquad [7.3]$$

where α denotes the cluster configuration, L=1, and the Ψ_i represent the internal cluster wave functions from Eqn. 7.1. The coefficient γ in the exponential determines the distance between the two clusters (for example, between the α-particle and the proton). For a bound nucleus, the γ's can also be used as free parameters in the variational calculation. However, the ^{5}Li ground state is unbound in the α+p channel. If the distance between α and proton clusters is used as a free parameter in the variational calculation, the result will be an infinite separation between them. It was therefore necessary to fix the distance between the clusters to values which reproduced the binding energy of ^{5}Li reasonably well. The calculated binding energy is -20.7476, which underestimates the experimental value of -26.331 MeV. This variational calculation was carried out using the phenomenological soft-core nucleon-nucleon potential of [Mer86].

The overlap integral of each cluster configuration with the total ground-state wave function is defined as:

$$\text{Overlap Integral} = \frac{\langle \alpha | {}^5\text{Li} \rangle}{\sqrt{\langle \alpha | \alpha \rangle} \sqrt{\langle {}^5\text{Li} | {}^5\text{Li} \rangle}} \qquad [7.4]$$

where $\langle\alpha|$ represents one of the three cluster-configuration wave functions and $\langle{}^5\text{Li}|$ represents the total ^{5}Li ground-state wave function. Table 7.2 gives the values for γ, the coefficients c_α^{LSJ} and the overlap integral for each cluster configuration. According to this calculation, the ^{5}Li nucleus is almost entirely in the $[\alpha+p]^{S=1/2}$ configuration, which is consistent with the shell model description. The non-zero value for the $[d+{}^3\text{He}]^{S=1/2}$ overlap is due to the non-orthogonality of the two S=1/2 configurations.

Table 7.2 For each of the three cluster configurations, the coefficients c_α^{LSJ} and the parameters γ of Eqns. 7.2 and 7.3 are listed. The values of the c_α^{LSJ} coefficients were obtained from a variational calculation which used the effective soft-core nucleon-nucleon potential of [Mer86]. Also given are the overlap integrals of each cluster-configuration wave function with the total ground-state wave function of ^{5}Li as defined in Eqn. 7.4.

Configuration	c_α^{LSJ}	γ (fm^{-2})	overlap
$[p+^4He]^{S=1/2}$	1.89×10^{-5}	0.005	0.9996
$[d+^3He]^{S=1/2}$	-23.70×10^{-5}	0.07	0.1424
$[d+^3He]^{S=3/2}$	1.98×10^{-5}	0.07	0.0010

7.4 The scattering wave function

The scattering wave function is described by the same cluster configurations which were used to describe the ground state of ^{5}Li and is constructed according to Eqn. 7.2, however now all values of J^π which are allowed by the angular-momentum coupling algebra are used. The scattering wave function includes an interaction region where all channels are open and a tail which reproduces the long-range Coulomb piece of the wave function. The interaction region is constructed as a sum of regular and irregular Coulomb waves and square-integrable functions of the form $R^{L+1}e^{-\delta R^2}$, where R is the relative-motion coordinate between the two clusters.

In order to simplify the calculation, the regular and irregular Coulomb waves are approximated by 20 square-integrable functions which are chosen in such a way that different partial waves (predominantly s, p, and d waves) can be reproduced by the 20 Gaussians over a wide range of energies. If the Gaussians are not carefully chosen, some terms may become linearly dependent within the numerical accuracy of the computer. Therefore, a trial-and-error procedure which was previously performed by H.M.

Hofmann [HofPri] started with a relatively small number of Gaussians and added more as needed. The 20 values of δ (fm^{-2}) used are:

5.0, 1.7, 0.7, 0.35, 0.15, 0.07, 0.04, 0.025, 0.015, 0.01, 0.007, 0.005, 0.0035, 0.0025, 0.0015, 0.001, 0.0007, 0.0004, 0.0002, and 0.0001.

Accurately describing the long-range behavior of the scattering wave function is important in low-energy reactions which are less sensitive to the interior of the wave function and in radiative-capture reactions where the electric-dipole operator weights the scattering wave function by r in the transition matrix element, thereby increasing the sensitivity to its long-range behavior.

7.5 The nuclear potential and phase shifts of the d+^{3}He and p+α reactions

The Resonating Group Model calculations performed for this experiment use the phenomenological local soft-core nucleon-nucleon potential of [Mer86] which is described by the same formalism as discussed in [Eik71]. This potential is derived from a realistic potential and transformed such that no D-state is necessary to bind the deuteron. The four states of the two-nucleon system have S = 0 or 1, and T = 0 or 1. Therefore, the two-nucleon potential is decomposed into four different potentials, with each operating on one of these four two-nucleon states. More specifically, the potential is written as:

$$V = V^{1+}P^{1+} + V^{1-}P^{1-} + V^{3+}P^{3+} + V^{3-}P^{3-} \qquad [7.5]$$

where the P's are projection operators for the four states. In the potential of [Eik71] no singlet-odd term is used. The three potentials are given by:

$$V^{1+} = V_C^{1+}(r), \qquad [7.6a]$$

$$V^{3+} = V_C^{3+}(r) + V_{LS}^{3+}(r)(\mathbf{L}\cdot\mathbf{S}) + r^2V_T^{3+}(r)S_{12}, \qquad [7.6b]$$

$$V^{3-} = V_C^{3-}(r) + V_{LS}^{3-}(r)(\mathbf{L}\cdot\mathbf{S}) + r^2V_T^{3-}(r)S_{12}, \qquad [7.6c]$$

where $V_C(r)$, $V_{LS}(r)$, and $V_T(r)$ give the radial dependence of the central, spin-orbit, and tensor pieces of the potential, respectively. The terms in the potentials are defined by:

$$V_C^{1+}(r) = \sum_{i=1}^{N} A_C^{1+,i} \exp(-B_C^{1+,i} r^2), \qquad [7.7]$$

$$\mathbf{L}\cdot\mathbf{S} = \frac{1}{2\hbar}\mathbf{r} \times \mathbf{p} \cdot (\sigma_1+\sigma_2), \qquad [7.8]$$

and $$S_{12} = \frac{3(\sigma_1\cdot r)(\sigma_2\cdot r)}{r^2} - \sigma_1\cdot\sigma_2, \qquad [7.9]$$

where the other radial functions V(r) are expressed analogously to $V_C^{1+}(r)$. The parameters A and B of the potential are given in Table 7.3.

In order to determine how well this potential describes the d+^{3}He reactions, phase shifts were calculated for the d+^{3}He and p+α elastic scattering reactions. Only one phase shift analysis [Jen80] of the d+^{3}He reaction exists. Unfortunately, multiple solutions were found. Therefore, it was necessary to compare the calculated p+α phase shifts to the experimentally determined phase shifts of [Hou78], [Pla72], and [Sch71]. Two phase shifts were found to be particularly sensitive to variations of the strengths of the spin-orbit and tensor forces. The $^2d_{3/2}$ phase shift clearly exhibits the $3/2^+$ fusion resonance. Although the energy of the fusion resonance is calculated to be too low (a general failing of most RGM models), the strength of the resonance was found to depend almost exclusively on the tensor force. By increasing the tensor force to 1.75 times its two-body value, agreement between the theory and experimental values was obtained. The spin-orbit force was also adjusted to 0.75 times its two-body value in order to reproduce the $^2d_{5/2}$ phase shift. Figs 7.1 through 7.3 plot the experimental ^{4}He(p,p)^{4}He phase shifts of [Hou78], [Pla72], and [Sch71] against three sets of RGM-calculated phase shifts . These three RGM calculations used the potential of [Mer86] with different

strengths of the spin-orbit and tensor forces, i.e. the two-body potential, the phase-shift adjusted strengths described above, and the two-body potential with the tensor-force strength set to 0. Figs. 7.4 through 7.6 plot the experimental ^{3}He(d,d)^{3}He phase shifts of [Jen80] against the three sets of RGM-calculated phase shifts.

Table 7.3 The coefficients of the phenomenological local soft-core nucleon-nucleon potential of [Mer86] are listed. The width parameters B are given in units of fm^{-2}, and the strength parameters A in units of MeV.

$A_C^{1+,1} = -692.60$	$A_C^{3+,1} = -510.32$	$B_C^{1+,1}=B_C^{3+,1}= 7.1199$
$A_C^{1+,2} = 904.72$	$A_C^{3+,2} = 681.06$	$B_C^{1+,2}=B_C^{3+,2}= 4.8092$
$A_C^{1+,3} = -77.031$	$A_C^{3+,3} = -8.004$	$B_C^{1+,3}=B_C^{3+,3}= 0.6409$
$A_C^{1+,4} = -692.60$	$A_C^{3+,4} = -510.32$	$B_C^{1+,4}=B_C^{3+,4}= 7.1199$
$A_{LS}^{3+,1} = 214.585$	$A_{LS}^{3-,1} = -262.507$	$B_{LS}^{3+,1}=B_{LS}^{3-,1}= 1.7888$
$A_{LS}^{3+,2} = -0.811$	$A_{LS}^{3-,2} = -25.772$	$B_{LS}^{3+,2}=B_{LS}^{3-,2}= 1.2851$
$A_T^{3+,1} = -102.692$	$A_T^{3-,1} = -8.129$	$B_T^{3+,1}=B_T^{3-,1}= 1.0942$
$A_T^{3+,2} = -2.740$	$A_T^{3-,2} = 25.105$	$B_T^{3+,2}=B_T^{3-,2}= 0.8364$
$A_T^{3+,3} = -1.863$	$A_T^{3-,3} = 0.613$	$B_T^{3+,3}=B_T^{3-,3}= 0.2380$

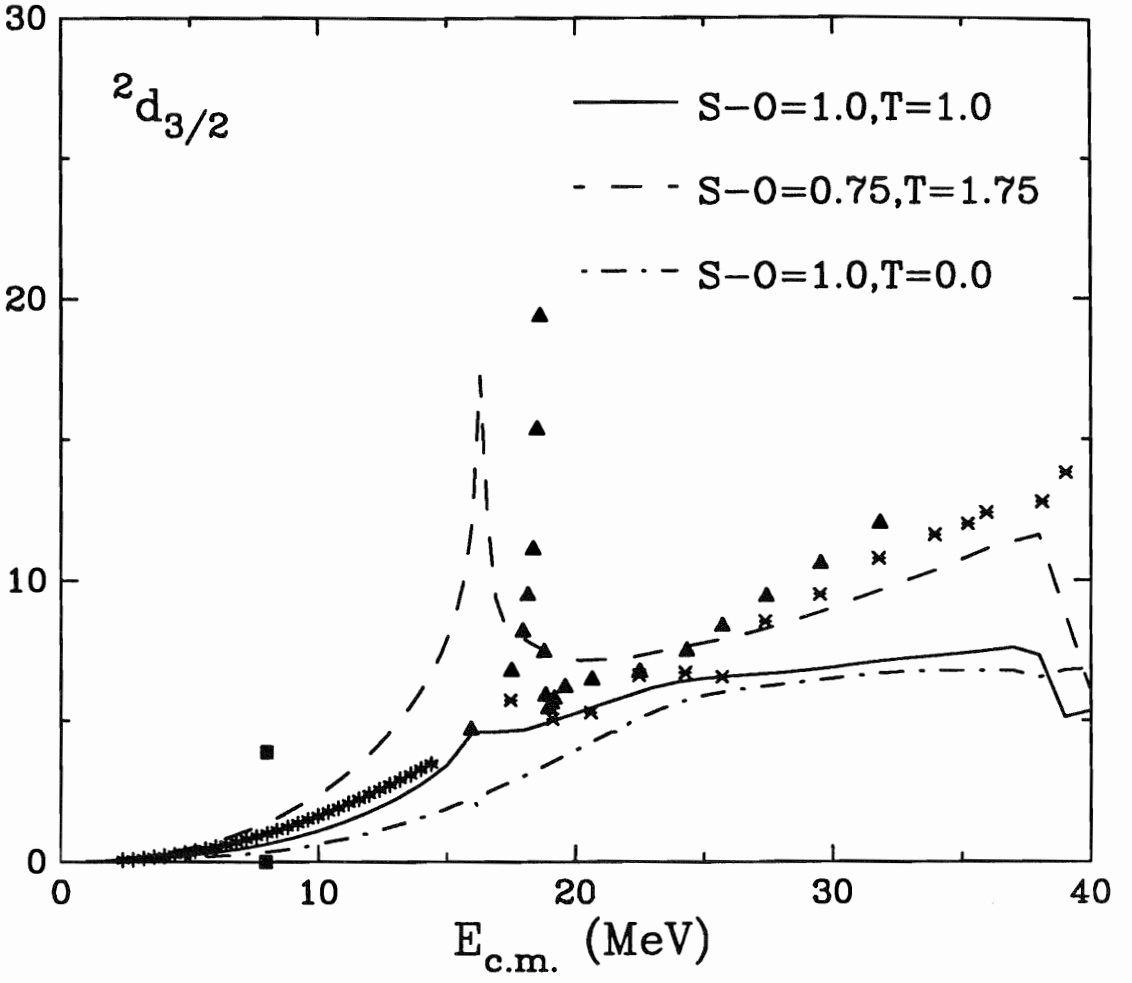

Fig. 7.1 The experimental ^{4}He(p,p)^{4}He phase shifts of [Hou78], [Pla72], and [Sch71] are plotted against the three sets of RGM-calculated phase shifts as described in the text.

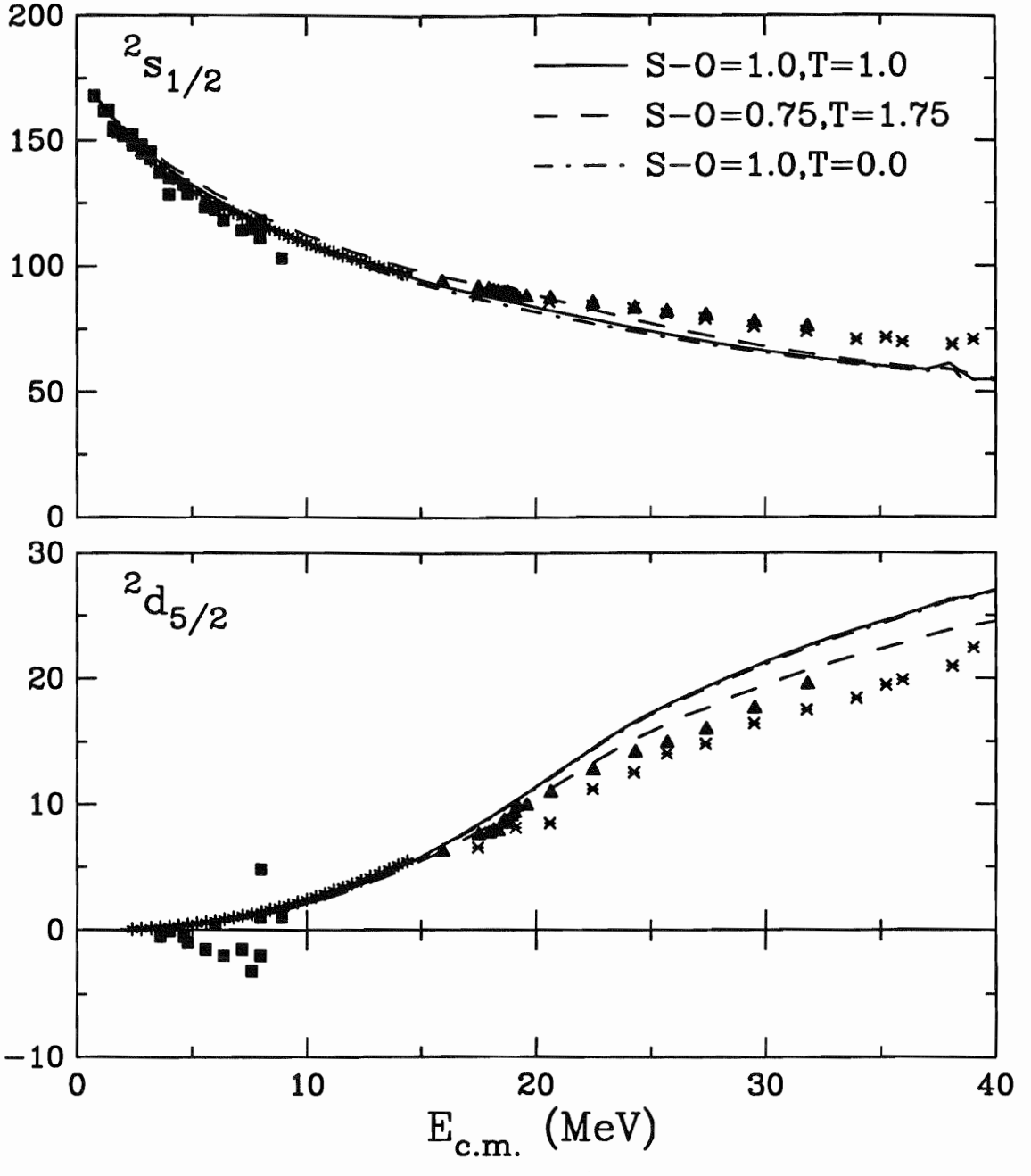

Fig. 7.2 More ^{4}He(p,p)^{4}He phase shifts from [Hou78], [Pla72], and [Sch71] and the three sets of RGM-calculated phase shifts as described in the text.

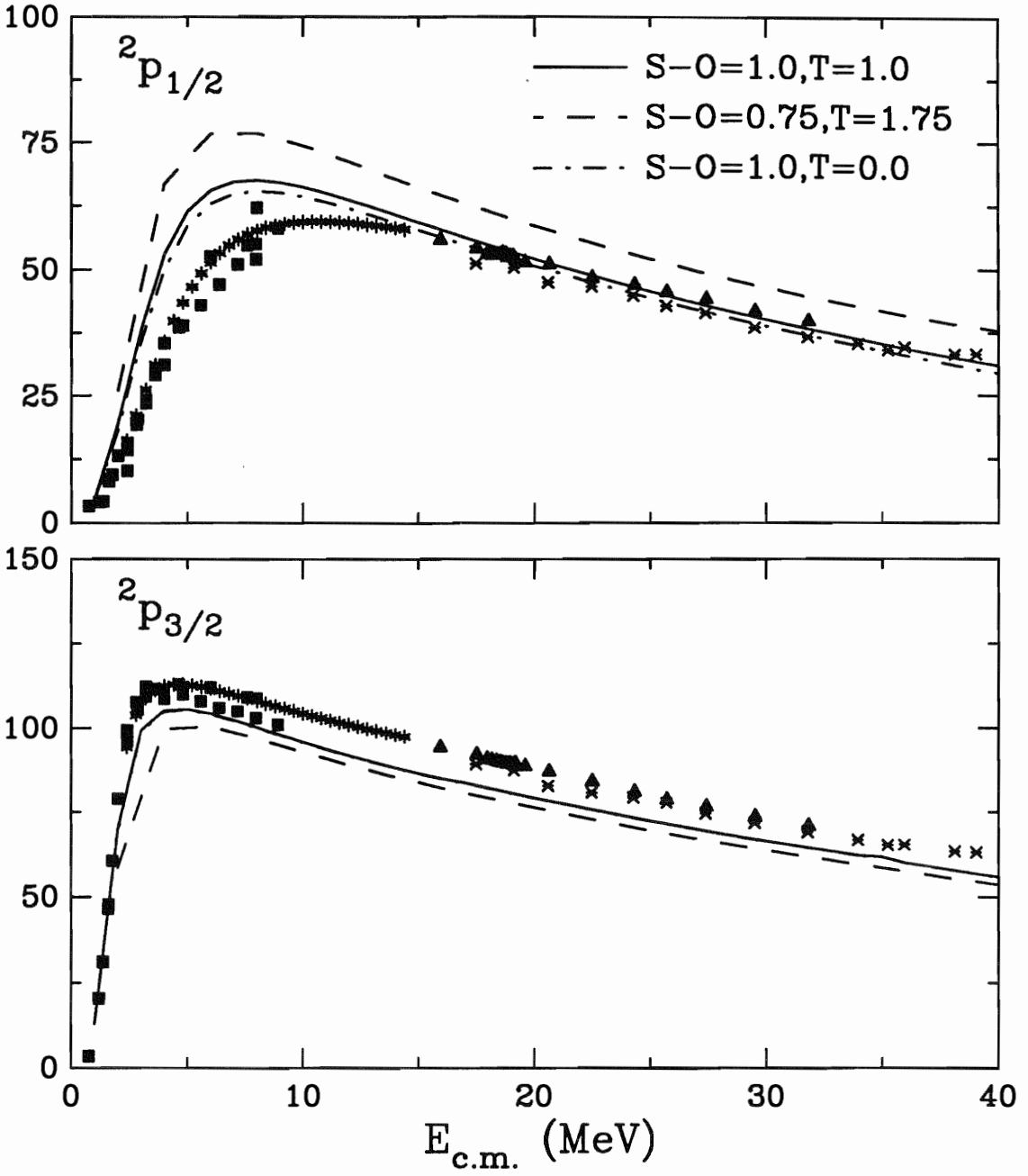

Fig 7.3 Still more ^{4}He(p,p)^{4}He phase shifts from [Hou78], [Pla72], and [Sch71] and the three sets of RGM-calculated phase shifts as described in the text.

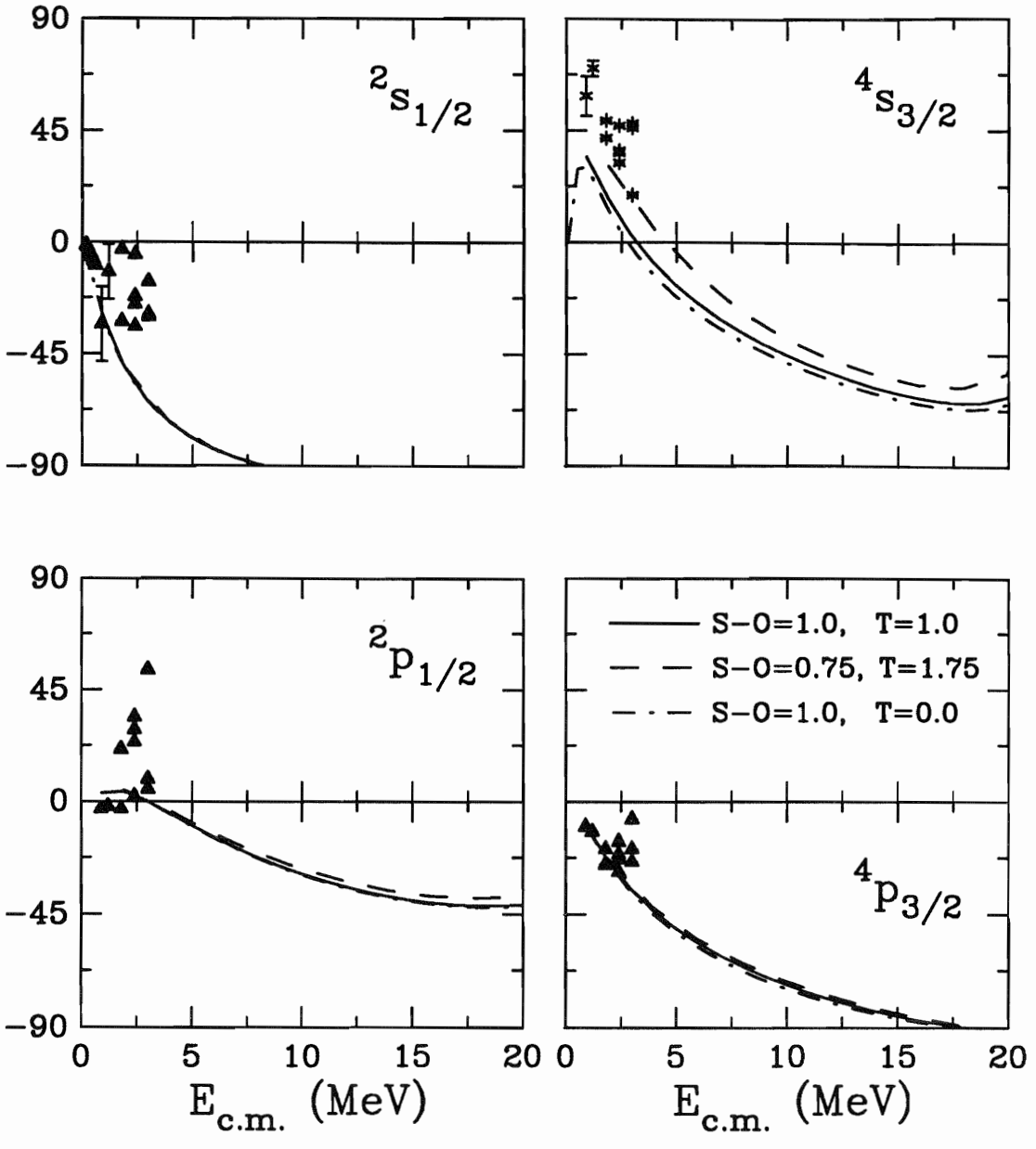

Fig. 7.4 The ^{3}He(d,d)^{3}He phase shifts of [Jen80] are plotted against the three sets of RGM-calculated phase shifts as described in the text.

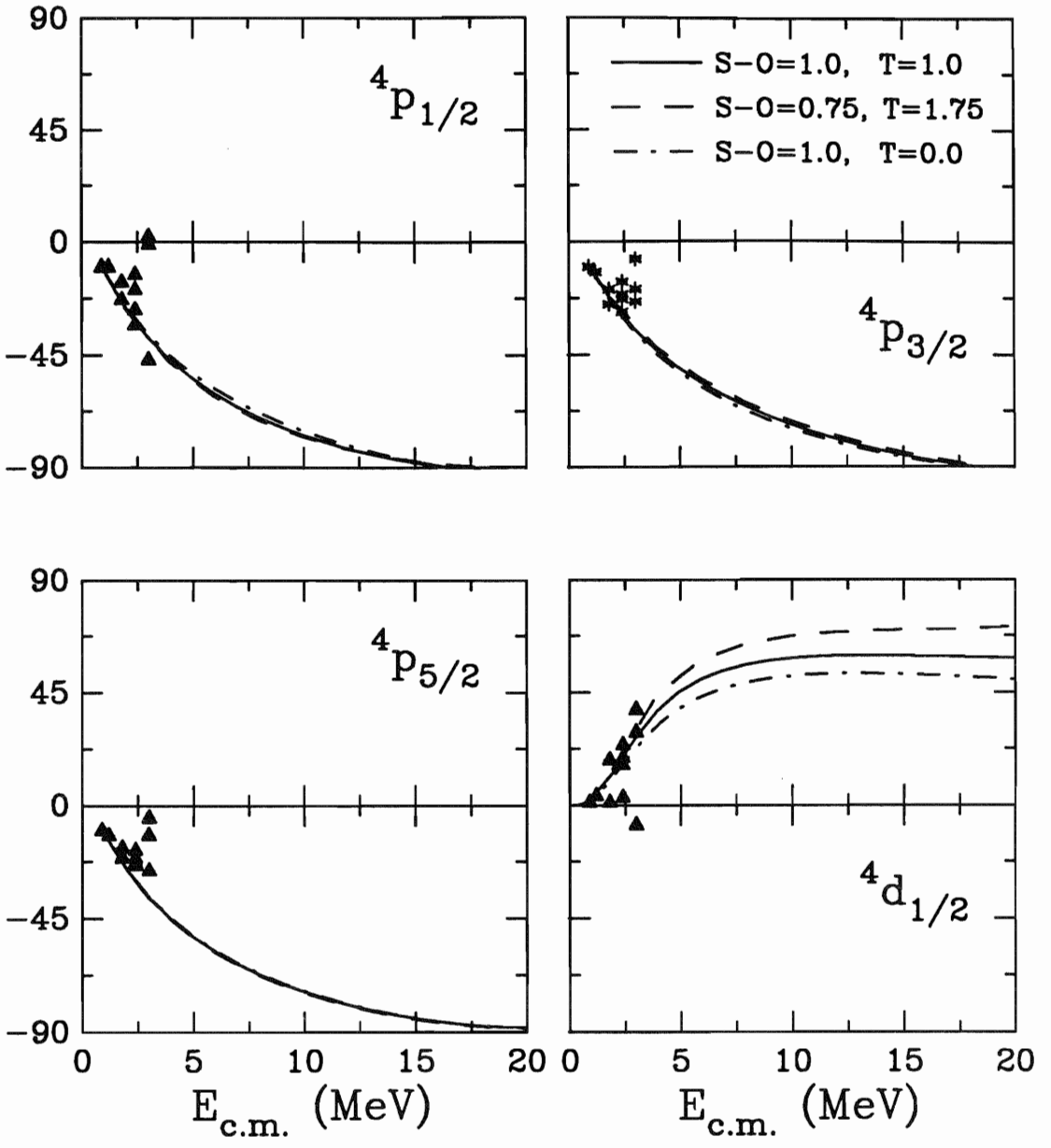

Fig. 7.5 More ^{3}He(d,d)^{3}He phase shifts from [Jen80] are plotted against the three sets of RGM-calculated phase shifts as described in the text.

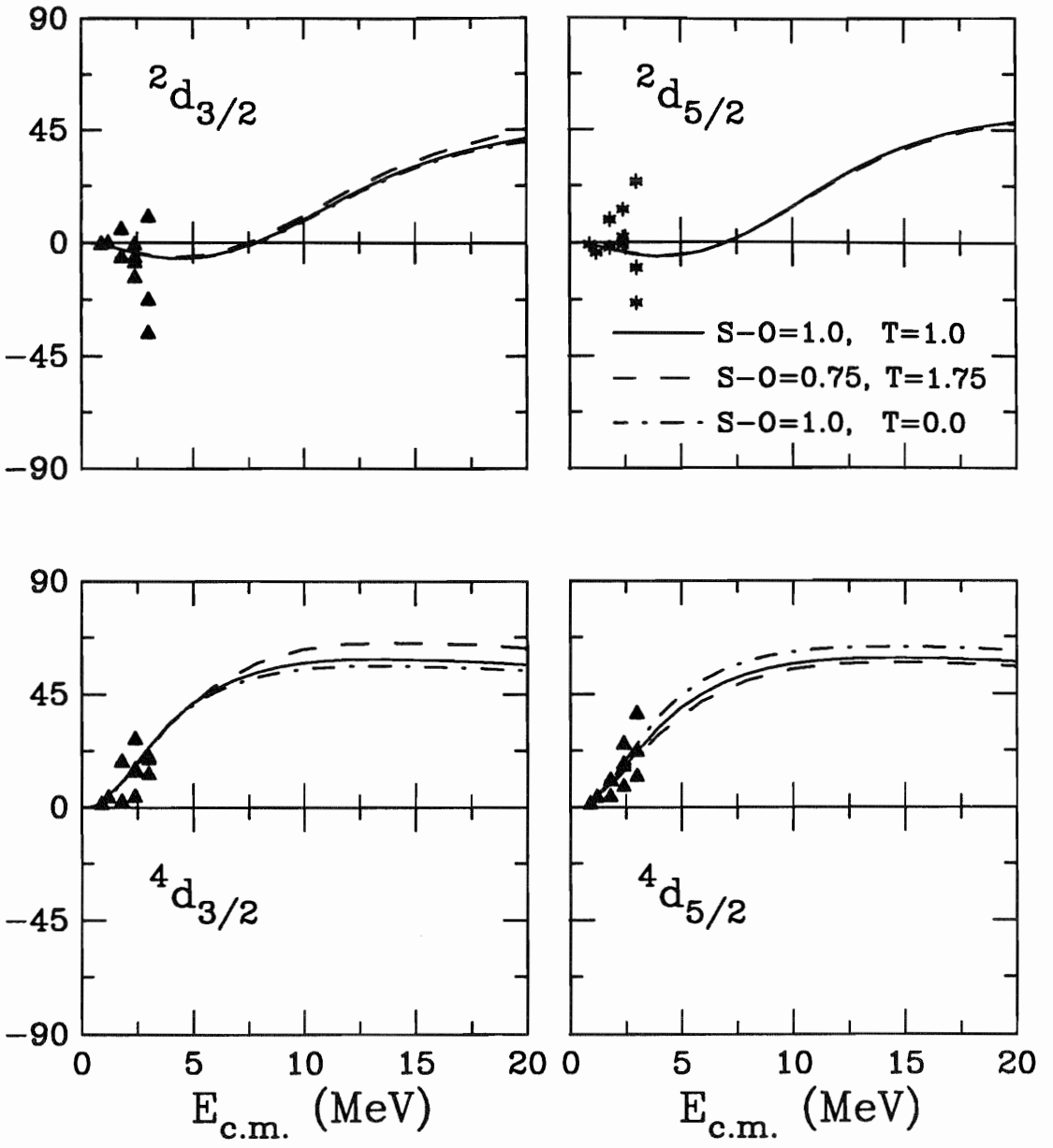

Fig. 7.6 Still more ^{3}He(d,d)^{3}He phase shifts from [Jen80] are plotted against the three sets of RGM-calculated phase shifts as described in the text.

7.6 The electromagnetic transition operators

A multipole expansion of the electromagnetic field in the long-wavelength limit yields the electromagnetic transition operators:

$$O(E,L\mu) = \sum_{j=1}^{A} e g_{l_j} r_j^L Y_{L\mu}(\hat{\mathbf{r}}_j), \qquad [7.10]$$

$$O'(E,L\mu) = -\sum_{j=1}^{A} g_{s_j} \frac{e}{2mc} \frac{k}{L+1} \mathbf{L}(r_j^L Y_{L\mu}(\hat{\mathbf{r}}_j)) \cdot \mathbf{S}_j \quad \text{where} \quad \mathbf{L} = -i\mathbf{r}\times\nabla \qquad [7.11]$$

$$O(M,L\mu) = \sum_{j=1}^{A} 2g_{l_j} \frac{e}{2mc} \frac{1}{L+1} \nabla(r_j^L Y_{L\mu}(\hat{\mathbf{r}}_j)) \cdot \mathbf{l}_j, \qquad [7.12]$$

$$O'(M,L\mu) = \sum_{j=1}^{A} g_{s_j} \frac{e}{2mc} \nabla(r_j^L Y_{L\mu}(\hat{\mathbf{r}}_j)) \cdot \mathbf{S}_j. \qquad [7.13]$$

where L and μ give the multipolarity of the transition and the electric and magnetic operators are labeled E and M, respectively. The g-factors for free nucleons are g_l(proton) = 1, g_l(neutron)=0, g_s(proton)=5.586, and g_s(neutron) = -3.826. Eqn. 7.10 is derived using Siegert's theorem and contains most meson-exchange current effects. The other operators do not include these effects.

7.7 Transition Matrix Element calculation at E_d = 0.45 MeV

Transition matrix elements were calculated at the $3/2^+$ fusion resonance (see Tables 7.4 and 7.5) for E1, M1, and E2 transitions using both the two-body potential (Calculation A) and the phase-shift adjusted potential (Calculation B). As shown in Figs. 7.7 through 7.10, both calculations reproduce the measured analyzing powers of the E_d=0.8-0.0 MeV and E_d=0.6-0.3 MeV experiments. Although the calculations were performed at the peak of the fusion resonance, energy averaging over the resonance (in

accordance with the data) does not change the results substantially since almost identical results were obtained at other energies in the averaging region. Of course, the calculated on-resonance absolute cross section is larger than the energy-averaged experimental values. However, even compared to the measured on-resonance cross sections of [Bla54] and [Bus68], Calculation A still overestimates the cross section by a factor of 2 and 5, respectively. It is interesting to note that a factor of 2 reduction in the calculated cross section can be obtained by reducing the tensor force strength to 0.75 times its two-body value (Calculation C). This reduction does not lead to any appreciable discrepancies with the measured analyzing powers.

In calculations A and B, the ${}^4s_{3/2}$(E1) transition matrix element dominates the capture cross section, contributing 98.5% and 99.8% of the cross section strength, respectively. The tensor force couples the $[d+{}^3He]^{S=3/2}_{J=3/2}$ scattering channel to the $[p+{}^4He]^{S=1/2}_{J=3/2}$ scattering channel, allowing the transition to the S=1/2 ground state to proceed via the dominant $\Delta S=0$ term of the E1 operator. To further examine the sensitivity of the calculation to the tensor force, a third calculation (Calculation D) was performed with the tensor force turned off. In this case (see Figs. 7.7 to 7.10), the tensor analyzing powers nearly vanish, the vector analyzing power becomes quite large, and the calculated cross section underestimates both measured cross sections by a factor of 16. These results differ from those of Calculations A and B due to the dramatic reduction in the strength of the ${}^4s_{3/2}$(E1) transition matrix element which now contributes less than 1% of the calculated cross section strength. This clearly demonstrates the importance of the tensor force in driving the $d+{}^3He$ fusion reaction in the region of the $3/2^+$ resonance.

Table 7.4 Transition matrix element relative intensities from a TME fit to the E_d=0.8 MeV data (two statistically significant solutions with χ^2=25) and the three RGM calculations. Calculation A uses the two-body potential. Calculation B uses the modified potential which has been adjusted to reproduce the ^{4}He(p,p)^{4}He phase shifts. Calculation C uses the two-body potential with the tensor force strength set to 0.75 times its two-body value. Calculation D uses the two-body potential with no tensor force.

	TME fits		RGM calculations			
	Solution 1	Solution 2	A	B	C	D
$^2s_{1/2}$ (E1)	0.03±0.03	0.48±0.06	0.013	0.002	0.026	0.913
$^4s_{3/2}$ (E1)	0.89±0.03	0.44±0.05	0.985	0.998	0.971	0.001
^2p	0.01±0.01	0.01±0.01	0.000	0.000	0.004	0.078
^4p	0.07±0.02	0.07±0.02	0.000	0.000	0.000	0.000

Table 7.5 Legendre polynomial coefficients from a direct fit to the E_d=0.8 MeV data, a TME fit to this data, and the RGM calculations. Calculation A uses the two-body potential. Calculation B uses the modified potential which has been adjusted to reproduce the ^{4}He(p,p)^{4}He phase shifts. Calculation C uses the two-body potential with the tensor force strength set to 0.75 times its two-body value. Calculation D uses the two-body potential with no tensor force. A_0 is given in units of μb/sr.

	Legendre fit	TME fit	RGM calculation			
			A	B	C	D
A_0	1.855 ± 0.012	1.85 ± 0.13	8.78	44.95	4.46	0.114
$\bar{a}_1$	-0.035 ± 0.013	-0.035 ± 0.011	0.004	0.002	0.006	0.010
$\bar{a}_2$	-0.061 ± 0.016	-0.065 ± 0.017	-0.005	-0.006	-0.006	-0.050
$\bar{b}_1$	0.032 ± 0.022	0.031 ± 0.020	-0.030	-0.007	-0.047	-0.371
$\bar{b}_2$	-0.009 ± 0.013	-0.010 ± 0.003	0.007	0.007	0.007	-0.034
$\bar{c}_0$	-0.030 ± 0.012	-0.001 ± 0.001	0.012	0.013	0.012	0.001
$\bar{c}_1$	0.011 ± 0.019	-0.020 ± 0.006	0.012	0.002	0.017	0.003
$\bar{c}_2$	-0.256 ± 0.023	-0.242 ± 0.025	-0.310	-0.293	-0.321	-0.011
$\bar{e}_2$	-0.046 ± 0.006	-0.099 ± 0.010	-0.127	-0.120	-0.131	-0.004

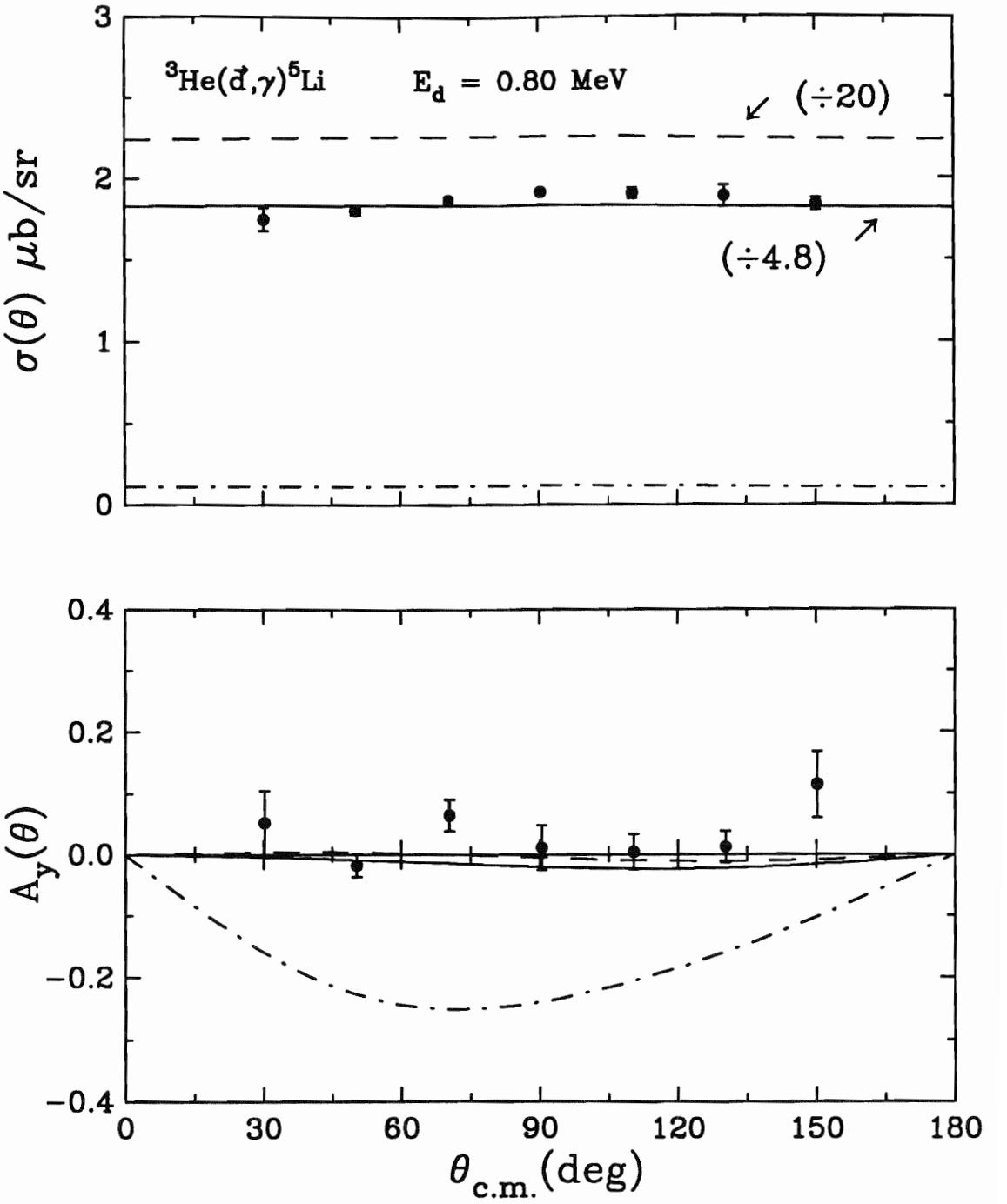

Fig. 7.7 $\sigma(\theta)$ and $A_y(\theta)$ from the ^{3}He($\vec{d}$,γ)^{5}Li reaction at E_d=0.8-0 MeV are shown along with the results of the three RGM calculations. The solid curve is Calculation A (two-body forces), the dashed curve is Calculation B (^{4}He(p,p)^{4}He phase shift adjusted forces), and the dashed-dotted curve is Calculation D which uses no tensor force.

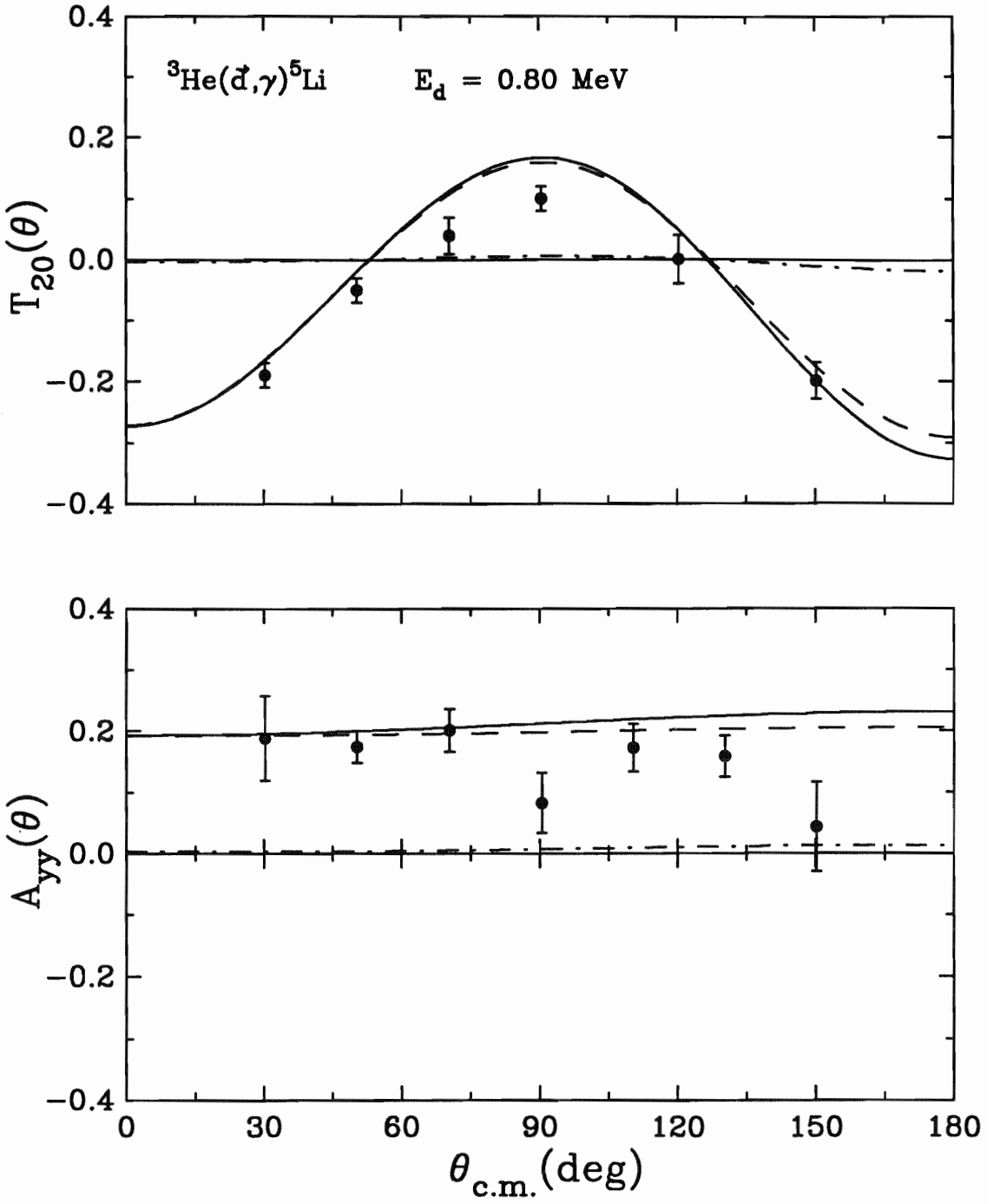

Fig. 7.8 $A_{yy}(\theta)$ and $T_{20}(\theta)$ from the ^{3}He($\vec{d}$,γ)^{5}Li reaction at E_d =0.8-0 MeV are shown along with the results of the three RGM calculations. The solid curve is Calculation A (two-body forces), the dashed curve is Calculation B (^{4}He(p,p)^{4}He phase shift adjusted forces), and the dashed-dotted curve is Calculation D which uses no tensor force.

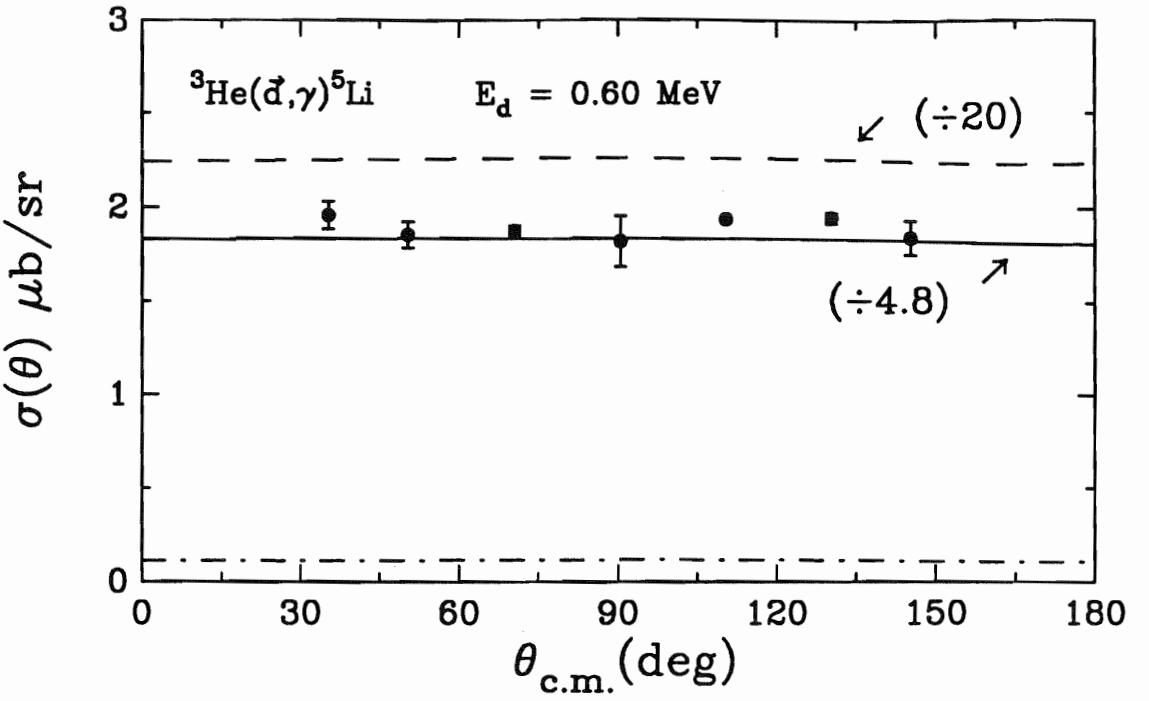

Fig. 7.9 $\sigma(\theta)$ from the ^{3}He($\vec{d}$,γ)^{5}Li reaction at E_d=0.6-0.3 MeV is shown along with the results of the three RGM calculations. The solid curve is Calculation A (two-body forces), the dashed curve is Calculation B (^{4}He(p,p)^{4}He phase shift adjusted forces), and the dashed-dotted curve is Calculation D which uses no tensor force.

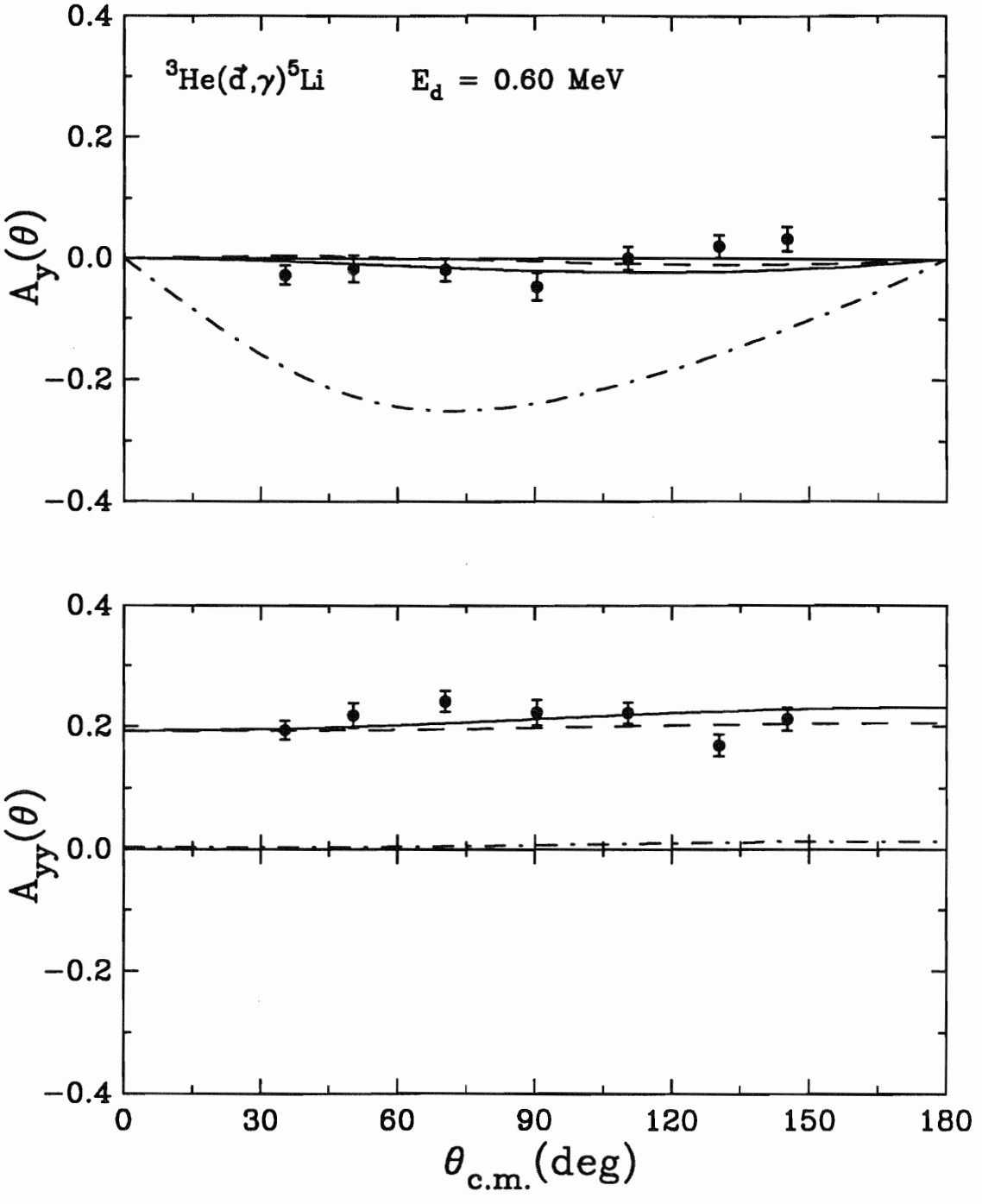

Fig. 7.10 $A_y(\theta)$ and $A_{yy}(\theta)$ from the ^{3}He($\vec{d}$,γ)^{5}Li reaction at E_d =0.6-0.3 MeV are shown along with the results of the three RGM calculations. The solid curve is Calculation A (two-body forces), the dashed curve is Calculation B (^{4}He(p,p)^{4}He phase shift adjusted forces), and the dashed-dotted curve is Calculation D which uses no tensor force.

7.8 Transition Matrix Element calculation at $E_d = 8.6$ MeV

Transition matrix elements have also been calculated for $E_d(\text{lab}) = 8.6$ MeV using the two-body potential (Calculation E), the phase-shift adjusted potential (Calculation F), and the two-body potential with the tensor-force strength set to 0 (Calculation G). All of the parameters of the calculation are exactly the same as were used for the calculation at $E_d(\text{lab}) = 0.45$ MeV. The results of these calculations are listed in Tables 7.6 and 7.7, and are plotted in Figs 7.11 and 7.12. At this energy, qualitative agreement with the measured cross section and analyzing powers was improved by turning off the tensor force (Calculation G). However, a comparison of transition matrix elements reveals that although these calculated observables reproduce the data better, the relative intensities of the transition matrix elements do not agree with those extracted from a TME fit to the data. In fact, a non-zero tensor force is necessary to get agreement between data and theory for the relative strengths of the TME's. As with the $E_d(\text{lab}) = 0.45$ MeV calculation, the ${}^4s_{3/2}(E1)$ transition matrix element dominates the capture cross section due to the coupling of the $[d+{}^3He]^{S=3/2}_{J=3/2}$ scattering channel to the $[p+{}^4He]^{S=1/2}_{J=3/2}$ scattering channel by the tensor force. In Calculation E, the ${}^4d_{3/2}(E1)$ TME contributes 14% to the cross section strength via this same tensor-force coupling mechanism and the ${}^2d_{5/2}(E1)$ TME contributes 22% of the cross section strength by coupling directly to the α+p channel. Only about 6% E2 radiation is present in the calculation and virtually no M1 radiation.

Table 7.6 Transition matrix element relative intensities from a TME fit to the E_d=8.6 MeV data (two statistically significant solutions) and the three RGM calculations.

	TME fit	RGM calculations		
		E	F	G
$^2s_{1/2}$ (E1)	0.148 ± 0.022	0.019	0.009	0.034
$^4s_{3/2}$ (E1)	0.653 ± 0.026	0.308	0.454	0.000
$^2d_{3/2}$ (E1)		0.061	0.036	0.101
$^2d_{5/2}$ (E1)		0.398	0.219	0.647
Total: ^{2}d(E1)	0.175 ± 0.015	0.459	0.255	0.748
$^4d_{1/2}$ (E1)		0.033	0.072	0.000
$^4d_{3/2}$ (E1)		0.043	0.142	0.000
$^4d_{5/2}$ (E1)		0.001	0.005	0.002
Total: ^{4}d(E1)	0.015 ± 0.006	0.077	0.219	0.002
$^2p_{1/2}$ (M1)		0.000	0.000	0.000
$^2p_{3/2}$ (M1)		0.001	0.000	0.001
$^4p_{1/2}$ (M1)		0.000	0.000	0.000
$^4p_{3/2}$ (M1)		0.000	0.000	0.000
$^4p_{5/2}$ (M1)		0.000	0.000	0.000
$^2p_{1/2}$ (E2)		0.003	0.001	0.009
$^2p_{3/2}$ (E2)		0.127	0.057	0.205
Total: ^{2}p(E2)	0.004 ± 0.004	0.131	0.058	0.215
$^4p_{1/2}$ (E2)		0.004	0.005	0.000
$^4p_{3/2}$ (E2)		0.000	0.000	0.000
$^4p_{5/2}$ (E2)		0.000	0.000	0.000
Total: ^{4}p(E2)	0.005 ± 0.001	0.004	0.005	0.000

Table 7.7 Legendre polynomial coefficients from a direct fit to the E_d=8.6 MeV data, a TME fit to this data, and the RGM calculations. Calculation E uses the two-body potential. Calculation F uses the modified potential which has been adjusted to reproduce the ^{4}He(p,p)^{4}He phase shifts. Calculation G uses the two-body potential with no tensor force.

	Legendre fit	TME fit	RGM calculation		
			E	F	G
A_0 (μb/sr)	2.147 ± 0.013	2.15 ± 0.082	4.96	7.82	3.07
$\bar{a}_1$	-0.138 ± 0.013	-0.140 ± 0.014	0.018	0.025	0.002
$\bar{a}_2$	-0.203 ± 0.017	-0.205 ± 0.024	-0.086	0.070	-0.189
$\bar{b}_1$	-0.015 ± 0.009	-0.015 ± 0.018	-0.107	-0.053	0.021
$\bar{b}_2$	-0.020 ± 0.007	-0.023 ± 0.009	0.122	0.127	-0.034
$\bar{c}_0$		0.229 ± 0.019	-0.004	-0.143	0.018
$\bar{c}_1$		-0.036 ± 0.005	-0.036	-0.059	-0.004
$\bar{c}_2$		-0.198 ± 0.015	-0.273	-0.344	-0.006
$\bar{e}_2$		-0.111 ± 0.006	-0.004	-0.024	-0.005

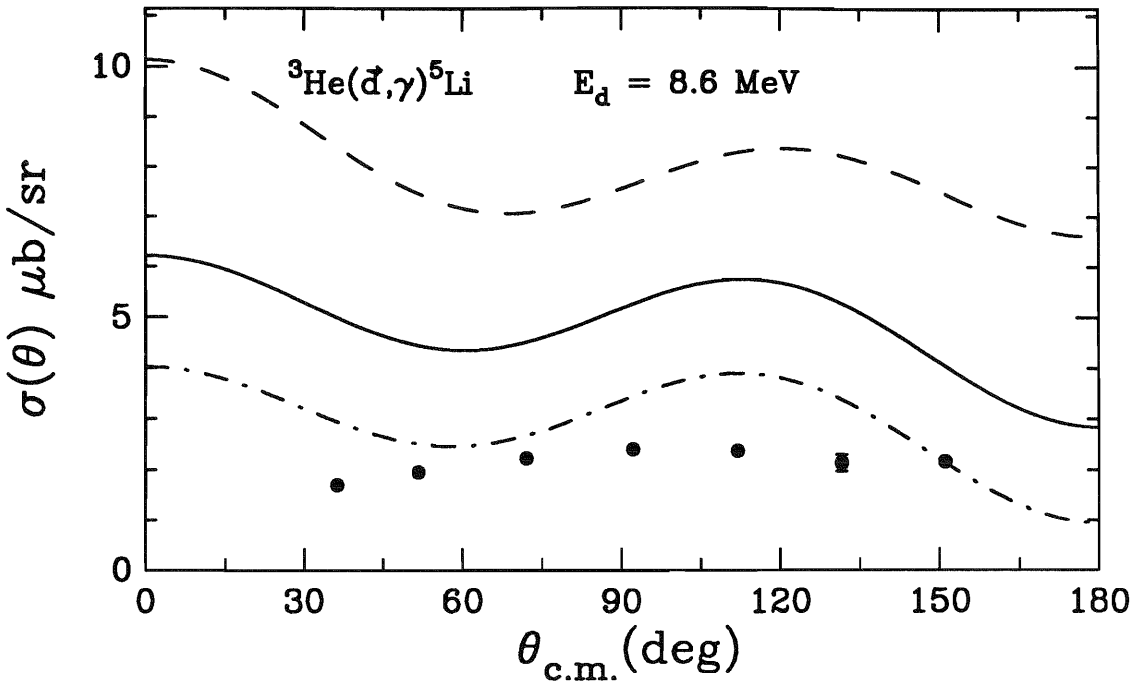

Fig. 7.11 $\sigma(\theta)$ from the ^{3}He($\vec{d}$,γ)^{5}Li reaction at E_d = 8.6 MeV is shown along with the results of the three RGM calculations. The solid curve is Calculation E (two-body forces), the dashed curve is Calculation F (^{4}He(p,p)^{4}He phase shift adjusted forces), and the dashed-dotted curve is Calculation G which uses no tensor force.

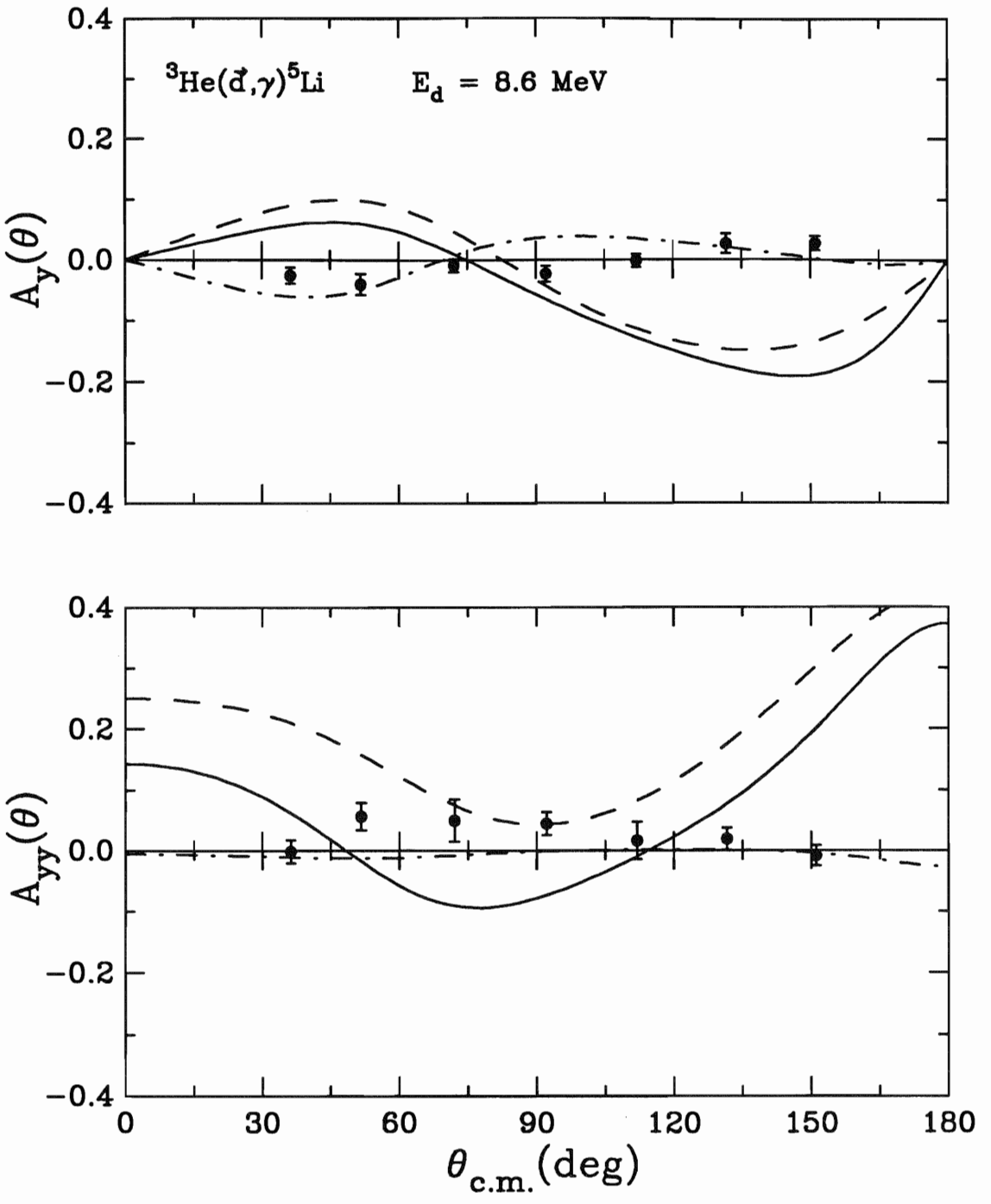

Fig. 7.12 $A_y(\theta)$ and $A_{yy}(\theta)$ from the ^{3}He($\vec{d}$,γ)^{5}Li reaction at E_d = 8.6 MeV are shown along with the results of the three RGM calculations. The solid curve is Calculation E (two-body forces), the dashed curve is Calculation F (^{4}He(p,p)^{4}He phase-shift adjusted forces), and the dashed-dotted curve is Calculation G which uses no tensor force.

Chapter 8: Conclusions

In conclusion, the absolute differential cross section and vector and tensor analyzing powers of the $^3He(\vec{d},\gamma)^5Li$ reaction have been measured in two energy regions. The first energy region spans the fusion resonance which lies at $E_d(lab) = 0.45$ MeV. The second energy region is at $E_d(lab) = 8.6$ MeV.

Transition matrix element analyses of the fusion resonance region observables indicated that the reaction proceeds predominantly through s-wave (E1) capture, with small admixtures of M1 or E2 radiation. While two solutions exist for the TME fits of the $E_d(lab) = 0.8$-0.0 MeV observables, and three solutions exist for the TME fits of the $E_d(lab) = 0.6$-0.3 MeV observables, the multichannel Resonating Group Model calculations unambiguously select the dominant $^4s_{3/2}(E1)$ solution (where the fitted $^4s_{3/2}(E1)$ TME contributes >89% of the cross section strength) as the physically preferred one. In the RGM picture, the strong capture cross section in the fusion resonance region is a consequence of the tensor force, which couples the $[d+^3He]^{S=3/2}_{J=3/2}$ channel to the $[p+^4He]^{S=1/2}_{J=3/2}$ channel, enabling the capture reaction to proceed via the $\Delta S=0$ (E1) transition to the ground state.

At $E_d = 8.6$ MeV, only one TME solution was found from a fit to the cross section and analyzing powers $A_y(\theta)$ and $A_{yy}(\theta)$. The fit indicates that the capture cross-section strength is dominated by s-wave E1 capture with an admixture of ~20% d-wave E1 capture. In an RGM calculation at this energy, qualitative agreement with the measured cross section and analyzing powers was improved by turning off the tensor force. However, a comparison of transition matrix elements revealed that although the calculated observables reproduce the data better, the relative intensities of the calculated transition matrix elements do not agree with those extracted from a TME fit to the data. In fact, a non-zero tensor force is necessary to get agreement between data and theory for the relative strengths of the TME's. As with the $E_d(lab) = 0.45$ MeV calculation, the strong

$^4s_{3/2}$ (E1) capture strength is due to the coupling of the $[d+^3He]^{S=3/2}_{J=3/2}$ scattering channel to the $[p+^4He]^{S=1/2}_{J=3/2}$ scattering channel by the tensor force.

As shown, the tensor force has a dominating effect in this reaction. In the fusion resonance region it is especially important since it enhances the cross section by a factor of 16 (in a comparision of the measured cross section to the RGM calculation with no tensor force). Since the branching ratio for the $^3He(d,\gamma)^5Li$ and $^3He(d,p)^4He$ reactions is flat about the fusion resonance [Cec85b], the present study shows that the tensor force actually drives the energy producing 3He(d,p)4He reaction. Furthermore, these results indicate that it is the tensor force which dramatically increases the feasibility of using the $^3He(\vec{d},\gamma)^5Li$ reaction as a diagnostic tool for deuterium-tritium reactors.

Appendix A

A.1 Ground-State Widths of ^{5}Li and ^{5}He

In the analysis of the data taken for the ^{3}He($\vec{d}$,γ)^{5}Li reaction, it was necessary to fit the peak in the γ-ray spectra in order to extract consistent sums with which to calculate the angular distributions. In order to perform this fitting procedure, the line-shape response function of the NaI spectrometers were convoluted with the energy distribution of the γ rays which come from this capture reaction to an unbound ground state. An important biproduct of this fitting procedure is the width of the ground state of ^{5}Li. This fitting procedure was also performed on γ-ray spectra obtained for the ^{3}H(d,γ)^{5}He reaction in order to compare the widths of the two nuclei which are related through the principle of charge symmetry. The following is a discussion of the results of these analyses which resolves some disagreements in the literature. The FORTRAN subroutine which performed the fitting procedure is also given.

The ground states of ^{5}He and ^{5}Li have $J^\pi = 3/2^-$ and are most easily pictured as a single nucleon in the $p_{3/2}$ shell-model orbital above a closed $s_{1/2}$ core. They are unbound by 0.89 and 1.97 MeV, respectively, in the n-α and p-α channels [Ajz88]. Previous charged-particle reactions established the widths of the ground states to be ~ 1 MeV, corresponding to lifetimes of ~10^{-22} seconds. These experimental widths varied widely depending on the experimental set-up and reactions used. For a review of experiments see [Ohl64] and [Ajz88]. The simplest measurement, nucleon scattering from ^{4}He at energies just above threshold, is complicated by potential scattering interference in the energy-dependent cross section. Warburton and McGruer [War57] used the ^{4}He(d,p)^{5}He reaction and fit a Gaussian to the high-energy side of the peak in their proton spectrum obtaining $\Gamma_{^5He}$=0.55±0.03 MeV. This fit the high-energy side well but failed to reproduce the long low-energy tail and therefore underestimated the width. Ohlsen and Young [Ohl64] used the same reaction and measured both the Full Width at Half

Maximum (FWHM) of a Gaussian fit and the FWHM of the observed spectrum. The Gaussian fit gave a value of $\Gamma_{^5He}$=0.57±0.02 MeV in agreement with Warburton and McGruer. The observed spectrum had a FWHM of $\Gamma_{^5He}$=0.85±0.05 MeV. Cerny et al. [Cer66] have studied both ^{5}He and ^{5}Li via the ^{7}Li(p,^{3}He)^{5}He and ^{7}Li(p,t)^{5}Li reactions respectively. Widths of $\Gamma_{^5He}$=0.80±0.04 MeV and $\Gamma_{^5Li}$=1.55±0.15 MeV are quoted although it is not stated how these widths were obtained. [Ajz88] quotes a best value for the width of ^{5}He from the work above and others to be $\Gamma_{^5He} = 0.6 \pm 0.02$ MeV. For ^{5}Li only a value of $\Gamma_{^5Li} \sim 1.5$ MeV is quoted. Table 1 summarizes these and other [Smi63 and Bus68] various experimental widths and the methods of measurement used.

According to the theory of resonance reactions, the energy dependent shape of an isolated resonance for an electric dipole transition and an N-α breakup channel (where N=p or n) can be described in terms of a Breit-Wigner form:

$$BW(E_\gamma) \propto \frac{1}{k^2} \frac{E_\gamma^3 \Gamma_N(E_N)}{\left[\left(E_\gamma - E_{res} + \Delta(E_N)\right)^2 + \left(\frac{\Gamma_N}{2}\right)^2\right]} \qquad [A.1]$$

where Γ_N is the width of the N-α channel, E_N is the nucleon emission energy, and E_γ^3 is the energy-dependent piece of the γ-ray width Γ_γ. We have assumed that Γ_γ is much less than Γ_N so that the total width $\Gamma = \Gamma_N + \Gamma_\gamma \approx \Gamma_N$. The energy dependence of the nucleon widths Γ_N is determined by the relation $\Gamma_N = 2P_L(E_N)\gamma^2$, where γ^2 is the reduced width and $P_L(E_N)$ is the penetrability of the nucleon, which for this case has an orbital angular momentum L=1. $P_1(E_N)$ was calculated directly from the confluent hypergeometric functions, F_1 and G_1, for several choices of channel radius. Similarly, the energy dependence of the level shift, $\Delta(E_N)$, is determined from the shift function $S_1(E_N)$ in the relation $\Delta(E_N) = -(S_1(E_N) - B)\gamma^2$ where B, the boundary condition, was chosen such that $\Delta(E_{res}) = 0.0$. Both the penetrability and the shift function are defined according to the Lane and Thomas definitions [Lan58]. The γ-ray energy is simply related to the nucleon

emission energy by kinematic considerations for both the $^3H(d,\gamma)^5He \rightarrow {}^4He + n$ and the $^3He(d,\gamma)^5Li \rightarrow {}^4He + p$ reactions. For the ^5He reaction, E_{res} corresponds to a neutron energy of E_n=0.89 MeV and a γ-ray energy of E_γ=21.8 MeV. For the ^5Li reaction, E_{res} corresponds to a proton energy of E_p=1.97 MeV and a γ-ray energy of E_γ=21.5 MeV. These values were taken from [Ajz88] and were not measured in this experiment.

The γ-ray spectra from our NaI spectrometer were fit using the minimization code MINUIT with a convolution of the measured energy-dependent response function of the NaI spectrometer (See Section 3.5) and the Breit-Wigner resonance shape described above. The functional form used is:

$$F(E) \propto \int NaI(E,E_\gamma)\ B\text{-}W(E_\gamma)\ dE_\gamma \qquad [A.2]$$

where $\Gamma_N(E_{res})$ and the overall height of F(E) were varied, and the entire convoluted form was shifted up or down in energy to allow for spectrum calibration errors. The lack of a precise spectrum calibration prevented us from extracting values for E_{res}. From the extracted widths, we reconstructed the resonance shape using Eqn. A.1. Figure A1 shows the best fits to the ^5He and ^5Li spectra (solid curve), as well as the NaI response function and the B-W shape used in the convolution.

Table A2 summarizes the results of the best fits to the data. Using a channel radius of $r = 1.4\ (4^{1/3} + 1^{1/3}) = 3.6$ fm, the FWHM of the resonance curves that we have extracted are comparable to the values of previous measurements as quoted in Table A1, but they differ from the average values quoted by [Ajz88]. The dependence of the widths, Γ_p and Γ_n, on the channel radius is plotted in Fig. A2. It was found that while the individual widths vary with radius, the ratio of the widths Γ_p/Γ_n is insensitive to the radius. We can make a simple prediction of this ratio by setting $\gamma_p^2=\gamma_n^2$, as expected from the charge symmetry of the nuclear force. With this assumption, the ratio of widths is given by:

$$\Gamma_p(E_{res})/\Gamma_n(E_{res}) = 2P_1^p(E_{res})\gamma_p^2/2P_1^n(E_{res})\gamma_n^2 \approx P_1^p(E_{res})/P_1^n(E_{res}) = 1.79.$$

This prediction is in agreement with the measured ratio $\Gamma_p/\Gamma_n = 1.79 \pm 0.29$.

Within the framework of resonance reaction theory, we have measured the ground-state widths of ^{5}He and ^{5}Li to be $\Gamma_n = 1.36 \pm 0.19$ MeV and $\Gamma_p = 2.44 \pm 0.21$ MeV, assuming pure E1 radiation. These values vary significantly from previously published widths due to the energy dependence of the penetrability and shift functions. The FWHM of the Breit-Wigner functions corresponding to these widths, however, do fall within the range of previous measurements. From our results, the relative magnitudes of $\Gamma_n(E_{res})$ and $\Gamma_p(E_{res})$ can be explained simply in terms of the relative penetrability of the neutron and proton through their respective Coulomb and angular momentum barriers. Furthermore, the ratio of these widths is consistent with the property of charge symmetry in the nuclear force.

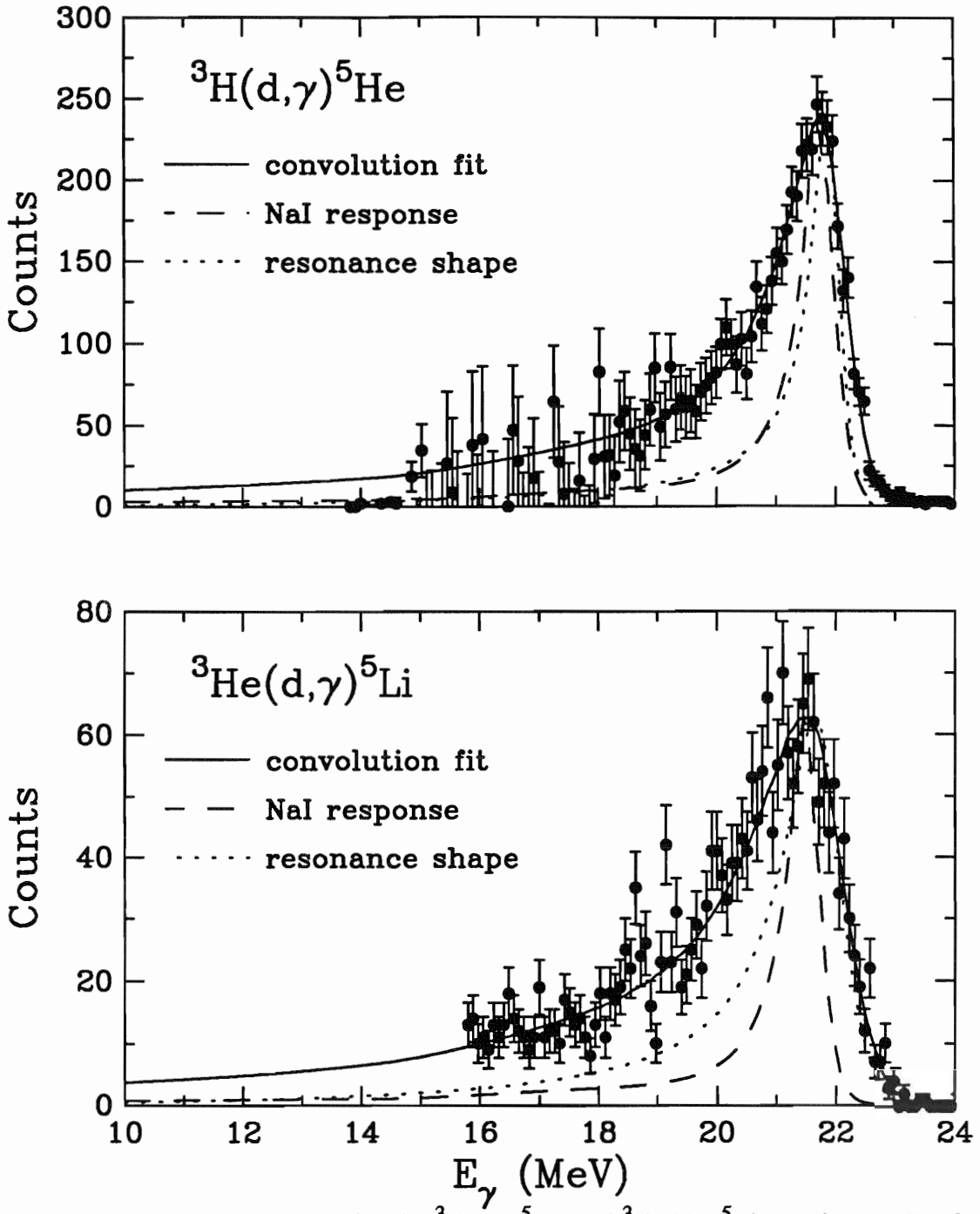

Fig. A1 Typical γ-ray spectra for the ^{3}H(d,γ)^{5}He and ^{3}He(d,γ)^{5}Li reactions at E_d=8.6 MeV and θ_{lab}=90°. The top spectrum was obtained by subtracting a pure titanium foil spectrum from a tritiated titanium foil spectrum. No background was subtracted in the bottom spectrum. The convolutions were fitted in the range 20.0 MeV ≤ E_γ ≤ 24.0 MeV and 19.0 MeV ≤ E_γ ≤ 24.0 MeV respectively.

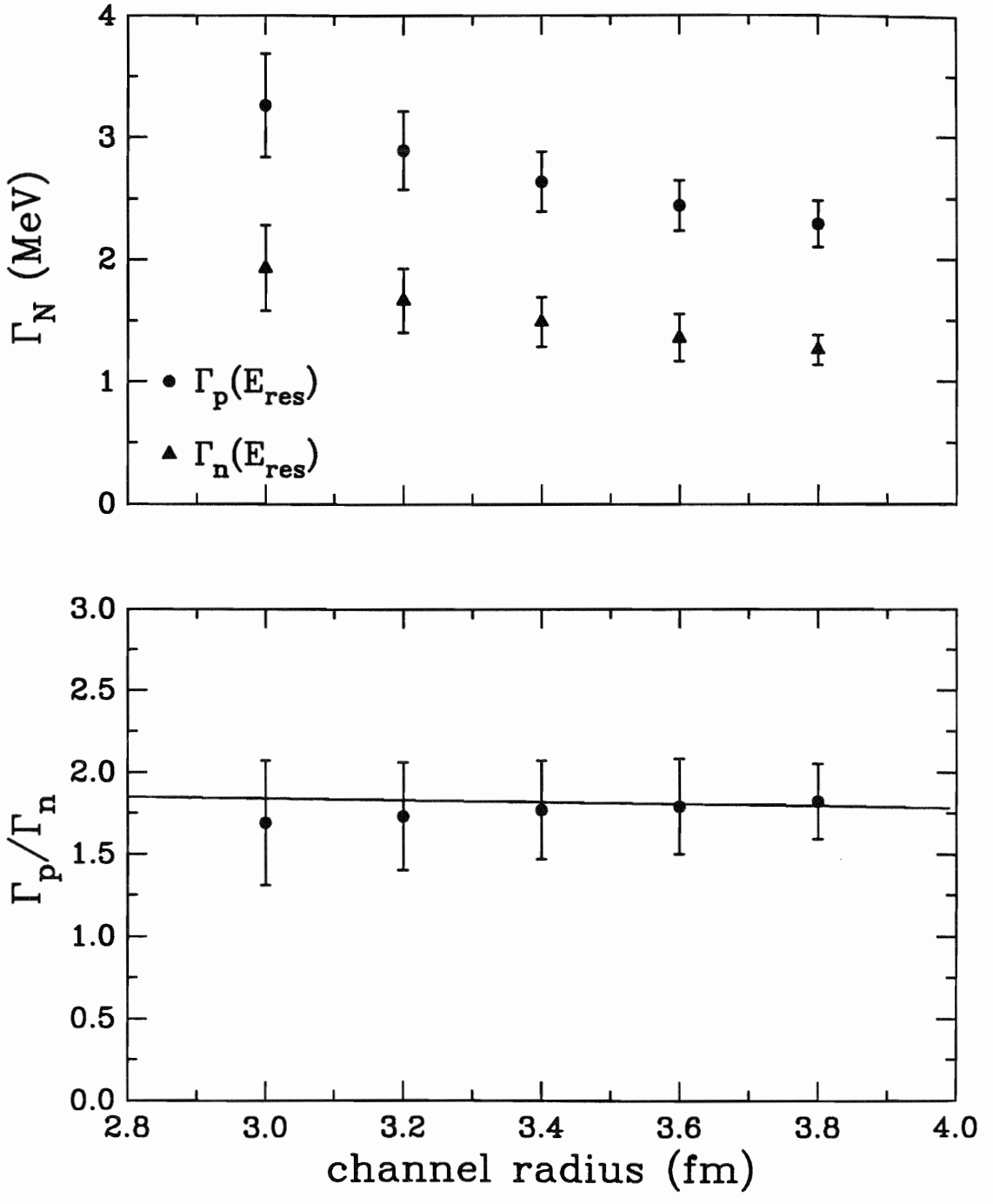

Fig. A2 Upper panel: The neutron resonance width Γ_n at the resonance energy $E_n = 0.89$ MeV and the proton resonance width Γ_p at the resonance energy $E_p = 1.97$ MeV are plotted as a function of the channel radius. Lower panel: The ratio of the widths demonstrates the insensitivity of this ratio to the channel radius. The solid curve is the ratio of penetrabilities $P_1^p(E_{res})/P_1^n(E_{res})$ as discussed in the text.

$\Gamma_{^5He}$ (MeV)	$\Gamma_{^5Li}$ (MeV)	Reaction	Method of Measurement	Ref.
1.36±0.19	2.44±0.21	$^3H(d,\gamma)^5He$, $^3He(d,\gamma)^5Li$	single-particle width in B-W shape	present work
0.61±0.03	1.24±0.03	$^3H(d,\gamma)^5He$, $^3He(d,\gamma)^5Li$	FWHM of resonance curve	present work
0.6±.02	~ 1.5		average value of several studies	[Ajz88]
0.57±0.02		$^4He(d,p)^5He$	Gaussian fit to proton spectrum	[Ohl64]
0.85±0.05		$^4He(d,p)^5He$	FWHM of proton spectrum	[Ohl64]
0.55±0.03		$^4He(d,p)^5He$	Gaussian fit to proton spectrum	[War57]
0.80±04	1.55±0.15	$^7Li(p,^3He)^5He$, $^7Li(p,t)^5Li$	not stated	[Cer66]
0.525±0.030		$^3He(t,p)^5He$	FWHM of proton spectrum	[Smi63]
	2.6±0.4	$^3He(d,\gamma)^5Li$	FWHM of resonance curve	[Bus68]

Table A1 A summary of various measurements of the ^5He and ^5Li ground-state widths, as well as the reactions and methods of measurement used.

	E_γ (MeV)	$E_N = E_{res}$ (MeV)	$P_1(E_{res})$	$S_1(E_{res})$	$\Gamma_N(E_{res})$ (MeV)	γ^2 (MeV)	FWHM (MeV)	χ_ν^2
^{5}He	21.8	0.89	0.205	-0.694	1.36 ± 0.19	3.32 ± 0.46	0.61 ± 0.03	1.01
^{5}Li	21.5	1.97	0.366	-0.635	2.44 ± 0.21	3.33 ± 0.29	1.24 ± 0.03	0.83

Table A2 The results of the present experiment. All energies, widths, and reduced widths are quoted in units of MeV in the center of mass system. The penetrability and shift functions are dimensionless and were calculated using the confluent hypergeometric functions. The γ-ray energy at the resonance E_γ and the nucleon energy at the resonance E_N are from [Ajz88]. Γ_N, γ^2, and FWHM were measured in this experiment as described in the text. The errors for our FWHM measurements were obtained by constructing a Breit-Wigner resonance for $\Gamma_N + \Delta\Gamma_N$ and $\Gamma_N - \Delta\Gamma_N$, and taking half the difference of their FWHM values.

A.2 The Convolution Code

In order to fit the spectra from the $^3He(\vec{d},\gamma)^5Li$ reaction, it was necessary to write a code that could convolute the NaI line-shape response function as measured with the $^3H(p,\gamma)^4He$ reaction (see Section 3.5) with a one-level Breit-Wigner function corresponding to the ground-state resonance. The MINUIT subroutine which accomplishes this is given below. The convolution is performed on a mesh corresponding to the channels of the spectrum which is being fit. It is accomplished simply by constructing response functions for every γ-ray energy on the mesh, weighting each by the value of the Breit-Wigner function at that channel energy, and summing all the weighted response functions. The fitted parameters are WIDTH, HEIGHT, ISHIFT, and GWIDTH. WIDTH is defined in equation A1 as Γ_N, Height is the overall height of the convoluted function, ISHIFT is the number of channels the convoluted function is shifted in order to line up with the spectrum, and GWIDTH is the Gaussian width as in the form $e^{-(x/GWIDTH)^2}$. This version of the subroutine was used to fit the fusion resonance spectra. An alternate version which does not perform the additional Gaussian convolution was used to fit the spectra at E_d= 8.6 MeV and to extract the widths quoted in Appendix A.1.

In both versions, the user supplies information about the projectile and target charges and masses, the projectile energy, and the angle of the detector so that the code can perform a kinematics calculation to determine the energy of the proton which is emitted from the residual nucleus. In order to calculate the penetrability and shift functions, the user also supplies L, R0, and RMAX, which are the relative angular momentum of the decaying system (L=1 for ^5Li breaking up into a proton and α particle) and the channel radius (where RMAX=R0*$A^{1/3}$, and R0 is not used if RMAX is supplied) which was taken to be RMAX=3.6 in this case. The parameters for the line-shape response function of the NaI spectrometer is also supplied by the user.

```
SUBROUTINE FCN(NPAR, GG,FF, X, IFLAG)
C
C
C       THIS PROGRAM IS DESIGNED TO BE A GENERAL FITTING PROGRAM
C       THAT FITS THE LINESHAPE OF A NaI DETECTOR
C               Mark Balbes 11/28/89
C
C
C Minuit subroutine
C Inputs:  npar=no. of ADJUSTABLE parameters
C          GG = derivitive vector (not used here)
C          FF = value of function to be minimized
C          X = parameter values
C          IFLAG = control value 1==> set up constants
C                                2==> not used here
C                                3==> write out information
C                                4==> calculate F (CHI-SQR)
C                               >4==> not used here
C
C -------------------------------------------------------------------------
C234567

        DOUBLE PRECISION GG(50),X(50),ALIM(50),BLIM(50)
        REAL XSPEC(2000),YSPEC(2000),ERR(2000)
        REAL XFORE(2000),YFORE(2000),ERRFORE(2000)
        REAL XBACK(2000),YBACK(2000),ERRBACK(2000)
        REAL FOREBCI BACKBCI,FOREDTC,FOREACC,BACKDTC,BACKACC
        REAL NAIR(2000),RES(2000),W(2000),SHAPE(2000),SHAPEOLD(2000)
        REAL TEMP(2000),PEN(2000),PENX(2000),DETR(512,512),P(51),SH(51)
        REAL LOWB, UPB
        REAL SHIFT(2000),SHIFTX(2000)
        REAL ERES,WIDTH,WIDTHOLD,HEIGHT,CHISQR,CHIPER
        INTEGER I,PENFLAG,ISHIFTFLAG,ISHIFT,IRESFLAG
        CHARACTER*50 FILENAME,BACKNAME
        REAL*8 T1, TM1, TM2, TM3, TM4, EX, ANG
        REAL*8 ANG3P, T3P, ANG4P, T4P, RATIOP, SHIFTP, QP
        REAL*8 ANG3M, T3M, ANG4M, T4M, RATIOM, SHIFTM, QM
        REAL*8 ECM,ANGL4P
        REAL APROJ1,ATARG1,ZPROJ1,ZTARG1
        REAL APROJ2,ATARG2,ZPROJ2,ZTARG2
        INTEGER IAPROJ1,IATARG1,IZPROJ1,IZTARG1
        INTEGER IAPROJ2,IATARG2,IZPROJ2,IZTARG2
        INTEGER IANUC1,IZNUC1,IANUC2,IZNUC2
        CHARACTER TITLE*60,ATIME*10,ADATE*10,AATIME*20
        DOUBLE PRECISION C1,C2,C3,C4,C5,C6,C7,C8,C9,C10,RJOINT
      COMMON/RESPONSE/C1,C2,C3,C4,C5,C6,C7,C8,C9,C10,
     &          RJOINT,CUTLO,CUTHI,STNCENT
        COMMON/REACTION/APROJ1,ZPROJ1,ATARG1,ZTARG1,EBEAM,ANGL
AB,QGAM
```

```
      COMMON/RESONANCE/APROJ2,ZPROJ2,ATARG2,ZTARG2,L,R0,RMAX,
QRES,
     &                          ISHIFTFLAG
      DOUBLE PRECISION U(50),WERR(50),XS(50),XTS1(50),WTS(50)
      COMMON/PAREXN/U,WERR
      COMMON/FIX/ IPFIX(50),XS,XTS1,WTS,NPFIX
      COMMON/PARM/P,SH
      COMMON/TITLEC/TITLE,FDATE
      REAL GWIDTH,GAUSS(512,512),SHAPE2(2000)
      GO TO (10,20,30,40,20),IFLAG


C
C Initialize
C
10    CONTINUE
C
C     READS IN SPECTRUM DATA AT THIS POINT
C
      READ(5,555)IFILE,FILENAME
555   FORMAT(I1,A50)
      READ(5,*)FOREBCI,FOREDTC,FOREACC
    OPEN(UNIT=20,FILE=FILENAME,STATUS='OLD')

      IF(IFILE.EQ.2) THEN
            I = 1
            WRITE(6,22)FILENAME
22          FORMAT(' READING 2 COLUMNS OF DATA FROM FILE',A50)
100         READ(20,*,END=101)XFORE(I),YFORE(I)
            YFORE(I)=YFORE(I)*FOREDTC*FOREACC
            ERRFORE(I)=SQRT(YFORE(I))
            IF(ERRFORE(I).LE.0.) ERRFORE(I)=1.
            I=I+1
            GOTO 100
101         NDATA=I-1          !NDATA IS NOW #OF DATA POINTS

      ELSE IF(IFILE.EQ.3) THEN
            I = 1
            WRITE(6,23)FILENAME
23          FORMAT(' READING 3 COLUMNS OF DATA FROM FILE',A50)
102         READ(20,*,END=103)XFORE(I),YFORE(I),ERRFORE(I)
            YFORE(I)=YFORE(I)*FOREDTC*FOREACC
            IF(ERRFORE(I).LE.0.) ERRFORE(I)=1.
            I=I+1
            GOTO 102
103         NDATA=I-1          !NDATA IS NOW #OF DATA POINTS
      ELSE
            WRITE(6,*)'DATA FILE FORMAT UNKNOWN.  CHECK UNIT 5'
            WRITE(6,*)'EXECUTION TERMINATED'
            STOP
      ENDIF
      CLOSE(20)
```

```
      WRITE(6,*)'NDATA=',NDATA

      READ(5,555)IFILEB,BACKNAME
      IF(IFILEB.EQ.2.OR.IFILEB.EQ.3) THEN
       READ(5,*)BACKBCI,BACKDTC,BACKACC
     OPEN(UNIT=20,FILE=BACKNAME,STATUS='OLD')

       IF(IFILEB.EQ.2) THEN
            I = 1
            WRITE(6,24)BACKNAME
24          FORMAT(' READING 2 COLUMNS OF BKGRND FROM FILE',A50)
200         READ(20,*,END=201)XBACK(I),YBACK(I)
            IF(XBACK(I).NE.XFORE(I))THEN
             WRITE(6,*)'BKGRND AND FOREGRND ENERGIES DIFFERENT'
             STOP
            ENDIF
            YBACK(I)=YBACK(I)*BACKDTC*BACKACC
            ERRBACK(I)=SQRT(YBACK(I))
            IF(ERRBACK(I).LE.0.) ERRBACK(I)=1.
            I=I+1
            GOTO 200
201         NBACK=I-1          !NBACK IS NOW #OF BKGRND POINTS

       ELSE IF(IFILEB.EQ.3) THEN
            I = 1
            WRITE(6,25)BACKNAME
25          FORMAT(' READING 3 COLUMNS OF BKGRND FROM FILE',A50)
202         READ(20,*,END=203)XBACK(I),YBACK(I),ERRBACK(I)
            IF(XBACK(I).NE.XFORE(I))THEN
             WRITE(6,*)'BKGRND AND FOREGRND ENERGIES DIFFERENT'
             STOP
            ENDIF
            YBACK(I)=YBACK(I)*BACKDTC*BACKACC
            IF(ERRBACK(I).LE.0.) ERRBACK(I)=1.
            I=I+1
            GOTO 202
203         NBACK=I-1          !NDATA IS NOW #OF DATA POINTS
       ELSE
            WRITE(6,*)'BKGRND FILE FORMAT UNKNOWN.  CHECK UNIT
5'
            WRITE(6,*)'EXECUTION TERMINATED'
            STOP
       ENDIF
       CLOSE(20)
        WRITE(6,*)'NBACK=',NBACK
      ELSE
       BACKBCI=1.
      ENDIF
C  Subtract the background and calculate the new errors.
      DO I=1,NDATA
       XSPEC(I)=XFORE(I)
       YSPEC(I)=YFORE(I)-(FOREBCI/BACKBCI)*YBACK(I)
```

```
ERR(I)=SQRT(ERRFORE(I)**2+((FOREBCI/BACKBCI)*ERRBACK(I))**2)
      ENDDO


C READ CARDS.INFO (UNIT 5)
      READ(5,*)
      READ(5,*)APROJ1,ZPROJ1,ATARG1,ZTARG1,EBEAM,ANGLAB
      IAPROJ1=APROJ1
      IZPROJ1=ZPROJ1
      IATARG1=ATARG1
      IZTARG1=ZTARG1
      READ(5,*)
      READ(5,*)
      READ(5,*)C1,C2,C3
      READ(5,*)C4,C5
      READ(5,*)C6,C7,C8
      READ(5,*)C9,C10
      READ(5,*)RJOINT,CUTLO,CUTHI,STNCENT
      READ(5,*)
      READ(5,*)
      READ(5,*)IRESFLAG
      READ(5,*)APROJ2,ZPROJ2,ATARG2,ZTARG2
      IAPROJ2=APROJ2
      IZPROJ2=ZPROJ2
      IATARG2=ATARG2
      IZTARG2=ZTARG2
      READ(5,*)L,R0,RMAX
      READ(5,*)PENFLAG
      READ(5,*)ISHIFTFLAG
      READ(5,*)
      READ(5,*)
      READ(5,*)LOWB,UPB
      READ(5,*)

C  Calculate the gamma ray resonance energy.
      TM1=IAPROJ1 + EMASS(IAPROJ1,IZPROJ1)/931.5016
      TM2= IATARG1 + EMASS(IATARG1,IZTARG1)/931.5016
      TM3=0.
      TM4=IATARG1+IAPROJ1+
     &    EMASS(IATARG1+IAPROJ1,IZTARG1+IZPROJ1)/931.5016
      EX=0.
      ANG=ANGLAB
      WRITE(6,*)'IAPROJ1,IZPROJ1=', APROJ1,ZPROJ1
      WRITE(6,*)'IATARG1,IZTARG1=',ATARG1,ZTARG1
      WRITE(6,*)'EBEAM=',EBEAM
      WRITE(6,*)'ANGLAB=',ANGLAB
      CALL SRKIN (EBEAM, TM1, TM2, TM3, TM4, EX, ANG,
     &       ANG3P, T3P, ANG4P, T4P, RATIOP, SHIFTP, QP,
     &       ANG3M, T3M, ANG4M, T4M, RATIOM, SHIFTM, QM,
     &       ECM,ANGL4P)
      ERES=T3P
```

```
      WRITE(6,*)'T3P=',T3P
      WRITE(6,*)'ERES=',ERES

C Calculate Q-Values of gamma ray reaction and exit channel reaction
      IANUC1=IATARG1+IAPROJ1
      IZNUC1=IZTARG1+IZPROJ1
      IANUC2=IATARG2+IAPROJ2
      IZNUC2=IZTARG2+IZPROJ2

      WRITE(6,*)'ATARG1,ZTARG1',IATARG1,IZTARG1
      WRITE(6,*)'ATARG2,ZTARG2',IATARG2,IZTARG2
      WRITE(6,*)'ANUC1,ZNUC1',IANUC1,IZNUC1
      WRITE(6,*)'ANUC2,ZNUC2',IANUC2,IZNUC2
      QGAM=EMASS(IATARG1,IZTARG1)+EMASS(IAPROJ1,IZPROJ1)
     &          -EMASS(IANUC1,IZNUC1)
      QRES=EMASS(IANUC2,IZNUC2)
     &          -EMASS(IATARG2,IZTARG2)-EMASS(IAPROJ2,IZPROJ2)
      WRITE(6,*)'QGAM=',QGAM
      WRITE(6,*)'QRES=',QRES

C Calculate the needed penetrabilities.
      IF(PENFLAG.NE.0) THEN
            WRITE(6,*)'CALCULATING PENETRABILITIES'
            CALL GETPEN(PEN,SHIFT,XSPEC,NDATA)
            WRITE(6,*)'PENETRABILITIES HAVE BEEN CALCULATED'
      ELSE
            OPEN(2,FILE='PEN.DAT',STATUS='OLD')
            OPEN(3,FILE='SHIFT.DAT',STATUS='OLD')
            DO 464 I=1,NDATA
                  READ(2,*)PENX(I),PEN(I)
                  READ(3,*)SHIFTX(I),SHIFT(I)
                  IF(PENX(I).NE.XSPEC(I)) THEN
                    WRITE(6,*)'WARNING: PENETRABILITIES
     & ARE FOR THE WRONG ENERGIES!!!'
                  ENDIF
                  IF(SHIFTX(I).NE.XSPEC(I)) THEN
                    WRITE(6,*)'WARNING: SHIFT FUNCTIONS
     & ARE FOR THE WRONG ENERGIES!!!'
                  ENDIF
464         CONTINUE
            CLOSE(2)
      ENDIF

      IF(PENFLAG.NE.0) THEN
            OPEN(19,FILE='PEN.DAT',STATUS='NEW')
            OPEN(18,FILE='SHIFT.DAT',STATUS='NEW')
            DO 465 I=1,NDATA
              WRITE(19,*)XSPEC(I),PEN(I)
              WRITE(18,*)XSPEC(I),SHIFT(I)
465         CONTINUE
            CLOSE(19)
      ENDIF
```

```
C  Calculate the NaI response function for all the gamma ray
C  energies going into the detector.
        WRITE(6,*)'ENTERING DETR CALCULATION'
        DO 13 I=1,NDATA
              CALL MKRESPSUB(NAIR,XSPEC,NDATA,XSPEC(I))
              DO 14 J=1,NDATA
                DETR(I,J)=NAIR(J)
14            CONTINUE
13      CONTINUE
        WRITE(6,*)'EXITING DETR CALCULATION'
C       OPEN(2,FILE='DETR.OUT',STATUS='NEW')
C       DO 141 I=1,NDATA
C             WRITE(2,*)XSPEC(I),DETR(NDATA-100,I)
C141    CONTINUE
C       DO 142 I=1,NDATA
C             WRITE(2,*)XSPEC(I),DETR(NDATA-50,I)
C142    CONTINUE
C       DO 143 I=1,NDATA
C             WRITE(2,*)XSPEC(I),DETR(NDATA-10,I)
C143    CONTINUE
C       DO 144 I=1,NDATA
C             WRITE(2,*)XSPEC(I),DETR(NDATA,I)
C144    CONTINUE

        RETURN

C -------------------------------------------------------------

20      CONTINUE
        RETURN

C -------------------------------------------------------------

30      CONTINUE
C  THIS IS THE LAST CALL TO FCN -- THE FITTING IS FINISHED BY NOW
        WIDTH = X(1)
        HEIGHT = X(2)
        ISHIFT = X(3)
        GWIDTH=X(4)
C  FIRST CALCULATE THE BREIT-WIGNER SHAPE

        CALL SIMPRESSUB(RES,W,PEN,SHIFT,ERES,WIDTH,XSPEC,NDATA)

C  NOW DO THE CONVOLUTION

        CALL SPREADSUB(SHAPE,XSPEC,DETR,RES,NDATA)

C  Calculate a gaussian to allow for beam energy straggling.
              DO I=1,NDATA
                DO J=1,NDATA
                  GAUSS(I,J)=EXP(-1.*((XSPEC(J)-XSPEC(I))/GWIDTH)**2)
```

```
                ENDDO
               ENDDO

C  Now convolute in the gaussian
                CALL SPREADSUB(SHAPE2,XSPEC,GAUSS,SHAPE,NDATA)

        DO 12 I=1,NDATA
                SHAPE2(I)=HEIGHT*SHAPE2(I)
12      CONTINUE

        OPEN(1,FILE='FITSPEC.FIT',STATUS='NEW')
        DO 35 I=1,NDATA
                WRITE(1,*)XSPEC(I),SHAPE2(I+ISHIFT)
35      CONTINUE
        CLOSE(1)
C   FIND PEAK OF SHAPE2(I) FOR B-W NORMALIZATION PURPOSES.

        CALL FINDMAX(XSPEC,SHAPE2,NDATA,IMAXS)

C   CALCULATE THE BREIT-WIGNER RESONANCE

        CALL SIMPRESSUB(RES,W,PEN,SHIFT,ERES,WIDTH,XSPEC,NDATA)

C   FIND ITS MAX VALUE
        CALL FINDMAX(XSPEC,RES,NDATA,IMAXR)

        OPEN(20,FILE='RESONANCE.OUT',STATUS='NEW')
        DO 41 I=1,NDATA
                WRITE(20,*)XSPEC(I),RES(I+IMAXR-IMAXS)*
     &             (SHAPE2(IMAXS)/RES(IMAXR))
41      CONTINUE
        CLOSE(20)

C    CALCULATE THE NaI RESPONSE AT THE RESONANCE
        CALL MKRESPSUB(NAIR,XSPEC,NDATA,XSPEC(IMAXR))
        OPEN(21,FILE='RESPONSE.OUT',STATUS='NEW')
        DO 43 I =1,NDATA
                WRITE(21,*)XSPEC(I),NAIR(I+IMAXR-IMAXS)*
     &             (SHAPE2(IMAXS)/NAIR(IMAXR))
43      CONTINUE

C  calculate the reduced width
        AION=APROJ2
        ZION=ZPROJ2
        ATARG=ATARG2
        ZTARG=ZTARG2
        L=L
        LMAX=L+3
        R0=1.4
        R=RMAX
        NEN=1
        E=(AION+ATARG)/ATARG * QRES
```

```
      CALL PENETSUB(E)
      PENRES = P(L+1)
      RW = WIDTH/(2.*PENRES)

C  Spit out the data being fit.
      OPEN(15,FILE='DATA.OUT',STATUS='NEW')
      DO 11 I=1,NDATA
        IF((I).GE.0.AND.(I).LE.NDATA) THEN
         WRITE(15,*)XSPEC(I),YSPEC(I),ERR(I)
        ENDIF
11    CONTINUE


C  Sum the calculated fit and data to get the yields for the spectrum.
      NDATA2=0
      YFITALL = 0.
      YFITRANGE = 0.
      YIELDFORE = 0.
      YIELDBCK=0.

      DO I = 1, NDATA
            YFITALL = YFITALL + SHAPE2(I)
            IF((XSPEC(I).GE.LOWB).AND.(XSPEC(I).LE.UPB)) THEN
                  YFITRANGE = YFITRANGE+SHAPE2(I+ISHIFT)
                  YIELDFORE = YIELDFORE+YFORE(I)
                  YIELDBACK  = YIELDBACK+YBACK(I)
                  NDATA2        = NDATA2 + 1
            ENDIF
      ENDDO
      YIELD = YIELDFORE-(FOREBCI/BACKBCI)*YIELDBACK
      YIELDERR =SQRT(YIELDFORE+(FOREBCI/BACKBCI)**2*YIELDBACK)
C  Write the FITSPEC.OUT file with the final results of the fit.
      OPEN(99,FILE='FITSPEC.OUT',STATUS='NEW')
   CALL TIME(ATIME)
   CALL DATE(ADATE)
   ENCODE (20,'(10A,10A)',AATIME)ADATE,ATIME
   WRITE(99,8000)TITLE,AATIME
8000  FORMAT(' ',4X,A50,5X,A20/)

      NDGFREE = NDATA2-(4-NPFIX)
      WRITE(99,*)'CHISQR=',CHISQR
      IF (NDGFREE.NE.0.) THEN
            CHIPER=CHISQR/FLOAT(NDGFREE)
            WRITE(99,*)'CHISQR/DGFREE=',CHIPER
      ENDIF
      WRITE(99,293)LOWB,UPB
293   FORMAT(/' FITTING REGION:',2F8.3/)
      WRITE(99,*)'# OF DATA POINTS=',NDATA2
      WRITE(99,*)'# OF VARIED PARAMETERS=',3-NPFIX
      WRITE(99,*)'# OF DEGREES OF FREEDOM=',NDGFREE
      IF(IPFIX(1).EQ.1.OR.IPFIX(2).EQ.1.OR.IPFIX(3).EQ.1)THEN
```

```
            WRITE(99,*)'WIDTH =',X(1),'FIXED'
        ELSE
            WRITE(99,*)'WIDTH =',X(1),'+-',WERR(1)
        ENDIF
        IF(IPFIX(1).EQ.2.OR.IPFIX(2).EQ.2.OR.IPFIX(3).EQ.2)THEN
            WRITE(99,*)'HEIGHT =',X(2),'FIXED'
        ELSE
            WRITE(99,*)'HEIGHT =',X(2),'+-',WERR(2)
        ENDIF
        IF(IPFIX(1).EQ.3.OR.IPFIX(2).EQ.3.OR.IPFIX(3).EQ.3)THEN
            WRITE(99,*)'ISHIFT =',X(3),'FIXED'
        ELSE
            WRITE(99,*)'ISHIFT =',X(3),'+-',WERR(3)
        ENDIF
        IF(IPFIX(1).EQ.4.OR.IPFIX(2).EQ.4.OR.IPFIX(3).EQ.4.OR.
     &  IPFIX(4).EQ.4)THEN
            WRITE(99,*)'GWIDTH =',X(4),'FIXED'
        ELSE
            WRITE(99,*)'GWIDTH =',X(4),'+-',WERR(3)
        ENDIF
        WRITE(99,*)
        WRITE(99,*)'PENETRABILITY AT ERES=',PENRES
        WRITE(99,*)'REDUCED WIDTH AT ERES=',RW

        WRITE(99,*)'YIELD OF DATA =',YIELD,'+-',YIELDERR
        WRITE(99,199)YFITRANGE/YFITALL
199     FORMAT(' RATIO OF FIT YIELD IN FITTING RANGE TO TOTAL FIT
YIELD ='
     &       ,F9.4)
        CLOSE(99)


        WRITE (6,*)'FINAL CALL'
      RETURN

C -------------------------------------------------------

40      CONTINUE

C#########################################################################
######

        FF = 0.
C
C*************************************************************
C       FITTING THE SPECTRUM WITH A CONVOLUTED LINESHAPE AND
C               BREIT-WIGNER
C*************************************************************
        WIDTH = X(1)
        HEIGHT = X(2)
        ISHIFT=X(3)
        GWIDTH=X(4)
```

```
C  FIRST CALCULATE THE BREIT-WIGNER SHAPE

                CALL
SIMPRESSUB(RES,W,PEN,SHIFT,ERES,WIDTH,XSPEC,NDATA)

C  NOW DO THE CONVOLUTION

                CALL SPREADSUB(SHAPE,XSPEC,DETR,RES,NDATA)

C  Calculate a gaussian to allow for beam energy straggling.
                DO I=1,NDATA
                 DO J=1,NDATA
                   GAUSS(I,J)=EXP(-1.*((XSPEC(J)-XSPEC(I))/GWIDTH)**2)
                 ENDDO
                ENDDO

C  Now convolute in the gaussian
                CALL SPREADSUB(SHAPE2,XSPEC,GAUSS,SHAPE,NDATA)

C  Vary the height of the convoluted shape.
                DO 98 I=1,NDATA
                        SHAPEOLD(I)=SHAPE2(I)
                        SHAPE2(I)=HEIGHT*SHAPE2(I)
98              CONTINUE

                DO 332 I=1,NDATA
                        SHAPE2(I)=HEIGHT*SHAPEOLD(I)
332             CONTINUE

        DO 99 I =1,NDATA
        IF(XSPEC(I).GE.LOWB.AND.XSPEC(I).LE.UPB) THEN
         FF = FF + ((YSPEC(I)-SHAPE2(I+ISHIFT))/ERR(I))**2
        ENDIF
99      CONTINUE

     CHISQR = FF
C
C#############################################################
        RETURN
        END

C_____________________________________________________________


C  This is a subroutine to find the maximum value of a function given
C   to it in x,y coordinate pairs.
C          Written by Mark Balbes
C                3/14/90

        SUBROUTINE FINDMAX(X,Y,NDATA,IMAX)
        REAL X(2000),Y(2000)
```

```
      REAL YMAX
      INTEGER IMAX

      IMAX = 0
      YMAX = 0

      DO 10 I =1,NDATA
            IF(Y(I).GT.YMAX) THEN
                  YMAX=Y(I)
                  IMAX=I
            ENDIF
10    CONTINUE
      END



      SUBROUTINE GETPEN(PEN,SHIFT,XSPEC,NDATA)

     REAL E,P(51),SH(51),T(100,10),RHO(100),ETA(100),FF(100,10
    1),F(150),G(147),GG(100,10),MU,EPRIME(100)
      REAL X(2000),Y(2000)
      REAL LIEX,QHEP
      REAL APROJ1,ATARG1,ZPROJ1,ZTARG1
      REAL APROJ2,ATARG2,ZPROJ2,ZTARG2
      INTEGER I, NUMBER, L

      REAL EGAM(2000),RES(2000),W(2000),PEN(2000),SHIFT(2000)
      REAL XSPEC(2000)
      REAL WIDTH,ERES,REDW,EI,EF,INC
      COMMON/REACTION/APROJ1,ZPROJ1,ATARG1,ZTARG1,EBEAM,ANGL
AB,QGAM
      COMMON/RESONANCE/APROJ2,ZPROJ2,ATARG2,ZTARG2,L,R0,RMAX,
QRES
      COMMON / PARM / P,SH
     COMMON F,G,FP,GP,SIGO
    COMMON /COM/AION,ZION,ATARG,ZTARG,LMAX,RO,R,E


C  SET UP THE INITIAL VALUES
      I=1
C-----------------------------------------------------------
C  Calculate the energy dependent penetrability and width.

      AION=APROJ2
      ZION=ZPROJ2
      ATARG=ATARG2
      ZTARG=ZTARG2
      LMAX=L+3
      R=RMAX
      NEN=1
      QHEP=QRES      ! Q VALUE FOR P+ALPHA=5LI REACTION IN C.O.M.
```

```
100     EGAM(I)=XSPEC(I)
        CALL CALCLIEXSUB(EGAM(I),LIEX) !LIEX=EX. ENERGY OF LI ABOVE
G.S.
        E= QHEP + LIEX      !C.O.M. ENERGY OF ALPHA+PROTON SYSTEM
        E=((ATARG+AION)/ATARG)*E        !E IN LAB FRAME
        IF(E.GT.0.01)THEN
                CALL PENETSUB(E)
                PEN(I)=P(L+1)
                SHIFT(I)=SH(L+1)
        ELSE
                PEN(I)=0.
                SHIFT(I)=0.
        ENDIF

C  SET UP I AND EGAM(I) FOR NEXT PASS
        I =I+1
        IF(I.LE.NDATA) GOTO 100
        RETURN
        END


C_____


        SUBROUTINE CALCLIEXSUB(EGAMLAB,EXLI)

        REAL*8 T1, TM1, TM2, TM3, TM4, EX, ANGLAB
        REAL*8 ANG3P, T3P, ANG4P, T4P, RATIOP, SHIFTP, QP
        REAL*8 ANG3M, T3M, ANG4M, T4M, RATIOM, SHIFTM, QM
        REAL*8 ECM,ANGL4P
        REAL*8 Q,EGAMLAB,EEX,BETA,GAMMA,EGAMCM,RM4
        REAL*8 EKLICM,RMLIEX,EKLILAB,EXLI
        REAL*8 E1CM,EK1CM,E2CM,EK2CM
        REAL ANUC,ZNUC
        REAL APROJ1,ATARG1,ZPROJ1,ZTARG1
        REAL APROJ2,ATARG2,ZPROJ2,ZTARG2

        INTEGER IAPROJ1,IATARG1,IZPROJ1,IZTARG1
        INTEGER IAPROJ2,IATARG2,IZPROJ2,IZTARG2

        COMMON/REACTION/APROJ1,ZPROJ1,ATARG1,ZTARG1,EBEAM,ANGL
AB,QGAM
        COMMON/RESONANCE/APROJ2,ZPROJ2,ATARG2,ZTARG2,L,R0,RMAX,
QRES

C       WRITE(6,*)'IN CALCLIEX SUBROUTINE'
C       WRITE(6,*)'EGAMLAB=',EGAMLAB
C       WRITE(6,*)APROJ1,ZPROJ1,ATARG1,ZTARG1,EBEAM,ANGLAB,QGAM
C       WRITE(6,*)APROJ2,ZPROJ2,ATARG2,ZTARG2,L,R0,RMAX,QRES
        IAPROJ1=APROJ1
        IATARG1=ATARG1
```

```
      IZPROJ1=ZPROJ1
      IZTARG1=ZTARG1
      IAPROJ2=APROJ2
      IATARG2=ATARG2
      IZPROJ2=ZPROJ2
      IZTARG2=ZTARG2

      T1=EBEAM
      TM1= IAPROJ1 + EMASS(IAPROJ1,IZPROJ1)/931.5016
      TM2= IATARG1 + EMASS(IATARG1,IZTARG1)/931.5016
      TM3=0.
      IANUC=IATARG1+IAPROJ1
      IZNUC=IZTARG1+IZPROJ1
      TM4=IANUC + EMASS(IANUC,IZNUC)/931.5016
      Q = (TM1+TM2-TM3-TM4)*931.5016

C     Set up to do relativistic transformations.
      E1LAB = T1+TM1*931.5016
      PC1LAB = SQRT(E1LAB**2 - (TM1*931.5016)**2)
      BETA = PC1LAB/(E1LAB + TM2*931.5016)
      GAMMA = 1./SQRT(1-BETA**2)

C Calculate the kinetic energy available in the center of mass frame (ECM)

      E1CM =GAMMA*(E1LAB-BETA*PC1LAB)
      EK1CM = E1CM - TM1*931.5016

      E2CM = GAMMA*TM2*931.5016
      EK2CM = E2CM - TM2*931.5016
      ECM = EK1CM+EK2CM
      EEX = ECM +Q
      EGAMCM= GAMMA*(1.-BETA*COSD(ANGLAB))*EGAMLAB

      RM4=TM4*931.5016
      EKLICM=(EEX+RM4-EGAMCM)-SQRT((EEX+RM4-EGAMCM)**2-
EGAMCM**2)

C  Calculate the mass of the excited Li nucleus
      RMLIEX=(EGAMCM**2-EKLICM**2)/(2.*EKLICM)
      EKLILAB =((EKLICM+RMLIEX)+BETA*SQRT((EKLICM+RMLIEX)**2-
RMLIEX**2))
     &                *GAMMA-RMLIEX

      EXLI=RMLIEX-RM4
      RETURN
      END
C_____


      SUBROUTINE MKRESPSUB(NAIR,XSPEC,N,CENT)
      REAL XSPEC(2000),NAIR(2000),TEMP(2000)
```

```
      DOUBLE PRECISION C1,C2,C3,C4,C5,C6,C7,C8,C9,C10,RJOINT
      DOUBLE PRECISION XCH,FUNCTION,SLOPE
      COMMON/RESPONSE/C1,C2,C3,C4,C5,C6,C7,C8,C9,C10,
     &                RJOINT,CUTLO,CUTHI,STNCENT

      DO 10 I=1,N
       XCH= XSPEC(I)*STNCENT/CENT
       IF (XCH .GE.RJOINT .AND. XCH.LE.CUTHI) THEN

      FUNCTION=DEXP(C6+C7*XCH+C8*XCH**2+C9*XCH**3+C10*XCH**4
)
            NAIR(I)=FUNCTION
       ELSE
            NAIR(I)=0.
       ENDIF
       IF(XCH.LT.RJOINT.AND. XCH.GE.CUTLO) THEN

      FUNCTION=DEXP(C1+C2*XCH+C3*XCH**2+C4*XCH**3+C5*XCH**4)
            NAIR(I)=FUNCTION
       ENDIF
       IF(XCH.LT.CUTLO)THEN
            SLOPE=DEXP(C1+C2*CUTLO+C3*CUTLO**2+
     &           C4*CUTLO**3+C5*CUTLO**4)/CUTLO
            NAIR(I)=SLOPE*XCH
        ENDIF
10    CONTINUE
```

C Normalize the response function to have a total area of one.

```
      SUM=0.
      DO 20 I=1,N
            SUM=SUM+NAIR(I)
20    CONTINUE
      DO 30 I=1,N
            NAIR(I)=NAIR(I)/SUM
30    CONTINUE
      RETURN
      END
```

C THIS PROGRAM WILL SIMPLY CALCULATE A SIMPLE NATURAL LINESHAPE
C USING THE ONE LEVEL SMALL WIDTH APPROXIMATION OF THE BREIT-WIGNER
C FORMULA.

```
      SUBROUTINE
SIMPRESSUB(RES,W,PEN,SHIFT,ERES,WIDTH,XSPEC,NDATA)
```

```
      REAL E,P(51),SH(51),T(100,10),RHO(100),ETA(100),FF(100,10
     1),F(150),G(147),GG(100,10),MU,EPRIME(100)
         REAL X(2000),Y(2000)
      COMMON F,G,FP,GP,SIGO
     COMMON /COM/AION,ZION,ATARG,ZTARG,LMAX,RO,R,E
         COMMON/RESONANCE/APROJ2,ZPROJ2,ATARG2,ZTARG2,L,R0,RMAX,
QRES,
     &          ISHIFTFLAG
         COMMON/PARM/P,SH
         INTEGER I, NUMBER, L

         REAL EGAM(2000),RES(2000),W(2000),DEL(2000)
         REAL XSPEC(2000),PEN(2000),SHIFT(2000)
         REAL WIDTH,ERES,REDW,EI,EF,INC,NORM


C-------------------------------------------------------------
C  calculate the reduced width and normalization to make value
C  of resonance 1 at the peak.
         AION=APROJ2
         ZION=ZPROJ2
         ATARG=ATARG2
         ZTARG=ZTARG2
         L=L
         LMAX=L+3
         R=RMAX
         NEN=1
         E=((ATARG+AION)/ATARG)*QRES  !E IN LAB FRAME

         CALL PENETSUB(E)
         RW = WIDTH/(2.*P(L+1))
         SHIFTRES=SH(L+1)
C        WRITE(6,*)'RW IN SIMPRES=',RW
         NORM= (ERES**3*WIDTH)/(WIDTH/2)**2/ERES
C        WRITE(6,*)'CALCULATED NORM'


C  SET UP THE INITIAL VALUES
         I=1
C-------------------------------------------------------------
C  Calculate the energy dependent penetrability and width.

100      EGAM(I)=XSPEC(I)
                 W(I) =2.*PEN(I)*RW
                 IF(ISHIFTFLAG.NE.0) THEN
                         DEL(I)=1.*(SHIFT(I)-SHIFTRES)*RW
                 ELSE
                         DEL(I)=0.
                 ENDIF
                 RES(I)=(EGAM(I)**3*W(I))/
     &           ((EGAM(I)-ERES-DEL(I))**2+(W(I)/2)**2)
```

```
     &          /EGAM(I)
          RES(I) = RES(I)/NORM

C  SET UP I AND EGAM(I) FOR NEXT PASS
          I =I+1
          IF(I.LE.NDATA) GOTO 100
          RETURN
          END



C  This is a modified convolution to take into
C  account the change of the NaI response function with energy
C  The each point of the function RES is
C  smeared out according to the NaI response
C  function for that energy.

          SUBROUTINE SPREADSUB(SPREAD,XSPEC,DETR,RES,NDATA)
          REAL XSPEC(2000),SPREAD(2000)
          REAL NAIR(2000),RES(2000),W(2000),SHAPE(2000)
          REAL TEMP(2000),PEN(2000),PENX(2000),DETR(512,512)
          INTEGER I,PENFLAG
        COMMON/RESPONSE/C1,C2,C3,C4,C5,C6,C7,C8,C9,C10,
     &          RJOINT,CUTLO,CUTHI,STNCENT

          DO 5 I=1,NDATA
               SPREAD(I)=0.
5         CONTINUE

          DO 10 I=1,NDATA
               DO 15 J=1,NDATA
                    SPREAD(J)=SPREAD(J)+DETR(I,J)*RES(I)
15             CONTINUE
10        CONTINUE

C  Normalize curve to have a max height of 1.
          CALL FINDMAX(XSPEC,SPREAD,NDATA,IMAX)
          YMAX=SPREAD(IMAX)
          DO 30 I=1,NDATA
               SPREAD(I)=SPREAD(I)/YMAX
30        CONTINUE
c         WRITE(6,*)'spread(imax)=',SPREAD(IMAX)
          RETURN
          END
```

Appendix B: Polarimeter Code

As discussed in Section 2.7, the polarization of the beam from the ABPIS was measured with a polarimeter which employed the $^3He(\vec{d},p)^4He$ reaction. The code which follows reads in yields from user-defined gates in a spectrum which contains peaks from each of the five detectors. It then carries out a search of χ^2 space using the MINUIT code to determine the beam polarization.

```
C  This program uses MINUIT to calculate the beam moments
C  of the TUNL Atomic Beam Source using the Stephenson polarimeter.
C        WRITTEN BY MARK BALBES 2/26/90
C
C  This program was modified to read previously set data gates directly from
C  XSYS data areas.
C           Modified by Zandy Williams  5/90


      SUBROUTINE FCN(NPAR, GG,FF, X, IFLAG)
C
C
C
C
C Minuit subroutine
C Inputs:  npar=no. of ADJUSTABLE parameters
C     GG = derivitive vector (not used here)
C     FF = value of function to be minimized
C     X = parameter values
C     IFLAG = control value 1==> set up constants
C                  2==> not used here
C                  3==> write out information
C                  4==> calculate F (CHI-SQR)
C                 >4==> not used here
C
C -------------------------------------------------------------------------
C234567


      DOUBLE PRECISION  EBEAM
      DOUBLE PRECISION  AP(9)   !REACTION MOMENTS FROM APCALC
      DOUBLE PRECISION  DAP(9)      !ERROR IN MEASURED MOMENTS
      DOUBLE PRECISION TR1(5,4)     !MOMENTS OF REACTION Tij
      DOUBLE PRECISION BETA(5)      !YIELD RATIO (SEE STEPHENSON REF.)
      DOUBLE PRECISION DBETA(5)     !ERROR IN BETA
      DOUBLE PRECISION CBETA(5)     !MINUITS GUESS FOR THE BETA'S
```

```
      REAL PAREA(36),PNETAREA(36),PERROR(36),PICHAN(2,36)
      REAL UAREA(36),UNETAREA(36),UERROR(36),UICHAN(2,36)

      DOUBLE PRECISION GG(50),X(50),ALIM(50),BLIM(50)
      CHARACTER*50 FILENAME,BACKNAME
      CHARACTER TITLE*60,ATIME*10,ADATE*10,AATIME*20
      DOUBLE PRECISION U(50),WERR(50),XS(50),XTS1(50),WTS(50)
      COMMON/PAREXN/U,WERR
      COMMON/FIX/ IPFIX(50),XS,XTS1,WTS,NPFIX
      COMMON/PARM/P,SH
      COMMON/TITLEC/TITLE,FDATE
      GO TO (10,20,30,40,20),IFLAG


C
C Initialize
C
10  CONTINUE

      WRITE(6,*)'WHAT IS THE DEUTERON BEAM ENERGY?'
      READ(5,*)EBEAM
C  Get the reaction moments from the literature.

      CALL APCALC(AP,DAP,EBEAM)

      T11A=AP(8)          !iT11 for alpha particles
      T20A=AP(2)          !T20 for alpha particles
      T21A=AP(4)          !T21 for alpha particles
      T22A=AP(6)          !T22 for alpha particles

      T11P=AP(9)          !iT11 for protons
      T20P=AP(3)          !T20 for protons
      T21P=AP(5)          !T21 for protons
      T22P=AP(7)          !T22 for protons

      T200=AP(1)          !T20 for 0 degree protons

C  Get yields from the detectors and calculate
C   beta= yield(pol)/yeild(unpol) - 1.

C   WRITE(6,*)'POL BCI'
C   READ(7,*)POLBCI
C   WRITE(6,*)'LEFT SSD POL YIELD'
C   READ(7,*)SSDLPOL
C   WRITE(6,*)'RIGHT SSD POL YEILD'
C   READ(7,*)SSDRPOL
C   WRITE(6,*)'LEFT CsI POL YEILD'
C   READ(7,*)CSILPOL
C   WRITE(6,*)'RIGHT CsI POL YEILD'
C   READ(7,*)CSIRPOL
C   WRITE(6,*)'0 DEGREE CsI POL YEILD'
C   READ(7,*)CSI0POL
```

```
      CALL PARSE
      CALL SUM(100,0,PAREA,PNETAREA,PERROR,PICHAN)
      CALL SUM(101,0,UAREA,UNETAREA,UERROR,UICHAN)

      IFLAG = 1
      DO 1000,IJ=1,6
       IF(PAREA(IJ) .EQ. -100) THEN
        WRITE(6,1010)IJ
1010      FORMAT(' GATE ',I1,' NOT SET IN DATA AREA 8')
       IFLAG = 0
       END IF
       IF(UAREA(IJ) .EQ. -100) THEN
        WRITE(6,1020)IJ
1020      FORMAT(' GATE ',I1,' NOT SET IN DATA AREA 9')
       IFLAG = 0
       END IF
1000   CONTINUE

      IF (IFLAG .EQ. 0) STOP

      POLBCI  = PAREA(1)
      SSDLPOL = PAREA(2)
      SSDRPOL = PAREA(3)
      CSILPOL = PAREA(4)
      CSIRPOL = PAREA(5)
      CSI0POL = PAREA(6)

      UNPOLBCI  = UAREA(1)
      SSDLUNPOL = UAREA(2)
      SSDRUNPOL = UAREA(3)
      CSILUNPOL = UAREA(4)
      CSIRUNPOL = UAREA(5)
      CSI0UNPOL = UAREA(6)

      SSDLPOLN = SSDLPOL/POLBCI
      SSDRPOLN = SSDRPOL/POLBCI
      CSILPOLN = CSILPOL/POLBCI
      CSIRPOLN = CSIRPOL/POLBCI
      CSI0POLN = CSI0POL/POLBCI

C     WRITE(6,*)'UNPOLBCI'
C     READ(7,*)UNPOLBCI
C        WRITE(6,*)'LEFT SSD UNPOL YIELD'
C     READ(7,*)SSDLUNPOL
C     WRITE(6,*)'RIGHT SSD UNPOL YEILD'
C     READ(7,*)SSDRUNPOL
C     WRITE(6,*)'LEFT CsI UNPOL YEILD'
C     READ(7,*)CSILUNPOL
C     WRITE(6,*)'RIGHT CsI UNPOL YEILD'
C     READ(7,*)CSIRUNPOL
C     WRITE(6,*)'0 DEGREE CsI UNPOL YEILD'
```

```
C  READ(7,*)CSI0UNPOL

     SSDLUNPOLN = SSDLUNPOL/UNPOLBCI
     SSDRUNPOLN = SSDRUNPOL/UNPOLBCI
     CSILUNPOLN = CSILUNPOL/UNPOLBCI
     CSIRUNPOLN = CSIRUNPOL/UNPOLBCI
     CSI0UNPOLN = CSI0UNPOL/UNPOLBCI

     BETA(1)=SSDLPOLN/SSDLUNPOLN -1.
     BETA(2)=SSDRPOLN/SSDRUNPOLN -1.
     BETA(3)=CSILPOLN/CSILUNPOLN -1.
     BETA(4)=CSIRPOLN/CSIRUNPOLN -1.
     BETA(5)=CSI0POLN/CSI0UNPOLN -1.

     RA = UNPOLBCI/POLBCI
     DBETA(1) =
RA*SQRT(SSDLPOL*(SSDLPOL+SSDLUNPOL))/SSDLUNPOL**1.5
     DBETA(2) =
RA*SQRT(SSDRPOL*(SSDRPOL+SSDRUNPOL))/SSDRUNPOL**1.5
     DBETA(3) = RA*SQRT(CSILPOL*(CSILPOL+CSILUNPOL))/CSILUNPOL**1.5
     DBETA(4) =
RA*SQRT(CSIRPOL*(CSIRPOL+CSIRUNPOL))/CSIRUNPOL**1.5
     DBETA(5) = RA*SQRT(CSI0POL*(CSI0POL+CSI0UNPOL))/CSI0UNPOL**1.5

     WRITE(6,*)'BETA1=',BETA(1),'+-',DBETA(1)
     WRITE(6,*)'BETA2=',BETA(2),'+-',DBETA(2)
     WRITE(6,*)'BETA3=',BETA(3),'+-',DBETA(3)
     WRITE(6,*)'BETA4=',BETA(4),'+-',DBETA(4)
     WRITE(6,*)'BETA5=',BETA(5),'+-',DBETA(5)
     RETURN

20     CONTINUE
     RETURN


30  CONTINUE


     CBETA(1) = 2.*T11A*X(1)+T20A*X(2)+2.*T21A*X(3)+2.*T22A*X(4)
     CBETA(2) = -2.*T11A*X(1)+T20A*X(2)-2.*T21A*X(3)+2.*T22A*X(4)
     CBETA(3) = 2.*T11P*X(1)+T20P*X(2)+2.*T21P*X(3)+2.*T22P*X(4)
     CBETA(4) = -2.*T11P*X(1)+T20P*X(2)-2.*T21P*X(3)+2.*T22P*X(4)
     CBETA(5) = T200*X(2)

     OPEN(1,FILE='POL.OUT',STATUS='NEW')
     FF= 0.
     DO I = 1,5
        FF = FF + ((BETA(I)-CBETA(I))/DBETA(I))**2

C       WRITE(1,*)'BETA, CBETA, DBETA,CHI'
C       WRITE(1,*)BETA(I),CBETA(I),DBETA(I),
C    &                ((BETA(I)-CBETA(I))/DBETA(I))**2
```

```
      ENDDO

      WRITE(1,*)'CHISQR=',FF
      WRITE(1,*)'CHISQR/DF=',FF/4.
      WRITE(1,21)X(1),WERR(1)
      WRITE(1,22)X(2),WERR(2)
      WRITE(1,23)X(3),WERR(3)
      WRITE(1,24)X(4),WERR(4)
      WRITE(1,*)
21      FORMAT(' it11 = ',F7.4,' +/- ',F7.4)
22      FORMAT('  t20 = ',F7.4,' +/- ',F7.4)
23      FORMAT('  t21 = ',F7.4,' +/- ',F7.4)
24      FORMAT('  t22 = ',F7.4,' +/- ',F7.4)
      T20IND= (CSI0POLN/CSI0UNPOLN -1.)/T200
      WRITE(1,*)'t20ind =',T20IND
      RETURN



40  CONTINUE

c  Calculate the betas (CALLED CBETA) from the reaction analyzing powers and
C  Minuits guess for the beam moments
C   X(1)= it11
C   X(2)= t20
C   X(3)= t21
C   X(4)= t22

      CBETA(1) = 2.*T11A*X(1)+T20A*X(2)+2.*T21A*X(3)+2.*T22A*X(4)
      CBETA(2) = -2.*T11A*X(1)+T20A*X(2)-2.*T21A*X(3)+2.*T22A*X(4)
      CBETA(3) = 2.*T11P*X(1)+T20P*X(2)+2.*T21P*X(3)+2.*T22P*X(4)
      CBETA(4) = -2.*T11P*X(1)+T20P*X(2)-2.*T21P*X(3)+2.*T22P*X(4)
      CBETA(5) = T200*X(2)

      FF= 0.
      DO I = 1,5
         FF = FF + ((BETA(I)-CBETA(I))/DBETA(I))**2
      ENDDO
      END

C*************************************************************
      SUBROUTINE APCALC (AP,DAP,ECELL)
       IMPLICIT REAL*8 (A-H,O-Z)
C   SEPTEMBER 11, 1979    APC CHANGED BY HRB
C    UPDATED BY JK ON NOV 12, 1980
C   CALCULATES ANALYZING POWERS FOR STEPHENSON POLARIMETER
C   GIVEN ECELL, THE ENERGY OF THE BEAM AT THE CENTER OF THE 3HE
C   GAS CELL. PARAMETERIZATION DESCRIBED IN INTERNAL REPORT ON
C   POLARIMETER
C   ANALYZING POWER ERRORS (DAP) NOT IMPLEMENTED IN THIS
ROUTINE.
      DIMENSION AP(9),DAP(9),ESEG(2,9),TH(5,9)
```

```
      DATA ESEG(1,1),ESEG(2,1)/5.74320,9.73664/
      DATA ESEG(1,2),ESEG(2,2)/5.66486,8.46368/
      DATA ESEG(1,3),ESEG(2,3)/7.16195,9.71793/
      DATA ESEG(1,4),ESEG(2,4)/3.57236,7.38535/
      DATA ESEG(1,5),ESEG(2,5)/5.00022,8.87300/
      DATA ESEG(1,6),ESEG(2,6)/5.25266,8.48731/
      DATA ESEG(1,7),ESEG(2,7)/3.94564,8.62899/
      DATA ESEG(1,8),ESEG(2,8)/4.78185,7.18520/
      DATA ESEG(1,9),ESEG(2,9)/5.31735,9.04752/
      DATA TH(1,1),TH(2,1),TH(3,1),TH(4,1),TH(5,1)
     *    /.5678260E-1,.6339732E-2,.3626511E+1,-.1288532E+1,-.1357468E-2/
      DATA TH(1,2),TH(2,2),TH(3,2),TH(4,2),TH(5,2)
     *    /-.1386417E-1,-.2157343E-1,.6658048E+1,.3954708E+0,.5704074E-2/
      DATA TH(1,3),TH(2,3),TH(3,3),TH(4,3),TH(5,3)
     *    /.1768071E-2,.101657E-1,.8875718E+1,-.5852313E+0,.2791001E-2/
      DATA TH(1,4),TH(2,4),TH(3,4),TH(4,4),TH(5,4)
     *    /.9926582E-1,.9827271E-3,43.18327,-1.269458,.1376273E-1/
      DATA TH(1,5),TH(2,5),TH(3,5),TH(4,5),TH(5,5)
     *    /-.3334001E-1,-.1531519E-1,.7052077E+1,.6524656,-.1869513E-2/
      DATA TH(1,6),TH(2,6),TH(3,6),TH(4,6),TH(5,6)
     *    /-.3873436E-1,.2417044E-1,.7998671E+1,-.5987587E+0,-.3338909E-3/
      DATA TH(1,7),TH(2,7),TH(3,7),TH(4,7),TH(5,7)
     *    /.1956599E-1,.4379229E-2,.9937902E+1,-.3045045E+0,.4836683E-2/
      DATA TH(1,8),TH(2,8),TH(3,8),TH(4,8),TH(5,8)
     *    /-.2020095E-1,.3360658E-1,.7457660E+1,-.5700812E+0,.3487879E-2/
      DATA TH(1,9),TH(2,9),TH(3,9),TH(4,9),TH(5,9)
     *    /-.1833195E-1,.1267094E-1,.1108175E+2,-.5992863E+0,.5430263E-2/
      DO 10 N=1,9
      A1=TH(1,N)
      A2=TH(2,N)
      B2=TH(3,N)
      C2=TH(4,N)
      A3=TH(5,N)
      IF (ECELL-ESEG(1,N)) 20,30,30
   30 IF (ECELL-ESEG(2,N)) 40,40,50
   40 AP(N)=A2*(ECELL-B2)**2+C2
C  TYPE *, 'IN 40'
      GO TO 10
   50 EM=ECELL-ESEG(2,N)
C  TYPE *, 'IN 50'
      X=A2/A3*(ESEG(2,N)-B2)
      AP(N)=A3*(2.*X*EM+EM**2)+(X*A3)**2/A2+C2
      GO TO 10
   20 EM=ECELL-ESEG(1,N)
C  TYPE *, 'IN 20'
      X=A2/A1*(ESEG(1,N)-B2)
      AP(N)=A1*(2.*X*EM+EM**2)+(X*A1)**2/A2+C2
   10 CONTINUE
      DO 60 N=1,9
   60 DAP(N)=0.
      RETURN
      END
```

Appendix C: $^3H(p,\gamma)^4He$ Line-shape Fitting Code

This appendix contains the FORTRAN code for a MINUIT subroutine which fits a $^3He(p,\gamma)^4He$ γ-ray spectrum with the composite function described in Section 3.5. Also included is a code which takes the parameters of the composite function and reconstructs the line-shape.

```
      SUBROUTINE FCN(NPAR, GG,FF, X, IFLAG)
C
C
C   THIS PROGRAM IS DESIGNED TO BE A GENERAL FITTING PROGRAM
C   THAT FITS THE LINESHAPE OF A NaI DETECTOR
C              Mark Balbes 11/28/89
C
C
C Minuit subroutine
C Inputs:  npar=no. of ADJUSTABLE parameters
C      GG = derivitive vector (not used here)
C      FF = value of function to be minimized
C      X = parameter values
C      IFLAG = control value 1==> set up constants
C                  2==> not used here
C                  3==> write out information
C                  4==> calculate F (CHI-SQR)
C                 >4==> not used here
C

C ---------------------------------------------------------------------------
C234567

      DOUBLE PRECISION GG(50),X(50),XDATA(2000),YDATA(2000),W(50),
     *  FNCT,ERR(2000),A0,XP(50),AP,BP,EN
      DOUBLE PRECISION UPB,LOWB,JNTLO,JNTHI,CENT,FUNC
      DOUBLE PRECISION A,B,C,D,F,G,H,J,K,S,T,RTBIS,TEST
      CHARACTER*80 CHAR(30)
      COMMON /KEEP/XDATA,YDATA,NDATA,ERR
      COMMON /ZERO/JNTHI,A,B,C,D
      GO TO (10,20,30,40,20),IFLAG


C
C Initialize
C
10  CONTINUE
C
```

```
C   READS IN DATA AT THIS POINT
C
C  Read in lower and upper bound of data to be fit.
     READ(5,*)LOWB,UPB              !Read from Cards.info file

C  Read in lineshape spectrum to be fit.
       OPEN(UNIT=20,STATUS='OLD')
     I = 1
100      READ(20,*,END=101)TEMPX,TEMPY,TEMPE    !Read one line of data.
                        !If end-of-file goto label 101
     IF(TEMPX.GE.LOWB.AND.TEMPX.LE.UPB) THEN     !Take log of the data
         XDATA(I)=TEMPX
         IF(TEMPY.NE.0.) THEN
             ERR(I)=TEMPE/TEMPY       !Avoid divide by zero error
             YDATA(I)=LOG(TEMPY)      !Avoid log(0) error
         ELSE
             ERR(I)=0.
             YDATA(I)=0.
         ENDIF
         IF(ERR(I).EQ.0.) ERR(I)=1.       !Avoid divide by zero error
                        !if ydata not zero but err is
                        !(this is almost redundent)
         I=I+1
     ENDIF
     GOTO 100
101      NDATA=I-1         !NDATA IS NOW #OF DATA POINTS
C    WRITE(6,*)'EXITED LOOP'
     CLOSE(20)
C    WRITE(6,*)'CLOSED 20'

     RETURN

C ---------------------------------------------------------------

20  CONTINUE
     RETURN

C ---------------------------------------------------------------

30  CONTINUE
C  THIS IS THE LAST CALL TO FCN -- THE FITTING IS FINISHED BY NOW
C
C  Define the constants in the Exponential functions

     C=X(1)
     D=X(2)
     F=X(3)
     G=X(4)
     H=X(5)
     J=X(6)
     CENT=X(7)
     JNTHI=X(8)
```

```
      S=X(9)
      T=X(10)
C  To get matching function and first derivative at the
C  jnthi two parameters become dependent.  I've chosen A and B.

      B=G+2*H*(JNTHI-CENT)+3*J*(JNTHI-CENT)**2
     &    -2*C*(JNTHI-CENT)-3*D*(JNTHI-CENT)**2
     &    +4.*T*(JNTHI-CENT)**3-4.*S*(JNTHI-CENT)**3

      A=F+G*(JNTHI-CENT)+H*(JNTHI-CENT)**2+J*(JNTHI-CENT)**3
     &    -B*(JNTHI-CENT)-C*(JNTHI-CENT)**2-D*(JNTHI-CENT)**3
     &    +T*(JNTHI-CENT)**4-S*(JNTHI-CENT)**4
C*************************************************
C The data has been fit to F(x-cent) because it is
C easier for Minuit.  It would
C be nice to have the parameters that give F(x) so
C that centroid doesn't need to be known to reconstruct
C the curve.  Also Mulfit needs this form of the parameters.

      AP=A-B*CENT+C*CENT**2-D*CENT**3+S*CENT**4
      BP=B-2*C*CENT+3*D*CENT**2-4.*S*CENT**3
      XP(1)=C-3*D*CENT+6*S*CENT**2
      XP(2)=D-4.*S*CENT

      XP(3)=F-G*CENT+H*CENT**2-J*CENT**3+T*CENT**4
      XP(4)=G-2*H*CENT+3*J*CENT**2-4.*T*CENT**3
      XP(5)=H-3*J*CENT+6.*T*CENT**2
      XP(6)=J-4.*T*CENT
      XP(7)=S
      XP(8)=T

      open (unit=44,name='FITLINE4.out',type='new',disp='save')
      WRITE(44,*)AP
      WRITE(44,*)BP
      WRITE(44,*)XP(1)
      WRITE(44,*)XP(2)
      WRITE(44,*)XP(7)
      WRITE(44,*)XP(3)
      WRITE(44,*)XP(4)
      WRITE(44,*)XP(5)
      WRITE(44,*)XP(6)
      WRITE(44,*)XP(8)
      WRITE(44,*)JNTHI
      WRITE(44,*)
      WRITE(44,*)'LOWB=',LOWB
      WRITE(44,*)'UPB=',UPB
      write(44,169)CHISQR
169     format (/,' Total chi-squared = ',F9.3)
      CHIPER=CHISQR/(NDATA-7.)
      write(44,168)CHIPER
168     format (/,' Chi-squared/degree of freedom = ',F9.3)
```

```
C Calculate the funtion and its slope at the joint to
C see that they match.
C  EN=JNTHI
C  FNCT1=A+B*(EN-CENT)+C*(EN-CENT)**2+D*(EN-CENT)**3+S*(EN-
CENT)**4
C  FNCT2=F+G*(EN-CENT)+H*(EN-CENT)**2+J*(EN-CENT)**3+T*(EN-
CENT)**4
C  WRITE(44,*)'F(JOINT LOW)=',FNCT1
C  WRITE(44,*)'F(JOINT HIGH)=',FNCT2
C  WRITE(44,*)'DIF=',FNCT1-FNCT2
C
C  FP1=B+2.*C*(EN-CENT)+3.*D*(EN-CENT)**2+4*S*(EN-CENT)**3
C  FP2=G+2.*H*(EN-CENT)+3.*J*(EN-CENT)**2+4*T*(EN-CENT)**3
C  WRITE(44,*)'SLOPE(JOINT LOW)=',FP1
C  WRITE(44,*)'SLOPE(JOINT HIGH)=',FP2
C  WRITE(44,*)'DIF=',FP1-FP2
C Calculate the funtion and its slope at the joint to
C see that they match.
    EN=JNTHI
    FNCT1=AP+BP*EN+XP(1)*EN**2+XP(2)*EN**3+XP(7)*EN**4
    FNCT2=XP(3)+XP(4)*EN+XP(5)*EN**2+XP(6)*EN**3+XP(8)*EN**4
    WRITE(44,*)'F(EN,JOINT LOW)=',FNCT1
    WRITE(44,*)'F(EN,JOINT HIGH)=',FNCT2
    WRITE(44,*)'DIF=',FNCT1-FNCT2

    FP1=BP+2.*XP(1)*EN+3.*XP(2)*EN**2+4*XP(7)*EN**3
    FP2=XP(4)+2.*XP(5)*EN+3.*XP(6)*EN**2+4*XP(8)*EN**3
    WRITE(44,*)'SLOPE(EN,JOINT LOW)=',FP1
    WRITE(44,*)'SLOPE(EN,JOINT HIGH)=',FP2
    WRITE(44,*)'DIF=',FP1-FP2

c Spit out the data being fit

    OPEN(2,FILE='DATA.OUT',STATUS='NEW')
    DO 23 I=1,NDATA
    WRITE(2,*)XDATA(I),EXP(YDATA(I)),ERR(I)*EXP(YDATA(I))
23  CONTINUE

c Make new cards.out file to be able to continue minimizing with

    OPEN(1,FILE='CARDS4.OUT',STATUS='OLD')
    I=1
24  READ(1,163,END=25)CHAR(I)
163     FORMAT(A80)
    I=I+1
    GOTO 24
25  CLOSE(1)
    INUM = I-1              !INUM=#OF LINES IN CARDS.OUT
    OPEN(1,FILE='CARDS4.OUT',STATUS='NEW')
    WRITE(1,163)CHAR(1)
    WRITE(1,167)'C',X(1),'.0001'
```

```
      WRITE(1,167)'D',X(2),'.0001'
      WRITE(1,167)'F',X(3),'.0001'
      WRITE(1,167)'G',X(4),'.0001'
      WRITE(1,167)'H',X(5),'.0001'
      WRITE(1,167)'J',X(6),'.0001'
      WRITE(1,171)'CENT',X(7),'.0001'
      WRITE(1,172)'JNTHI',X(8),'.0001'
      WRITE(1,167)'S',X(9),'.0001'
      WRITE(1,167)'T',X(10),'.0001'
      DO 26 I=12,INUM
         WRITE(1,163)CHAR(I)
26  CONTINUE
167     FORMAT(A1,3X,F15.6,3X,A5)
171     FORMAT(A4,3X,F15.6,3X,A5)
172     FORMAT(A5,3X,F15.6,3X,A5)
      CLOSE(1)
      WRITE (6,*)'FINAL CALL'
       RETURN

C -------------------------------------------------------------

40  CONTINUE

C#########################################################################
######

      FF = 0.
C
C*************************************************************
C   LINESHAPE EQUATION
C*************************************************************
C   WRITE(6,*)'ENTERED LINESHAPE EQN'
C
C  Define the constants in the Exponential functions

      C=X(1)
      D=X(2)
      F=X(3)
      G=X(4)
      H=X(5)
      J=X(6)
      CENT=X(7)   !Not true centroid, but is used to help Minuit fit
      JNTHI=X(8)  !Matching energy located between the two functions.
              !Value should be just less than the true centroid.
      S=X(9)
      T=X(10)
C  To get matching function and first derivative at the
C  jnthi two parameters become dependent.  I've chosen A and B.

      B=G+2*H*(JNTHI-CENT)+3*J*(JNTHI-CENT)**2+4*T*(JNTHI-CENT)**3
     &    -2*C*(JNTHI-CENT)-3*D*(JNTHI-CENT)**2-4*S*(JNTHI-CENT)**3
```

```
      A=F+G*(JNTHI-CENT)+H*(JNTHI-CENT)**2+J*(JNTHI-CENT)**3
     &    -B*(JNTHI-CENT)-C*(JNTHI-CENT)**2-D*(JNTHI-CENT)**3
     &    +T*(JNTHI-CENT)**4-S*(JNTHI-CENT)**4



      DO 211 I = 1, NDATA     !Loop calculates lineshape.
      EN=XDATA(I)
      IF(EN.LT.JNTHI) THEN
        FNCT=A+B*(EN-CENT)+C*(EN-CENT)**2+D*(EN-CENT)**3
     &        +S*(EN-CENT)**4
      ELSE
        FNCT=F+G*(EN-CENT)+H*(EN-CENT)**2+J*(EN-CENT)**3
     &        +T*(EN-CENT)**4
      ENDIF

211       FF = FF + ((YDATA(I)-FNCT)/ERR(I))**2    !Calculate chi squared

       CHISQR = FF
C     WRITE(6,*)'ABOUT TO EXIT LINESHAPE EQN'
C
C#############################################################
      RETURN
      END



      DOUBLE PRECISION ILO,IHI,INC
      DOUBLE PRECISION C1,C2,C3,C4
      DOUBLE PRECISION C5,C6,C7,C8
      DOUBLE PRECISION C9,JNTHI,S,T
      DOUBLE PRECISION X,Y
C     TYPE *,'INPUT LINESHAPE PARAMETERS (TAIL AND LOW ENERGY) C1-
C4'
     READ (11,*)C1,C2,C3,C4,S
C     TYPE *,'INPUT LINESHAPE PARAMETERS (PEAK AND HIGH ENERGY) C5-
C8'
     READ (11,*)C5,C6,C7,C8,T
C     TYPE *,'INPUT MATCHING POINT C9 (JOINT)'
      READ (11,*)JNTHI
      TYPE *,' JOINT = ',JNTHI
      TYPE *,'INPUT PLOTTING RANGE FOR LINESHAPE (LOW,HIGH,INC)'
      READ (5,*)ILO,IHI,INC
      OPEN (UNIT=9,NAME='LINESHAPE4.OUT',TYPE='NEW',DISP='SAVE')
      WRITE(6,*)C1,C2,C3,C4,C5,C6,C7,C8,S,T,JNTHI
      X=ILO
10    IF (X .LT. JNTHI) THEN
        Y=EXP(C1+C2*X+C3*X*X+C4*X*X*X+S*X*X*X*X)
      ELSE
        Y=EXP(C5+C6*X+C7*X*X+C8*X*X*X+T*X*X*X*X)
      ENDIF
C     type *,x,y
```

```
      WRITE (9,*)X,Y
      X=X+INC
      IF(X.LE.IHI) GOTO 10
C     WRITE (9,*) C1,C2,C3,C4
C     WRITE (9,*) C5,C6,C7,C8
C     WRITE (9,*) IC9
99    STOP
      END
```

Appendix D: The J-Independent TME Coefficients

Listed below are the J-independent TME coefficients that have been used in the analysis of the current experiment. The coefficients are identified by the spin and orbital angular momentum quantum numbers of the two transition matrix elements which it multiplies and the mode and multipolarity of the radiation. The Legendre coefficients A_i,C_i, and E_i are given as the real part of the sum of complex transition matrix element products. The B_i coefficients are given as the imaginary part of the sum. For example:

$$A_0 = 2\,(^2s(E1))^2 + 12\,(^4d(E1))^2 + 10\,(^2d(E1))^2 + 4\,(^4s(E1))^2 + 6\,(^2p(M1))^2 + 12\,(^4p(M1))^2 + 6\,(^2p(E2))^2 + 12\,(^4p(E2))^2$$

$$\begin{aligned} A_1 = {} & 8.325\,{}^2s(E1)\,{}^2p(M1)\cos(\theta_{2p}-\theta_{2s}) + 8.363\,{}^2s(E1)\,{}^2p(E2)\cos(\theta_{2p}-\theta_{2s}) \\ & + 4.731\,{}^4d(E1)\,{}^4p(E2)\cos(\theta_{4p}-\theta_{4d}) + 13.543\,{}^2d(E1)\,{}^2p(M1)\cos(\theta_{2p}-\theta_{2d}) \\ & -1.989\,{}^2d(E1)\,{}^2p(E2)\cos(\theta_{2p}-\theta_{2d}) + 16.617\,{}^4s(E1)\,{}^4p(E2)\cos(\theta_{4p}-\theta_{4s}) \end{aligned}$$

$$\begin{aligned} B_3 = {} & 3.957\,{}^4d(E1)\,{}^4p(E2)\sin(\theta_{4p}-\theta_{4d}) + 1.056\,{}^2d(E1)\,{}^2p(E2)\sin(\theta_{2p}-\theta_{2d}) \\ & -4.383\,{}^2d(E1)\,{}^4p(E2)\sin(\theta_{4p}-\theta_{2d}) + 3.063\,{}^4d(E1)\,{}^2p(E2)\sin(\theta_{2p}-\theta_{4d}) \end{aligned}$$

Table D.1 A lists of all of the coefficients for the TME's which were used in the analysis of the data. The code which calculates these coefficients from the J-dependent coefficients follows the table.

COEF	VALUE	MULT	2S+1	2L+1	MULT	2S+1	2L+1
A0	2.000	E1	2	1	E1	2	1
A0	12.000	E1	4	5	E1	4	5
A0	10.000	E1	2	5	E1	2	5
A0	4.000	E1	4	1	E1	4	1
A0	6.000	M1	2	3	M1	2	3
A0	12.000	M1	4	3	M1	4	3
A0	6.000	E2	2	3	E2	2	3

A0	12.000	E2	4	3	E2	4	3
A1	8.325	E1	2	1	M1	2	3
A1	8.363	E1	2	1	E2	2	3
A1	4.731	E1	4	5	E2	4	3
A1	13.543	E1	2	5	M1	2	3
A1	-1.989	E1	2	5	E2	2	3
A1	16.617	E1	4	1	E2	4	3
A2	5.913	E1	2	1	E1	2	5
A2	-9.593	E1	4	5	E1	4	1
A2	-5.648	E1	4	5	E1	4	5
A2	-3.739	E1	2	5	E1	2	5
A2	2.865	M1	2	3	M1	2	3
A2	-12.000	M1	4	3	M1	4	3
A2	17.669	E2	2	3	M1	2	3
A2	2.828	E2	2	3	E2	2	3
A2	0.001	E2	4	3	M1	4	3
A2	5.648	E2	4	3	E2	4	3
A3	-23.745	E1	4	5	E2	4	3
A3	15.157	E1	2	5	E2	2	3
B1	-1.162	E1	2	1	M1	2	3
B1	-4.243	E1	2	1	M1	4	3
B1	1.015	E1	2	1	E2	2	3
B1	-3.964	E1	2	1	E2	4	3
B1	8.097	E1	4	5	M1	2	3
B1	16.088	E1	4	5	M1	4	3
B1	-3.139	E1	4	5	E2	2	3
B1	-4.731	E1	4	5	E2	4	3
B1	4.447	E1	2	5	M1	2	3
B1	-6.270	E1	2	5	M1	4	3
B1	-5.000	E1	2	5	E2	2	3
B1	3.115	E1	2	5	E2	4	3
B1	3.581	E1	4	1	M1	2	3
B1	-13.416	E1	4	1	M1	4	3
B1	-3.646	E1	4	1	E2	2	3
B1	-2.437	E1	4	1	E2	4	3
B2	-0.917	E1	2	1	E1	2	5
B2	-1.765	E1	2	1	E1	4	5
B2	0.717	E1	4	5	E1	2	5
B2	2.729	E1	4	5	E1	4	1
B2	2.584	E1	4	5	E1	4	5
B2	2.449	E1	2	5	E1	2	5
B2	2.515	E1	4	1	E1	2	5
B2	-0.632	M1	2	3	M1	2	3
B2	-2.943	M1	2	3	M1	4	3
B2	4.600	M1	4	3	M1	4	3
B2	-0.837	E2	2	3	M1	2	3
B2	-2.957	E2	2	3	M1	4	3
B2	-1.414	E2	2	3	E2	2	3
B2	-0.193	E2	2	3	E2	4	3
B2	5.437	E2	4	3	M1	2	3
B2	-9.289	E2	4	3	M1	4	3
B2	-2.584	E2	4	3	E2	4	3

B3	3.957	E1	4	5	E2	4	3
B3	1.056	E1	2	5	E2	2	3
B3	-4.383	E1	2	5	E2	4	3
B3	3.063	E1	4	5	E2	2	3
C0	4.000	E1	2	1	E1	4	5
C0	1.616	E1	4	5	E1	4	5
C0	1.121	E1	2	5	E1	4	5
C0	-5.657	E1	4	1	E1	2	5
C0	5.657	E1	4	1	E1	4	5
C0	1.470	M1	2	3	M1	4	3
C0	1.470	E2	2	3	E2	4	3
C1	1.915	E1	2	1	E2	4	3
C1	8.333	E1	4	5	M1	2	3
C1	9.428	E1	4	5	E2	2	3
C1	11.323	E1	4	5	E2	4	3
C1	-11.751	E1	2	5	E2	4	3
C1	-3.341	E1	4	1	M1	2	3
C1	-0.204	E1	4	1	E2	2	3
C1	0.693	E1	4	1	E2	4	3
C2	-0.894	E1	2	1	E1	4	1
C2	-0.863	E1	2	1	E1	4	5
C2	9.023	E1	4	5	E1	2	5
C2	-2.145	E1	4	5	E1	4	1
C2	-4.530	E1	4	5	E1	4	5
C2	-0.185	E1	4	1	E1	2	5
C2	-1.131	E1	4	1	E1	4	1
C2	-1.470	M1	2	3	M1	4	3
C2	0.001	M1	4	3	M1	4	3
C2	0.000	E2	2	3	M1	4	3
C2	1.917	E2	2	3	E2	4	3
C2	-3.394	E2	4	3	M1	2	3
C2	-0.001	E2	4	3	M1	4	3
C2	0.941	E2	4	3	E2	4	3
C3	-2.028	E1	2	1	E2	4	3
C3	-4.782	E1	4	5	E2	4	3
C3	1.937	E1	2	5	E2	4	3
C3	-2.629	E1	4	1	E2	2	3
C3	-5.281	E1	4	1	E2	4	3
C3	-1.694	E1	4	5	E2	2	3
C4	-5.678	E2	2	3	E2	4	3
C4	-5.864	E2	4	3	E2	4	3
E2	-0.365	E1	2	1	E1	4	1
E2	0.352	E1	2	1	E1	4	5
E2	0.876	E1	4	5	E1	4	1
E2	-0.414	E1	4	5	E1	4	5
E2	-0.073	E1	2	5	E1	4	5
E2	0.075	E1	4	1	E1	2	5
E2	-0.462	E1	4	1	E1	4	1
E2	-1.171	E2	2	3	M1	4	3
E2	0.368	E2	2	3	E2	4	3
E2	1.479	E2	4	3	M1	4	3
E2	1.328	E2	4	3	E2	4	3

```
E2      -1.120      E2    4    3        M1    2    3
E3      -0.276      E1    2    1        E2    4    3
E3       1.057      E1    4    5        E2    4    3
E3      -0.032      E1    2    5        E2    4    3
E3      -0.358      E1    4    1        E2    2    3
E3      -0.719      E1    4    1        E2    4    3
E3       0.002      E1    4    5        E2    2    3
E4      -0.386      E2    2    3        E2    4    3
E4      -0.399      E2    4    3        E2    4    3
```

```
      PROGRAM MODLS

C  THIS PROGRAM IS DESIGNED TO READ THE FOR022 OUTPUT FILE FROM
C  LS (OR TEST2 OR COEF) AND MODIFY THE FILE TO A NO J DEPENDENCE
C  FORMAT.  I.E.  ALL TERMS WITH LIKE S,S',L,L' QUANTUM #'S BUT
DIFFERENT
C  J AND J' VALUES WILL HAVE THEIR COEFFICIENTS ADDED.
C
C  EXAMPLE:
C     A0 =(3.5)(2S2)(2P2) + (1.5)(2S2)(2P4) = (5.0)(2S)(2P)
C
C     WHERE NOTATION = 2S+1 L 2J+1
C
C
      INTEGER COUNT(100,100)
      DIMENSION A(0:4),B(0:4),C(0:4),D(0:4),E(0:4),FRAC(20)
      DIMENSION TME(10,10,10,2,4),PHASE(10,10,10,2,4)
       DIMENSION ISS(20),ILL(20),IJJ(20),IEEMM(20),IMMMM(20)
      CHARACTER*80 TITLE
      CHARACTER*1 NAME,EM1,EM2

      DOUBLE PRECISION G(50),X(50),XDATA(50),YDATA(50),W(50),
     *  FNCT,ERR(50),A0
      COMMON /KEEP/XDATA,YDATA,NDATA1,NDATA2
     *  ERR, tme, phase,radtodeg,NDATA3,NDATA4,ndata5
      COMMON /LSCOEF/IMAX(5,0:4),COEFF(5,0:4,500),IEM1(5,0:4,500),
     &  IMULT1(5,0:4,500),IS1(5,0:4,500),IL1(5,0:4,500),IJ1(5,0:4,500),
     &  IEM2(5,0:4,500),IMULT2(5,0:4,500),IS2(5,0:4,500),IL2(5,0:4,500),
     &  IJ2(5,0:4,500)

C
C-----------------------------------------------------------------
C READ IN THE TME QUANTUM #'S
      OPEN(UNIT=22,STATUS='OLD')
      READ(22,200,END=99)BLANK
      READ(22,200,END=99)TITLE
      READ(22,200,END=99)BLANK
200     FORMAT(A80)

C
```

```
C ***      First time through sets values of ICF and IK and IMAX(ICF,IK)
C ***      where ICF and IK give the ang. dist. coeff. (A1 or B3 or C2 etc.)
C ***      and IMAX tells the number of terms in the LS eqn. for that coeff.
C
199    READ (22,201,END=99)NAME,IK,IM,MAX,DCOEF,EM1,IDMUL1,IDS1,
     &IDL1,IDJ1,EM2,IDMUL2,IDS2,IDL2,IDJ2
201    FORMAT (2X,A1,I1,3X,I3,2X,I3,3X,F7.3,5X,A1,I1,4X,I2,4X,I2,4X,I2,
      &6X,A1,I1,4X,I2,4X,I2,4X,I2)
      IF (NAME .EQ. 'A')ICF=1
      IF (NAME .EQ. 'B')ICF=2
      IF (NAME .EQ. 'C')ICF=3
      IF (NAME .EQ. 'D')ICF=4
      IF (NAME .EQ. 'E')ICF=5
      IMAX(ICF,IK)=MAX
      COEFF(ICF,IK,1)=DCOEF
      IMULT1(ICF,IK,1)=IDMUL1
      IEM1(ICF,IK,1)=1
      IF (EM1 .EQ. 'M')IEM1(ICF,IK,1)=2
      IS1(ICF,IK,1)=IDS1
      IL1(ICF,IK,1)=IDL1
      IJ1(ICF,IK,1)=IDJ1
      IMULT2(ICF,IK,1)=IDMUL2
      IEM2(ICF,IK,1)=1
      IF (EM2 .EQ. 'M')IEM2(ICF,IK,1)=2
      IS2(ICF,IK,1)=IDS2
      IL2(ICF,IK,1)=IDL2
      IJ2(ICF,IK,1)=IDJ2
C
C ***      Succeeding reads, values of ICF, IK, IMAX already set from above
C
      DO 51 I=2,IMAX(ICF,IK)
      READ (22,201)NAME,KK,IM,MAX,COEFF(ICF,IK,I),EM1,IMULT1(ICF,IK,I),
       &IS1(ICF,IK,I),IL1(ICF,IK,I),IJ1(ICF,IK,I),EM2,IMULT2(ICF,IK,I),
       &IS2(ICF,IK,I),IL2(ICF,IK,I),IJ2(ICF,IK,I)
      IEM1(ICF,IK,I)=1
      IF (EM1 .EQ. 'M')IEM1(ICF,IK,I)=2
      IEM2(ICF,IK,I)=1
      IF (EM2 .EQ. 'M')IEM2(ICF,IK,I)=2
51    CONTINUE
      GO TO 199
99    CLOSE(22)
C
C-----------------------------------------------------------------------
C
C     ADD COEFFICIENTS WITH THE SAME S AND L QUANTUM #'S

      DO 100 ICF=1,5
      DO 250 IK=0,4
      DO 300 I1=1,IMAX(ICF,IK)-1
        S1 = IS1(ICF,IK,I1)
        L1 = IL1(ICF,IK,I1)
        REM1 = IEM1(ICF,IK,I1)
```

```
      MULT1= IMULT1(ICF,IK,I1)
      S2 = IS2(ICF,IK,I1)
      L2 = IL2(ICF,IK,I1)
      REM2 = IEM2(ICF,IK,I1)
      MULT2= IMULT2(ICF,IK,I1)

    IF (COEFF(ICF,IK,I1).EQ.0.) GOTO 300

    DO 400 I2=I1+1,IMAX(ICF,IK)
      S1P = IS1(ICF,IK,I2)
      L1P = IL1(ICF,IK,I2)
      REM1P = IEM1(ICF,IK,I2)
      MULT1P= IMULT1(ICF,IK,I2)
      S2P = IS2(ICF,IK,I2)
      L2P = IL2(ICF,IK,I2)
      REM2P = IEM2(ICF,IK,I2)
      MULT2P= IMULT2(ICF,IK,I2)
      COEFP= COEFF(ICF,IK,I2)


    IF(S1.EQ.S1P.AND.L1.EQ.L1P.AND.REM1.EQ.REM1P
    &     .AND.MULT1.EQ.MULT1P .and.
    &     S2.EQ.S2P.AND.L2.EQ.L2P.AND.REM2.EQ.REM2P
    &     .AND.MULT2.EQ.MULT2P) then
      COEFF(ICF,IK,I1) = COEFF(ICF,IK,I1)+COEFF(ICF,IK,I2)
      COEFF(ICF,IK,I2)=0.
    ELSEIF(S1.EQ.S2P.AND.L1.EQ.L2P.AND.REM1.EQ.REM2P
    &     .AND.MULT1.EQ.MULT2P .and.
    &     S2.EQ.S1P.AND.L2.EQ.L1P.AND.REM2.EQ.REM1P
    &     .AND.MULT2.EQ.MULT1P) THEN
     IF(ICF.EQ.2) COEFF(ICF,IK,I2)=-1.*COEFF(ICF,IK,I2)
      COEFF(ICF,IK,I1) = COEFF(ICF,IK,I1)+COEFF(ICF,IK,I2)
      COEFF(ICF,IK,I2)=0.
    ENDIF
400     CONTINUE
300     CONTINUE
250     CONTINUE
100     CONTINUE

C-----------------------------------------------------------------
C  COUNT HOW MANY NONZER0 TERMS THERE ARE PER COEFFICIENT

    DO 500 ICF = 1,5
    DO 600 IKP = 1,5
      IK= IKP-1
      COUNT(ICF,IK) = 0
    DO 700 I = 1,IMAX(ICF,IK)
    IF(COEFF(ICF,IK,I).NE.0.) COUNT(ICF,IK)=COUNT(ICF,IK)+1
700     CONTINUE
600     CONTINUE
500     CONTINUE
```

```
C-------------------------------------------------------------
C
C  WRITE A NEW LS FILE IN UNIT 23
      open(unit=23,status='NEW')
      WRITE (23,200)BLANK
      WRITE (23,200)TITLE
      WRITE (23,200)BLANK
      DO 10 ICF = 1,5
      DO 20 IK=0,4
      J=0
      DO 30 I = 1,IMAX(ICF,IK)
C     IF (ABS(COEFF(ICF,IK,I)).LE. .02) COEFF(ICF,IK,I)=0.
      IF (ICF.EQ.1)NAME='A'
      IF (ICF.EQ.2)NAME='B'
      IF (ICF.EQ.3)NAME='C'
      IF (ICF.EQ.4)NAME='D'
      IF (ICF.EQ.5)NAME='E'
      EM1 = 'E'
      IF (IEM1(ICF,IK,I).EQ.2) EM1 = 'M'
      EM2 = 'E'
      IF (IEM2(ICF,IK,I).EQ.2) EM2 = 'M'
      IF (COEFF(ICF,IK,I).NE.0.)THEN
      J=J+1
       WRITE(23,201)NAME,IK,J,COUNT(ICF,IK),COEFF(ICF,IK,I),EM1,
       &IMULT1(ICF,IK,I),IS1(ICF,IK,I),IL1(ICF,IK,I),
      &-1,EM2,IMULT2(ICF,IK,I),
       &IS2(ICF,IK,I),IL2(ICF,IK,I),-1
      ENDIF
30    CONTINUE
20    CONTINUE
10    CONTINUE
      CLOSE(23)

      END
```

References

[Ajz88] F. Ajzenberg-Selove, *Energy Levels of Light Nuclei A=5-10*, Nucl. Phys. **A490**, 1 (1988).

[Bal91] M.J. Balbes, G.Feldman, L.H. Kramer, H.R. Weller, and D.R. Tilley, *Ground-State Widths of ^{5}He and ^{5}Li determined in the ^{3}H(d,γ)^{5}He and ^{3}He(d,γ)^{5}Li reactions*, Phys. Rev. C **43**, 343 (1991).

[Bar71] H. H. Barschall, and W. Haeberli, ed., *Polarization Phenomena in Nuclear Reactions*, University of Wisconsin Press, Madison, Wisconsin (1971).

[Bev69] P.R. Bevington, Data Reduction and Error Analysis for the Physical Sciences, McGraw-Hill Inc., USA (1969).

[Bla54] J.M. Blair, N.M. Hintz, and D. M. Van Patter, *Radiative Capture of Deuterons by ^{3}He*, Phys. Rev. **96**, 1023 (1954).

[Blu90] G. Blüge and K. Langanke, Phys. Rev **C41**, 1191 (1990).

[Bon52] T.W. Bonner, J.P. Conner, and A.B. Lillie, *Cross Section and Angular Distribution of the ^{3}He(d,p)^{4}He Nuclear Reaction*, Phys. Rev. **88**, 473 (1952).

[Bro64] G.E. Brown, *Direct and Semi-Direct (p,γ) and (n,γ) Reactions*, Nucl. Phys. **57**, 339 (1964).

[Bur83] J. Burger, H.M. Hofmann, H. Kellermann, and T. Mertelmeier, Proceedings of the International Conference on Nuclear Physics, Vol. 1, Tipografia Compositori, Bologna, B9 (1983).

[Bus68] W. Buss, W. Del Bianco, H. Wäffler, and B. Ziegler, *Deuteron Capture on ^{3}He*, Nucl. Phys. **A112**, 47 (1968).

[Cec85a] F.E. Cecil, D.M. Cole, F.J. Wilkinson III, and S.S. Medley, *Measurement and Application of DDγ, DTγ and D^3Heγ Reactions at Low Energy*, Nucl. Instr. and Meth. **B10/11**, 411 (1985).

[Cec85b] F.E. Cecil, D.M. Cole, R. Philbin, N. Jarmie, and R. Brown, *Reaction $^2H(^3He,\gamma)^5Li$ at center-of-mass energies between 25 and 60 keV*, Phys. Rev. **C32**, 690 (1985).

[Cer66] J. Cerny, C. Detraz, and R.H. Pehl, *Study of Mass 5 and 7 Nuclei by (p,t) and (p,^{3}He) Reactions on ^7Li and ^9Be*, Phys. Rev. **C152**, 950 (1966).

[Cle74] T. B. Clegg, G. A. Bissinger, and T. A. Trainor, *A Lamb-Shift Polarized Ion Source for the TUNL Tandem Accelerator*, Nucl. Instr. and Meth. **120**, 445 (1974).

[CleTBP] T.B. Clegg et al., to be published.

[Dar71] S.E. Darden, "Description of Polarization and Suggestions for Additional Conventions", H. H. Barschall, and W. Haeberli, ed., *Polarization Phenomena in Nuclear Reactions*, University of Wisconsin Press, Madison, Wisconsin 39 (1971).

[Del68] W. Del Bianco, F. Lemire, F.J.A. Lévesque, and J.M. Poutissou, *$D(^3He, \gamma)^5Li$ reaction from 2 to 11 MeV*, Canadian Journal of Physics **46**, 1585 (1968).

[Eik71] H. Eikemeier and H.H. Hackenbroich, *A Phenomenological Local Soft-Core Nucleon-Nucleon Potential*, Nucl. Phys. **A169**, 407 (1971).

[Hae75] W. Haeberli, "Polarization Experiments", *Nuclear Spectroscopy and Reactions*, ed. J. Cerny, Academic Press, New York, 156 (1975).

[HayPri] E. Hayward (private communication).

[Hof86] H.M Hofmann, "Resonating Group Calculations in Light Nuclear Systems", *Lecture Notes in Physics* **273**, Springer-Verlag, 1986.

[HofPri] H.M. Hofmann (private communication).

[Hou78] A. Houdayer, N.E. Davidson, S.A. Elbakr, A.M.Sourkes, W.T.H. Van Oers, and A.D. Bacher, *Cross-section measurements and phase shift analysis of p-^{4}He elastic scattering in the energy range 20-55 MeV*, Phys. Rev. **C18**, 1985 (1978).

[How82] C.R. Howell and S.A. Wender, *A Linear Voltage Ramp Generator For A Three Stage Bunching System*, Nucl. Instr. and Meth. **195**, 443 (1982).

[Jen80] B. Jenny, W. Gruebler, P.A. Schmelzbach, V. Konig, and H.R. Burge, *Phase-Shift Analysis of ^{3}He(d,d)^{3}He Scattering*, Nucl. Phys. **A337**, 77 (1980).

[Kin72] H.T. King, *The ^{2}H(^{3}He,γ)^{5}Li Reaction from 2-26 MeV*, Nucl. Phys. **A178,** 337 (1972).

[Kin83] S.E. King, *Radiative Capture of Protons and Deuterons Into ^{3}He*, Unpublished Disertation, Duke University (1983).

[Kra68] L. Kraus, M. Suffert, and D. Magnac-Valette, Nucl. Phys. A109, 593 (1968).

[Lan58] A.M. Lane and R.G. Thomas, *R-Matrix Theory of Nuclear Reactions*, Rev. Mod. Phys. **30**, 257 (1958).

[Mar77] R.E. Marrs, E.G. Adelberger, and K.A. Snover, *Electromagnetic transitions in ^{13}C and ^{13}N*, Phys. Rev. C **16**, 61 (1977).

[Mat80] W. Braker, A. Mossman, *Matheson Gas Data Book 6th Edition*, Matheson Gas Products (1980).

[McB82] R.C.McBroom, H.R. Weller, N.R. Roberson, and D.R. Tilley, *^{3}H(p,γ)^{4}He reaction below E_p=30 MeV*, Phys. Rev. C **25**, 1644 (1982).

[McK68] J.L. McKibben, G.P. Lawrence, and G.G. Ohlsen, *Nuclear Spin Filter*, Phys. Rev. Lett **20**, 1180 (1968)

[Mer86] T. Mertelmeier and H.M. Hofmann, *Consistent Cluster Model Description of the Electromagnetic Properties of Lithium and Beryllium Nuclei*, Nucl. Phys. **A459,** 387 (1986).

[Mil79] W.T. Milner, *Double-Drift Beam Bunching Systems*, IEEE Trans. Nucl. Sci. **NS-26**, 1445 (1979).

[Ohl64] G.G . Ohlsen and P.G. Young, *Protons from the Deuteron Bombardment of Helium-4*, Phys. Rev. **C136**, 1632 (1964).

[Ohl71] G.G. Ohlsen et al., *Absolute Beam Polarization Determination for the LASL Lamb-Shift Source by the Quench Ratio Method*, H. H. Barschall, and W. Haeberli, ed., *Polarization Phenomena in Nuclear Reactions*, University of Wisconsin Press, Madison, Wisconsin 842 (1971).

[Pau74] P. Paul, "Large NaI Detectors", J. Cerny, ed., *Nuclear Spectroscopy and Reactions Part A*, Academic Press, New York, New York 345 (1974).

[Per76] C.M. Perey and F.G. Perey, *Compilation of Phenomenological Optical-Model Parameters*, Atomic Data and Nuclear Data Tables **17**, 1 (1976).

[Pla72] G.R. Plattner, A.D. Bacher, and H.E. Conzett, *Phase Shifts for p-^{4}He Elastic Scattering Between 20 and 40 MeV*, Phys. Rev. **C5**, 1158 (1972).

[Ril89] J.C. Riley, H.R. Weller, and D.R. Tilley, *Radiative Capture of Tensor and Vector Polarized Deuterons by ^{3}H at 400 keV*, Phys. Rev. **C40**, 1517 (1989).

[Sch70] H. Schröder and W. Mausberg, *Study of ^{5}Li around 20 MeV Excitation Energy by a Radiative Capture Reaction*, Z. Physik **235**, 234 (1970).

[Sch71] P. Schwandt, T.B. Clegg, and W. Haeberli, *Polarization Measurements and Phase Shifts for p-^{4}He Scattering Between 3 and 18 MeV*, Nucl. Phys. **A163**, 432 (1971).

[Sey79] R.G. Seyler and H.R. Weller, *Angular distribution theory for particle-capture-γ reactions*, Phys. Rev. **C20**, 453 (1979).

[Smi63] D.B. Smith, N. Jarmie, and A.M. Lockett, *^{3}He+t Reactions*, Phys. Rev. **C129**, 785 (1963)

[Ste80] K. Stephenson and W. Haeberli, *A Precision Polarimeter For 5-12 MeV Deuteron Beams*, Nucl. Instrum. Methods **169**, 483 (1980).

[Tom67] T.A. Tombrello, R.J. Spiger, A.D. Bacher, *Deuteron Elastic Scattering from ^{3}He and ^{3}H*, Physical Review **154**, 935 (1967).

[Van83] A.G.M. Van Hees and P.W.M. Glaudemans, Nucl. Phys. **A396**, 105c (1983).

[War57] E.K. Warburton and J.N. McGruer, *Deuteron-Induced Reactions from ^{14}N, ^{15}N, and ^{4}He*, Phys. Rev. **C105**, 639 (1957).

[Wel81] H.R. Weller and N.R. Roberson, *Proton and Neutron Radiative Capture*, IEEE Trans. Nucl. Sci. **NS_28**, 1268 (1981).

[Wen80] S.A. Wender et al., *A High Efficiency Bunching System for Polarized Beams*, Nucl. Instrum. Methods **174**, 341 (1980).

[Wes84] C.R. Westerfeldt, E.G. Bilpuch, M.E.Bleck, D.A. Outlaw, W.K. Wells, J.F. Wilkerson, and T.B. Clegg, *A System for Producing High-Resolution Polarized and Unpolarized Beams with a Tandem Accelerator*, Nucl. Instrum. Methods **219**, 284 (1984).

[Whe37] J.A. Wheeler, *Molecular Viewpoints in Nuclear Structure*, Phys. Rev. **52**, 1083 (1937).

[Yar53] J.L. Yarnell, R.H. Lovberg, and W.R. Stratton, *Angular Distribution of the Reaction $^{3}He(d,p)^{4}He$ between 240 keV and 3.56 MeV*, Phys. Rev. **90**, 292 (1953).

Biography

Mark Joseph Balbes

Personal: Born in Los Angeles, CA, February 12, 1965.

Education: B.A. Physics, Washington University, St. Louis, MO, 1986.
M.A. Physics, Duke University, Durham, NC, 1989.
Ph. D. Nuclear Physics, Duke University, Durham, NC, 1992.

Positions: Research Assistant
Triangle Universities Nuclear Laboratory, 1987-1992

Graduate Teaching Assistant
Duke University, 1986-1988

Selected Publications:

Polarized d + ^{3}He capture into the $3/2^+$ fusion resonance of ^{5}Li and the role of the tensor force, M.J. Balbes, G. Feldman, D.R. Tilley, and H.R. Weller, Physical Review C **45** R487 (1992).

Ground-State Widths of ^{5}He and ^{5}Li Determined in the ^{3}H(d,γ)^{5}He and the ^{3}He(d,γ)^{5}Li Reactions, M.J. Balbes, G. Feldman, L.H. Kramer, D.R. Tilley, H.R. Weller, Physical Review C **43** 343 (1991).

Tensor Polarized Deuteron Capture Reactions and D-State Effects in Light Nuclei, H.R. Weller, G. Feldman, L.H. Kramer, M.J. Balbes, J.Z. Williams, D.R. Tilley, 7th Intl. Symposium on Capture Gamma-Ray Spectroscopy, Asilomar, California (1990).

^{3}H(p,γ)^{4}He Reaction and the (γ,p)/(γ,n) ratio in ^{4}He, G. Feldman, M.J. Balbes, L.H. Kramer, J.Z. Williams, D.R. Tilley, H.R. Weller, Physical Review C **42** 1167 (1990).

Ground-State Widths of ^{5}He and ^{5}Li, M.J. Balbes, L.H. Kramer, G. Feldman, H.R. Weller, D.R. Tilley, Bulletin of the American Physical Society **35** 1660 (1990).

Radiative Capture of 800 keV Polarized Deuterons by ^{3}He, M.J. Balbes, G. Feldman, H.R. Weller, D.R. Tilley, Bulletin of the American Physical Society **34** 1810 (1989).

The ^{3}H(p,γ)^{4}He Reaction and the (γ,p)/(γ,n) ratio in ^{4}He, G. Feldman, M.J. Balbes, L.H. Kramer, J.Z. Williams, H.R. Weller, D.R. Tilley, Bulletin of the American Physical Society **34** 1810 (1989).